HIGH PRESSURE RESEARCH
https://doi.org/10.1080/08957959.2022.2059366

Taylor & Francis
Taylor & Francis Group

Review



# Progress and prospects for cuprate high temperature superconductors under pressure

Alexander C. Mark [a], Juan Carlos Campuzano[a] and Russell J. Hemley [b]

[a]Department of Physics, University of Illinois Chicago, Chicago, IL, USA; [b]Department of Physics, Chemistry, and Earth and Environmental Sciences, University of Illinois Chicago, Chicago, IL, USA

**ABSTRACT**

Since the discovery of high temperature superconductivity in $La_{5-x}Ba_xCu_5O_{5(3-y)}$ at an unprecedented $T_c$ of 35 K over 35 years ago, high pressure experiments have played a critical role in bdeveloping cuprate superconductivity. Soon after its discovery, compression experiments on $La_{5-x}Ba_xCu_5O_{5(3-y)}$ revealed a large $dT_c/dP$, motivating the study of 'chemical pressure' in the material that led to the 90 K Superconductor $YBa_2Cu_3O_{7-y}$. Cuprate superconductors discovered subsequently exhibited a range of $T_c$ from 30 K to 140 K, including the commonly studied Bi, Tl, and Hg based families. Pressure has large effects on superconductivity in these materials, including raising $T_c$ in the Hg based cuprates from 140 K to 166 K at 30 GPa. Reviewing past experiments indicate that pressure dopes holes into the $CuO_2$ planes common to all cuprates. Further detailed high pressure studies of these materials should deepen our understanding of cuprate superconductivity and the possibility of reaching still higher $T_c$ in cuprates.

**ARTICLE HISTORY**
Received 11 January 2022
Accepted 25 March 2022

**KEYWORDS**
High temperature superconductivity; cuprates; high pressure; diamond anvil cell

## 1. Introduction

Experiments over the past several decades have established that pressures now achievable in the laboratory can induce dramatic effects on the superconducting properties of materials. Particularly notable has been the use of pressure in studies of high temperature superconductivity (HTS) of the cuprate superconductors. In 1986 Bednorz and Müller [1] reported a superconducting critical temperature ($T_c$) of 30 K in $La_{2-x}Ba_xCuO_{4-y}$ (LBCO). In their 1988 review of the discovery of HTS in LBCO [2], the authors discuss how the work was in part motivated by predictions of superconductivity in materials under pressure [3,4]. Less than a year after the discovery of HTS in LBCO, Chu et al. [5] found a steep and unprecedented pressure-induced increase of $T_c$ in the material. This group hypothesized that substituting the La in LBCO with the smaller Y would induce a chemical pressure in the lattice that would enhance $T_c$, leading to their discovery of $YBa_2Cu_3O_{7-y}$ (YBCO), the first superconductor with a critical temperature above the boiling point of liquid nitrogen (ambient pressure $T_c \sim 93$ K) [6].

**CONTACT** A. C. Mark amark5@uic.edu Department of Physics, University of Illinois Chicago, Chicago, IL60607, USA; Russell J. Hemley rhemley@uic.edu Department of Physics, Chemistry, and Earth and Environmental Sciences, University of Illinois Chicago, Chicago, IL, USA

Within the next few years multiple cuprate families were discovered, having a range of ambient pressure critical temperatures from 33 K in $Bi_2Sr_2CuO_{6+\delta}$ (BSCCO) [7,8] to above 130 K in $HgBa_2Ca_2Cu_3O_{8+\delta}$ (HgBCCO) [9]. Meanwhile, high pressure studies, most conducted with diamond anvil cells (DACs), revealed intriguing $T_c$ pressure dependencies in these materials Figure 1, *e.g*. LBCO [5,10] YBCO [11–13], BSCCO [14–16] and HgBCCO [17–20]. For some oxygen doping levels, increasing pressure leads to $T_c$ values that are significantly higher than those obtained at ambient pressure. This pressure enhancement is best exemplified in optimally doped $HgBa_2Ca_2Cu_3O_{8+\delta}$ where samples typically exhibit an ambient pressure optimally doped $T_c$ around 130 K which rises to 166 K at 30 GPa, the highest critical temperature reported to date for a cuprate [19] Figure 1. This article reviews experimental high pressure studies of HTS in cuprates over the past 35 years. Building on early reviews by Wijngaarden et al. [21,22], we begin with an overview of the ambient pressure phenomenology of the cuprates followed by a discussion of how this frames an understanding of $T_c$ under pressure. The paper then reviews key properties of different cuprate families, in rough chronological order of their discovery. The use of high oxygen partial pressures for sample growth, the synthesis of novel cuprates that have only been reported under pressure, and electron-doped cuprate superconductors under pressure are then discussed. We conclude with summary remarks and prospects for future research on this interesting class of materials.

## 2. Phenomenology of the cuprate superconductors

At ambient pressure, $T_c$ in the cuprate superconductors is most commonly varied by altering the oxygen doping. Unlike elemental low temperature superconductors, the value of $T_c$ in these HTS materials depends on the inclusion of dopants that alter the electronic structure near the Fermi surface [45]. In addition to the cuprates, the superconducting properties of the iron-pnictides are affected by doping [46–50]. In temperature-doping parameter space $T_c$ is reported to rise and then fall as doping is increased, forming a dome. Presland et al. [51] proposed a phenomenological $T_c$ versus doping relation that has been used to characterize the cuprates,

$$\frac{T_c}{T_{c,\max}} = 1 - 82.6(\delta - \delta_{op})^2, \tag{1}$$

where $\delta_{\mathrm{op}}$ is the optimal oxygen doping corresponding to the maximum $T_c$ ($\delta_{op} \sim 0.16$ for most cuprates), and $T_{c,\max}$ the maximum critical temperature for a particular cuprate family. Samples are denoted as overdoped or underdoped depending on if $\delta$ is greater or smaller than $\delta_{\mathrm{op}}$, respectively.

Since the discovery of HTS in cuprates, numerous experiments indicated that superconductivity in these materials arises from a fundamentally different mechanism than that of conventional phonon-mediated superconductors. Hanzawa [52] showed that $T_c$ in the underdoped and optimally doped cuprates is largely uncorrelated with changes in the phonon density of states induced by isotope replacement as would be expected for phonon-mediated superconductivity [53,54], although small changes in $T_c$ can still be ascribed to phonons [55–57]. The presence of superconductivity despite the existence of strong magnetic interactions was also highly unusual since, in the conventional superconductors, increasing magnetism is found to lead to a suppression – and eventual

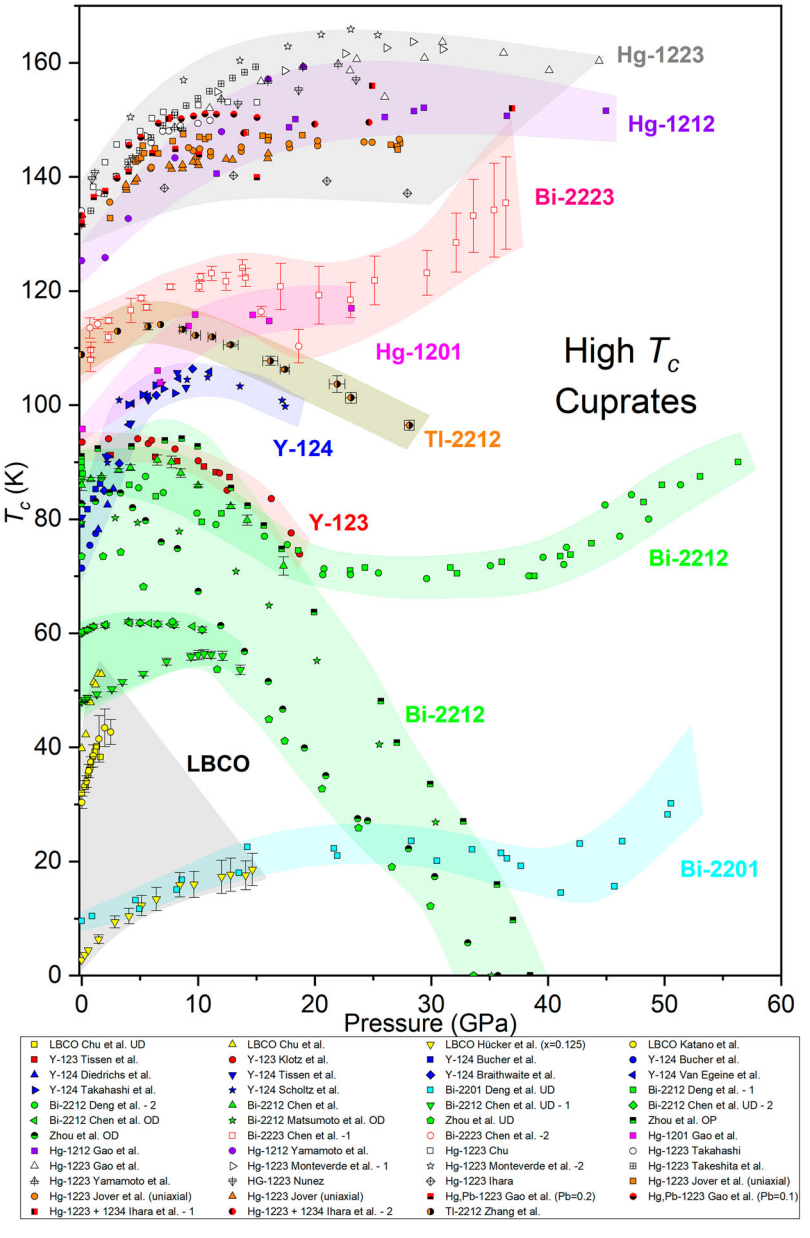


**Figure 1.** *P* dependence of superconducting critical temperature ($T_c$) of various hole doped cuprates discussed in this review. Data are presented for $La_{2-x}Ba_xCuO_{4-y}$ (LBCO) [10,23,24], $YBa_2Cu_3O_{7-y}$ (Y-123) [25,26], $YBa_2Cu_4O_{8-y}$ (Y-124) [27–33], $Tl_2Ba_2CaCu_2O_{8+\delta}$ (Tl-2212) [34], $Bi_2Sr_2CuO_{6+\delta}$ (Bi-2201) [35], $Bi_2Sr_2CaCu_2O_{8+\delta}$ (Bi-2212) [14,35–37] $Bi_2Sr_2Ca_2Cu_3O_{10+\delta}$ (Bi-2223) [14], $HgBa_2CuO_{4+\delta}$ (Hg-1201) [38], $HgBa_2CaCu_2O_{6+\delta}$ (Hg-1212) [38], $HgBa_2Ca_2Cu_3O_{8+\delta}$ (Hg-1223) [18–20,39–43], Pb doped Hg-1223 [44], and mixed phase Hg-1223 + Hg-1234 [43]. Changing the oxygen doping leads to different values and pressure dependencies of $T_c$. Unless specified, samples were optimally doped. Different curves for the same cuprate correspond to different ambient pressure doping levels and different pressure transmitting media used in the experiments (see text).

destruction - of superconductivity [58,59]. It was also noted that upon entering the superconducting state the entire cuprate sample was found to superconduct irrespective of doping level and/or dopant induced magnetic effects [60–62].

Cuprate superconductors studied to date can exhibit one of up to four electronic phases as a function of doping: the antiferromagnetic Mott insulating phase, the 'strange metal' phase, a Fermi liquid phase, and superconductivity [62–64]. The stability regions of these phases are shown schematically in Figure 2. In addition to these four phases, a phenomenon known as the pseudogap is observed in underdoped cuprates for $T_c < T < T^*$, where $T^*$ is the onset temperature of the pseudogap [65,66]. The pseudogap has been identified as a partial suppression of the electron density of states that appears to continuously evolve into the full superconducting gap as the temperature is lowered (For a review see Norman and Pèpin [67]).

Upon entering the superconducting state, HTS cuprates exhibit changes in bulk properties that parallel those found for conventional superconductors ( *i.e.* optical [71], electronic [72,73], and thermal [62,74] properties). On the other hand, the measured electronic contribution to the specific heat in cuprates is significantly lower than what phonon-mediated theories require to predict such high $T_c$'s. Batlogg et al. [75] pointed out that

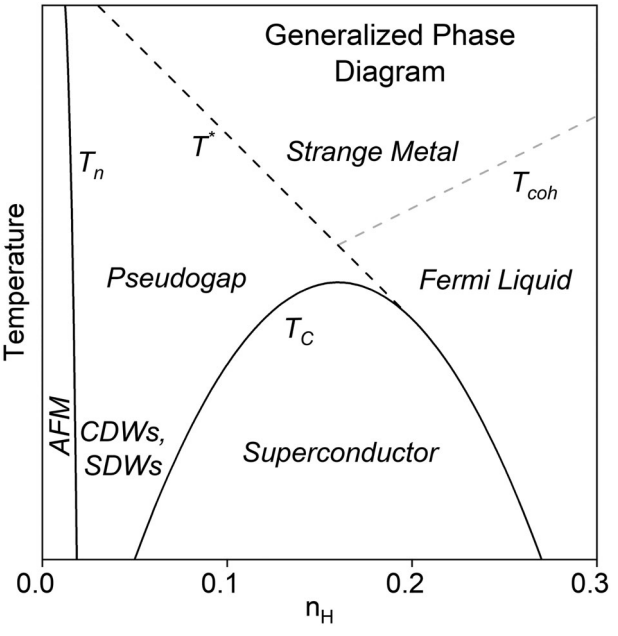


**Figure 2.** Generalized temperature-doping phase diagram of the electronic phases present in cuprates. The antiferromagnetic, pseudogap, superconducting, strange metal and Fermi liquid phase boundaries are plotted as a function of temperature and doping. Temperature scales of phase boundaries are adapted from Hashimoto et al. [68] and Chatterjee et al. [65]. $T_n$ is the Néel temperature, $T^*$ indicates the PG onset temperature, $T_c$ is the superconducting critical temperature, and $T_{coh}$ indicates the strange metal – Fermi liquid crossover temperature as determined via ARPES measurements [65]. CDW and SDW indicate regions of the phase diagram where charge density wave and spin density waves exist [69,70]. For the vast majority of cuprates, $T_c$ is maximized at an optimal oxygen doping of $n_H \sim 0.16$. A note on nomenclature; in this review $n_H$ will refer to the hole doping, instead of the more common abbreviation p, so as to avoid confusion with pressure.

the relatively small values of the electronic specific heat coefficient ($\gamma$) [75–77] and high $T_c$ measured in cuprates indicate that their HTS is incompatible with conventional phonon-mediated theories (See Kittel [78] for a general discussion of the relationship between $\gamma$ and superconductivity).

Early on it was suggested that the superconducting order parameter ($\Delta(k)e^{-i\phi(k)}$) should have *d*-wave symmetry [79,80]; that is, the order parameter changes sign under a $90^o$ rotation in momentum space. This behavior contrasts with the conventional *s*-wave symmetry of the order parameter found in conventional superconductors. The *d*-wave nature of the order parameter was later confirmed by phase-sensitive Josephson junction [81] and SQUID [82] experiments. Subsequently Ding et al. [83] found that the magnitude of the superconducting gap ($\Delta(k)$, the magnitude of the order parameter) can be described by the equation

$$\Delta(k) = \frac{\Delta_0}{2}\big(\cos(k_x) - \cos(k_y)\big), \tag{2}$$

where $\Delta_0$ is the maximum gap width and $k_{x,y}$ is the electron *x* and *y* momenta, respectively.

At temperatures between $T_c$ and some $T^*$ above $T_c$, cuprate superconductors exhibit a partial suppression in the electron density of states around the Fermi level, giving rise to the pseudogap discussed above. The pseudogap was first hinted at by a drastic reduction of the Knight shift in NMR measurements at temperatures well above $T_c$ by several groups [84–87]. Finally, the pseudogap was later observed in angle-resolved photoemission spectroscopy (ARPES) experiments by Ding et al. [88]. The gap width of the pseudogap ($\Delta^*$) exhibits a momentum dependence proportional to $\cos(k_x) - \cos(k_y)$, similar to the *d*-wave symmetry of the superconducting gap. The pseudogap transition temperature ($T^*$) extends throughout the underdoped region of temperature-doping space and appears to terminate at a point tangent to the superconducting dome at a doping level slightly higher than $\delta_{op}$ [65] Figure 2. This point corresponds to a change in Fermi surface topology that was first observed in BSCCO [89]. With increasing temperature, the nodal points of the pseudogap just above $T_c$ expand into apparent Fermi arcs, which eventually fill in the pseudogap, forming a complete Fermi surface [90]. Currently there is no accepted theory that adequately describes the pseudogap or how it might arise.

For undoped and highly underdoped samples (typically $\delta < 0.05$), cuprates are antiferromagnetic Mott insulators, with Néel temperatures ranging from 300 K to 500 K, depending on the compound [91–95]. Throughout the underdoped side of the phase diagram, many (but not all) cuprates appear to exhibit charge and spin density waves (CDW and SDW) or 'stripes' that are spatially incommensurate with the underlying $CuO_2$ lattice [69,96–98]. When stripes coexist with superconductivity they are observed to suppress $T_c$ [99]. Recent theoretical [100] and experimental [101] reports indicate the existence of spin-stripe order within cuprate superconductors may be fundamental to the existence of HTS in cuprates. Above $T^*$, the normal state of the high $T_c$ cuprates are often referred to as strange metals [65,102,103]. Within the strange metal phase the electrical resistivity scales linearly with temperature [$\rho(T) \sim T$] as opposed to the $\rho(T) \sim T^2$ dependence expected for metals [104]. As doping is increased, cuprates begin to behave more like Fermi liquids, with heavily overdoped cuprates appearing metallic [102,105]. On the

other hand, the electronic structures of the overdoped cuprates is much simpler than those of underdoped materials. As Lee et al. [106] stated 'Beyond optimal doping (the overdoped region) sanity gradually returns'. It has been demonstrated that $T_c$ decreases parabolically as doping increases beyond the optimal value. As the doping further increases, there is a crossover region where the resistivity scaling gradually changes to that of a Fermi liquid. Highly overdoped ($\delta > 0.28$) cuprates behave like metals with the resistivity exhibiting a $\rho(T) \sim T^2$ temperature dependence [102,107].

Early reviews of cuprates such as those by Wijngaarden et al. [21,22] pointed out similarities between the pressure and oxygen doping effects on $T_c$, and observation that has been discussed in many reviews since [108,109]. As either pressure or oxygen doping is increased, $T_c$ is found to first rise and then fall, forming a superconducting dome in both the temperature versus doping and the temperature versus pressure curves. In the case of variable doping this relation is parabolic, with a maximum value of $T_c$ corresponding to an optimal oxygen doping level $\delta_{op}$. Thus, to first approximation increasing pressure would appear to increase the doping, causing $T_c$ to trace out the phenomenological $T_c$ versus doping dome. Under pressure the $T_c$ versus doping relation approaches a skewed parabola, with $\delta_{op}$ shifting to lower values upon compression [41,110]. At ambient pressure, the non-stoichiometric oxygen doping parameter uniquely determines the hole concentration within the $CuO_2$ planes, which in turn determines $T_c$. Under pressure the relationship between them is more complex, with pressure also increasing the hole concentration at a constant chemical composition. To remain consistent with nomenclature used in the literature, below we use $y$ and $\delta$ for the oxygen doping parameter for LBCO/LSCO/YBCO and Bi-Th-Hg-bearing cuprates respectively.

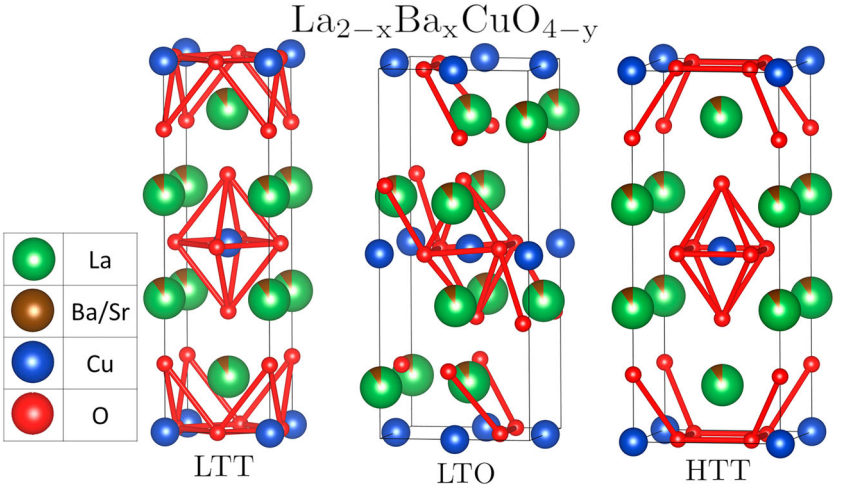


**Figure 3.** Unit cells of the observed structures of $La_{2-x}Ba_xCuO_{4-y}$: From left to right, the low temperature tetragonal (LTT), low temperature orthorhombic (LTO), and high temperature tetragonal (HTT) phases. The phases are derived from the parent lanthanum copper oxide in which some sites containing La are filled with Sr or Ba. HTS is primarily attributed to the LTO phase. Structural parameters used to generate HTT ($a$ =5.323 Å, $c$ = 13.21 Å) are from Wesche et al. [111]. Structural parameters for LTO ($a$ = 5.335 Å, $b$ = 5.415 Å, $c$ = 13.16 Å) and LTT ($a$ = 3.80 Å, $c$ = 13.20 Å) from Radaelli et al. [112]. LBCO and $La_{2-x}Sr_xCuO_{4-y}$ (LSCO) exhibits the same LTO and HTT phases, but the LTT phase has apparently not been reported for LSCO. Structural drawings in this paper were created using VESTA [113].

## 3. Lanthanum Barium Copper Oxide (LBCO)

Bednorz and Müller's [1] 1968 discovery of HTS in $La_{2-x}Ba_xCuO_{4-y}$ (LBCO) ushered in a new era of superconductivity in which pressure has consistently been used as a valuable experimental parameter. It is now common to describe LBCO using the formula $La_{2-x}Ba_xCuO_{4-y}$; in older literature the formula $La_{5-x}Ba_xCu_5O_{5(3-y)}$ was often used. Crystal structures of the observed phases of LBCO are presented in Figure 3.

Chu et al.'s [5] discovery of the large pressure effect on the critical temperature, with $T_c$ increasing from 30 K at ambient pressure to ~40 K at 1.7 GPa ($dT_c/dP \sim 9 \times 10^{-3}$ K/GPa) [10], contrasted with that observed in conventional superconductors for which much smaller (and typically negative) values of $dT_c/dP$ were reported. This pressure effect led Cava et al. [114] to synthesize a similar cuprate with smaller Sr instead of Ba in order to induce a 'chemical pressure' that would increase $T_c$. The resultant material was isostructural to LBCO, with Sr occupying the Ba sites, and had the formula $La_{2-x}Sr_xCuO_{4-y}$ (LSCO) with a $T_c$ of 36 K. Likewise, Wu et al. [6] continued this hypothesis, synthesizing cuprates with the smaller Y instead of La. The use of Y bearing materials in the synthesis process resulted in the discovery of $YBa_2Cu_3O_{7-y}$ (YBCO) with a $T_c$ of 93 K as discussed in the next section.

### 3.1. Structural studies of LBCO/LSCO

LBCO and LSCO have layered perovskite structures, similar to all known high $T_c$ cuprates. These materials consist of alternating layers of $CuO_2$ planes separated by charge reservoir layers that stabilize the structure [115]. In addition to the superconducting, antiferromagnetic, strange metal, and Fermi liquid phases and the pseudogap, two structural phases are reported to exist near the superconducting dome, an HTS low temperature orthorhombic (LTO) phase and a low temperature tetragonal (LTT) phase are both stable within the vicinity of the dome [116]. The HTS LTO phase competes with other structural and electronic phases that exist within a similar region of the phase diagram [70,117] Figure 2. The existence of these phases is dependent on the barium doping, with the LTT phase preferentially forming when the barium doping is near $x \sim 0.125$, and subsequently suppresses $T_c$. It is not clear if superconductivity at $x \sim 1/8$ is due to the small fraction of LTO phase still present in the sample, or if the LTT phase becomes superconducting at much lower temperatures [23]. Orthorhombicity in the LTO phase appears to be mainly due to the tilting of the $CuO_2$ planes, elongating the unit cell along the *b* direction [118]. Superconductivity has been correlated with the reduced symmetry of the LTO structure [118,119].

Above 200 K, a high temperature tetragonal (HTT) phase exists that is structurally similar to the superconducting phases. It contains two-dimensional $CuO_2$ planes, but only exists as a minority phase at temperatures low enough to induce superconductivity [111]. The HTT, LTO, and LTT *P-T* phase boundaries are presented in Figure 4. Irrespective of the majority phase, at ambient pressures there is typically a significant volume fraction of the other two present in the material [23,120]. The structurally analogous $La_{2-x}Sr_xCuO_{4-y}$ (LSCO) superconductor exhibits the same HTT and LTO phases, but to our knowledge the LTT phase has not been reported.

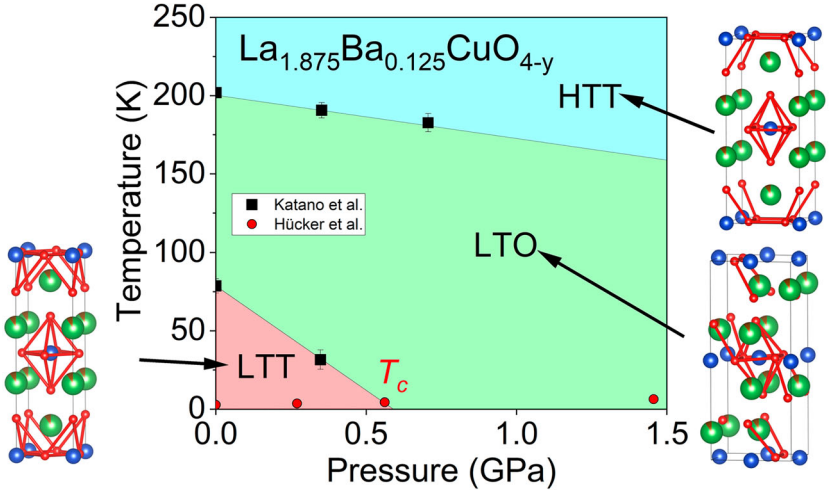


**Figure 4.** Pressure dependence of the phase boundaries of $La_{2-x}Ba_xCuO_4$ for x ~ 1/8 as reported by by Katano et al. [23]. $T_c$ data at $x \sim 1/8$ from Hücker et al. [24].

Moodenbaugh et al. [121] reported a decrease in $T_c$ from close to 30 K to 5 K in $La_{2-x}Ba_xCuO_{4-y}$ at a barium concentration of $x \approx 1/8$ ($La_{1.875}Ba_{0.125}CuO_{4-y}$). This '1/8 anomaly' was attributed to the formation of the LTT phase suppressing superconductivity [23,70,122–124]. Billinge et al. [116] showed that $T_c$ decreases with increasing volume fraction of the LTT phase within the material. Xiong et al. [125] demonstrated that, even though LTT does not form in LSCO, a noticeable dip in $T_c$ is still found at $x \sim 1/8$. The authors interpret this as evidence that an effect unrelated to the competing structural phase found in LBCO is responsible for the anomalies in $T_c$ around $x \sim 1/8$, instead proposing a possible Lifshitz transition that would alter the electronic structure. [126].

Tranquada et al. [98,127] reported neutron scattering evidence that stripe order is greatly enhanced within the LTT phase. The enhancement of stripes results in greater charge carrier scattering and enhanced magnetism that greatly suppresses superconductivity. Experiments reported by Zhou et al. [128] suggested that pressure destroys the LTT phase, allowing the superconducting LTO phase to dominate. The transition from LTO → LTT corresponds to the destruction of the antiferromagnetic stripes that are present in cuprates. Guguchia et al. [129] observed the complete destruction of the LTT phase in a sample at 1.8 GPa in a sample with doping of $x = 1/8$. However, suppression of the LTT phase does not entirely describe the pressure effects on $T_c$; Hücker et al. [24] reported that $T_c$ will continue to rise with further increase in pressure even after the LTT phase is completely destroyed. No pressure induced structural phase transitions to new phases have been observed up to ~15 GPa, the highest pressures reported for studies of LBCO [24].

### *3.2. Superconductivity under pressure in LBCO/LSCO*

As discussed above, the effect of pressure on $T_c$ of superconducting cuprates is often described as being analogous to the effect of oxygen doping. The critical temperature

is observed to increase, decrease, and in some cuprate families increase followed by a decrease (Figure 1). Many of these effects may be understood in terms of the $T_c$ – doping relation proposed by Presland et al. [51] discussed above (Equation 1). In general, $dT_c/dP$ is observed to be large and positive for underdoped samples, and decreases in magnitude as the ambient pressure oxygen doping is increased, commonly observed through transport [18,130] and magnetization measurements [14,131]. Additionally, Raman [132,133] and NMR measurements [134] are consistent with the $CuO_2$ planes being hole doped with pressure. According to this framework, barring an electronic or structural phase transition, pressure and doping are altering the same intrinsic quantity in cuprates, namely the charge carrier density ($n_H$) within the $CuO_2$ planes [39,44,110,135–138]. This framework is the basis of the phenomenological pressure induced charge transfer (PICT) model [135,136,139,140], in which the pressure effect on $T_c$ is written,

$$\frac{dT_c}{dP} = \frac{\partial n_H}{\partial P}\left(\frac{\partial T_c}{\partial n_H}\right)_P + \left(\frac{\partial T_c}{\partial P}\right)_{n_H}. \tag{3}$$

where the first term is that of pressure-induced doping and the second describes the intrinsic (non-doping related) pressure effect on the structure [141]. While it is generally agreed that $n_H$ increases with pressure and therefore alters $T_c$ accordingly, it is not believed to be the only contribution to the pressure dependence of $T_c$ [39]. In the

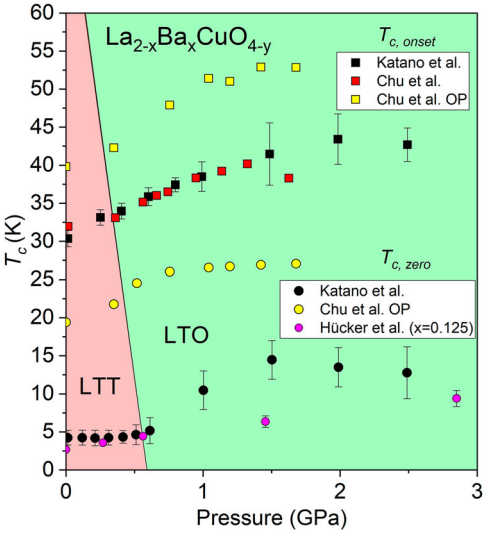


**Figure 5.** Pressure dependence of $T_c$ of $La_{2-x}Ba_xCuO_{4-y}$ (LBCO). Solid squares indicate the onset of superconductivity from Katano et al. [23], Hücker et al. [24], and Chu et al. [5,10]. OP denotes optimally doped; other data reported by Chu et al. [10] were of an unknown doping and measured as-grown. data from Hücker et al. [24] was from a sample with a Ba doping of x ∼ 1/8, and $T_c$ was suppressed due to the 1/8 anomaly (see text). $T_{c,onset}$ is defined as the temperature at which the resistivity versus temperature relation deviates from linearity. $T_{c,zero}$ was defined as the temperature at which the value of the resistivity is below the instrumental noise floor. Red region is the measured LTT phase and green is the LTO phase. The decrease in the highest pressure data point from Chu et al. [5] (red) was attributed to sample damage.

LBCO system the intrinsic pressure response appears to arise from structural changes ( *e.g.* the destruction of the LTT phase [129]) and a suppression of the magnetically ordered stripes [142,143].

As-grown LBCO has been reported to exhibit a $T_c$ of 42.5 K at 1.3 GPa, with a $dT_c/dP \approx 6$ K /GPa [10,23] (Figure 5). The onset of superconductivity in optimally doped LBCO was reported to rise to 52.5 K under similar pressures [10]. The pressure dependence was also positive, unlike that observed in conventional superconductors at the time [5]. In addition to quasi-hydrostatic compression, uniaxial strain has shown to have a similar effect on the transport properties of LBCO. Locquet et al. [144] reported that compressive epitaxial strain on thin film LSCO generated through an appropriate choice of substrate nearly doubles $T_c$ from 25 K to 49 K. The same resistivity measurements indicate a decrease in $T^*$. Bozovic et al. [145] reported that tensile strain suppresses superconductivity.

### 3.3. Magnetic and electrical resistivity measurements of LBCO/LSCO

Similar to doping, pressure has significant effects on the magnetic and electronic properties of LBCO and LSCO. Many of the magnetic effects on LBCO appear to be related to the spin-stripe order that predominantly exists in the LTT phase. Stripes, proposed independently by Zaanen and Gunnarson [69] and Machida [146], are charge and spin density waves present in the $CuO_2$ planes that are incommensurate with the underlying lattice. Their existence in many cuprate families is well documented [69,70]. Guguchia et al. [143] studied the interplay between static stripe order and superconductivity in LBCO using muon spin relaxation ($\mu$SR) spectroscopy and reported that magnetic ordering appears to be related to the presence of the LTT phase. The destruction of the LTT

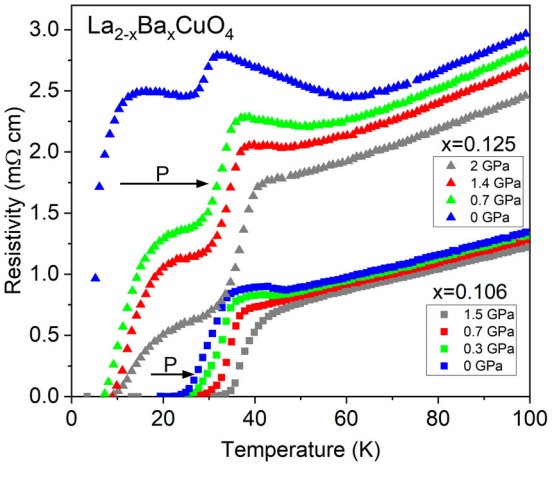


**Figure 6.** Temperature dependence of resistivity at various pressures for $La_{2-x}Ba_xCuO_4$ at barium dopings of $x = 0.106$ (squares) and $x = 0.125$ (triangles). Arrows indicate application of pressure. For both compositions pressure tends to increase both the onset of superconductivity and the zero resistivity temperature. For $x = 0.125$ the step-like behavior associated with the LTT phase and stripe order due to the 1/8 anomaly is reported to decrease under pressure. Figure adapted from Ido et al. [147].

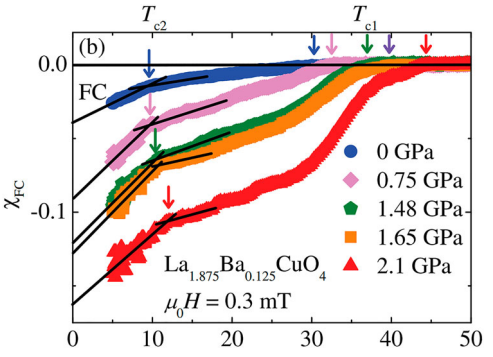


**Figure 7.** Temperature dependence of magnetic susceptibility of $La_{1.875}Ba_{0.125}CuO_{4-y}$ (LBCO) at different pressures. The enhancement of step-like behavior in the susceptibility has been explained as arising from a suppression of the magnetically ordered stripes under pressure. As the LTT phase and stripe order is destroyed, more of the sample becomes superconducting. This allows for the Meissner effect to be more strongly evident at higher temperatures. Figure reproduced from Guguchia et al. [129] with permission.

phase with pressure corresponds to the reduction in the volume fraction of the magnetically ordered phase and the corresponding increase in the volume fraction of the LTO phase [143].

In LBCO and LSCO a step-like feature has been reported in ambient pressure resistivity experiments, particularly when the sample is placed in a magnetic field, and has been observed since the discovery of cuprate superconductors (see Figure 1 in [10]). Ido et al. [147] reported a step-like behavior in resistivity measurements on LBCO under pressure Figure 6. Both the upper and lower temperature scales ($T_{c1}$ and $T_{c2}$ respectively) were observed to increase with pressure. At dopings around $x = 1/8$ the step like feature is especially prominent. As pressure is increased, the step-like behavior is suppressed [148]. Ido et al. [147] correlated the reduction in the step-like behavior to the destruction of the LTT phase.

Guguchia et al. [129,143] reported magnetization measurements exhibiting a similar two-step behavior that also indicate an upper and lower critical temperature. The authors attributed the upper critical temperature ($T_{c1}$) to the onset of the Meissner effect within the $CuO_2$ planes and the lower critical temperature ($T_{c2}$) to the complete expulsion of magnetic fields from the bulk. Under pressure, the step-like behavior in the susceptibility is enhanced [129,143]. As the pressure is increased, the magnetically ordered antiferromagnetic phase is suppressed at all doping levels, as indicated by the neutron scattering data of Traquada et al. [70] and $\mu$SR results by Guguchia et al. [129,143]. $T_{c1}$ increases under pressure from 30 K at ambient pressure to almost 45 K at 2.1 GPa, while $T_{c2}$ increases from 10 K to above 12 K over the same pressure range [129] Figure 7. The magnitude of the step in the susceptibility drastically increases upon compression, consistent with the disappearance of the LTT phase and subsequent suppression of the magnetically ordered stripes. Although stripe formation is greatly suppressed, Guguchia et al. [129,143] and Hücker et al. [24] reported weak stripes persisting even after the LTT phase is destroyed at higher pressures. The results suggest that whereas the LTT phase helps stabilize stripe order, weak stripes are still able to exist in the LTO phase [24,129,143].

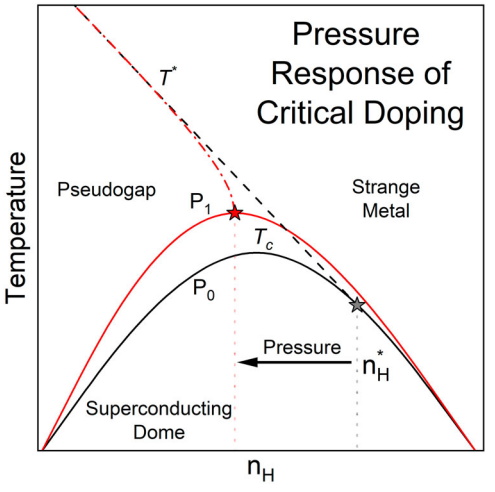


**Figure 8.** *P* response of $T^*$. As reported by Doiron-Leyraud et al. [149], the critical doping level corresponding to the termination of the pseudogap phase boundary, $n_H^*$ has been observed to shift to lower doping levels under hydrostatic pressure using transport measurements. Elevated pressure phase boundaries adapted from Doiron-Leyraud et al. [149] and Rullier et al. [64] Low pressure boundaries adapted from Wang et al. [151,152], Cyr-Choiniere et al. [153], Xu et al. [154], and Fujii et al. [155].

### *3.4. Pseudogap under pressure in LBCO/LSCO*

The pseudogap onset temperature, $T^*$ is defined as the temperature where the partial depletion in the electron density of states begins to appear. $T^*$ appears to be independent of pressure, disorder, and structural changes [64,149]. This behavior of the pseudogap provides no clue as to the nature of the pseudogap, and its origin remains to be understood. Doiron-Leyraud et al. [149] reported that the value of $T^*$ appears to be unaffected by pressure, with the the linear relationship between $T^*$ and doping as presented in the universal phase diagram (Figure 2) persists up to tens of gigapascals, and appears to be unaffected by the LTO $\rightarrow$ LTT phase transition. At ambient pressure, $T^*$ terminates at a point tangent to the superconducting dome slightly above optimal doping, meeting the dome at a critical doping ($n_H^*$). Campuzano et al. [150] argue that, at ambient pressure, this critical doping corresponds to a change in the Fermi surface topology from hole-like to electron-like. Resistivity measurements by Doiron-Leyraud et al. [149] (following the methods of Cooper et al. [104]) indicate that the value of $n_H^*$, and therefore the pseudogap boundary, moves to lower doping levels with pressure, truncating the pseudogap phase boundary (Figure 8).

The major effect of pressure on $T^*$ is on the maximum allowed doping for which the pseudogap can exist. This observation implies that pressure is simply shifting the termination point of the $T^*$ versus doping relation to lower dopings, not changing any of the properties of the pseudogap itself. It should be noted that many experiments that probe the pseudogap in LBCO/LSCO, both at ambient and elevated pressures, were performed on Eu – doped [156,157] and Nd – doped [149,157,158] samples, two dopants which are known to enhance stripe formation in the underdoped cuprates [153,155]. More experiments are needed to determine the nature of the relationship between the pseudogap and pressure.

### 3.5. Uniaxial compression of LBCO

The application of uniaxial stress has also been used as a probe into the interplay between superconducting and magnetic effects in LBCO, particularly in measuring the enhanced magnetism in the region of phase space around the 1/8 anomaly. Guguchia et al. [159] report uniaxial compression of LBCO with doping around 1/8 to exhibit a steep increase in $T_c$ along with an enhancement of spin-stripe order as measured using $\mu$SR. This has been interpreted as a destruction of the stripes associated with the 1/8 anomaly and subsequent enhancement of 3D superconductivity within the sample as opposed to the 2D superconductivity traditionally associated with cuprates. Evidence for the existence of 3D superconductivity that is fundamentally different from the 2D superconductivity exhibited in cuprates has previously been presented by Tranquada et al. [160] and by Guguchia et al. [143] in LBCO around the 1/8 anomaly.

Takeshita et al. [161] demonstrated that the superconducting and magnetic properties of Eu-doped LBCO are highly dependent on the direction of the applied stress. Stress along the (110) axis enhances $T_c$ about 3 times more than stress along the (100) axis. The discrepancy in these stress responses was attributed to stress induced stripe formation/destruction. Recently, Kamminga et al. [162] have reported uniaxial compression along the (110) direction in LBCO ($x \sim 1/8$) to destroy stripe order as probed by neutron diffraction.

## 4. Yttrium Barium Copper Oxide (YBCO)

As described above, the measured increase in $T_c$ under pressure observed by Chu et al. [10] in LBCO led to the 'chemical pressure' hypothesis that replacement of $La^{3+}$ in the cuprate with $Y^{3+}$ would give rise to a further $T_c$ enhancement. The first compound synthesized was the most common variety of YBCO, $YBa_2Cu_3O_{7-y}$ (Y-123). Later, Zandbergen et al. [163] identified a second member of the YBCO family with doubled $CuO_2$ chains in each unit cell with chemical formula $YBa_2Cu_4O_{8-y}$ (Y-124) as a separate structural phase rather than a crystallographic defect. In addition to the Y-123 and Y-124 phases, a Y-237 phase [164] and a Y-247 phase [165] exist, which may be thought of as heterostructures consisting of alternating blocks of Y-123 and Y-124. Both Y-237 and Y-247 require high oxygen partial pressures to form [166]. Structures, along with definitions of the crystallographic axes used in this paper, are presented in Figure 9. YBCO differs structurally from many of the other cuprate superconductors, in that it contains $CuO_2$ chain structures between the superconducting planes. These chains are oriented along the *b* axis of the unit cell, and cause YBCO to be significantly more orthorhombic than other cuprates. The broken four-fold rotational symmetry of the *ab* plane due to the chains means compounds of the YBCO family cannot be described using tetragonal or pseudo-tetragonal symmetry as is common for other cuprates.

A major open question for YBCO compounds under pressure is the nature of the complex interplay between the charge density waves and superconductivity. While it is agreed that the charge density waves are in general suppressed via hydrostatic or quasi-hydrostatic pressure and by uniaxial stress [169,170], it is debated if this observation is due to a complete destruction of the CDW phase under pressure, as proposed by Cyr-Choiniere et al. [142]. Alternatively, Vinograd et al. [171] have proposed that charge

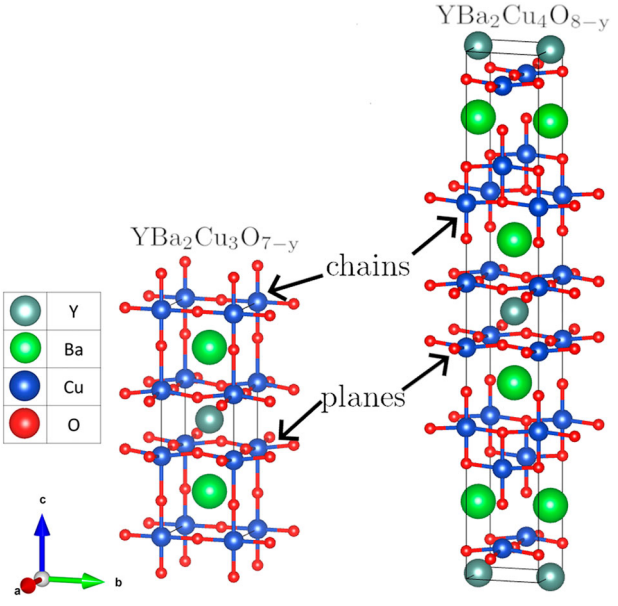


**Figure 9.** Left: $YBa_2Cu_3O_{7-y}$ (Y-123) unit cell. The two parallel $CuO_2$ planes in the center of the structure are believed to be responsible for superconductivity. The $CuO_2$ chains are on the top and bottom of the unit cell and run parallel to the *b* axis. Right: $YBa_2Cu_4O_{8-y}$ (Y-124) crystal structure. Y-124 has a significantly longer *c* parameter due to the doubling of the $CuO_2$ chains. Structural parameters for Y-123 ($a = 3.837$ Å, $b = 3.897$ Å, $c = 11.73$ Å) from Junod et al. [167] and Y-124 ($a = 3.840$ Å, $b = 3.871$ Å, $c = 27.23$ Å) from Karpinski et al. [168].

density waves continue to exist at high pressures, but correlation lengths are much shorter and are therefore unable to effectively scatter the charge carriers, as suggested by NMR experiments. The later group has argued that a destruction of the charge density waves implies that the majority of the rise in $T_c$ below 2 GPa would be due to the suppression of the CDW phase, whereas their continued existence at high pressure would suggest that *P* induced doping is responsible for the rise of $T_c$.

There is evidence of significant oxygen relaxation effects from the weakly bonded $CuO_2$ chains present in Y-123. Sadewasser et al. [130,172] reported that the $T_c$ versus pressure curve is dependent not only on the oxygen content and the pressure, but also on the temperature at which the pressure was changed, and how long the sample was left to relax after any change in *P-T* conditions. Little to no relaxation effect has been reported for Y-124, with Veal and Paulikas [173] suggesting that this difference is due to the doubling of the length of the chains in the unit cell of Y-124. Almasan et al. [136] observed that this allows for the majority of the chain Cu to have a closer to optimal valency.

### *4.1. Structural studies of YBCO*

The oxygen relaxation effects reported in Y-123 discussed above greatly complicate the interpretation of compression experiments. Sadewasser et al. [172] and Calamiotou et al. [174] have demonstrated that large hysteresis effects are present in Y-123, with

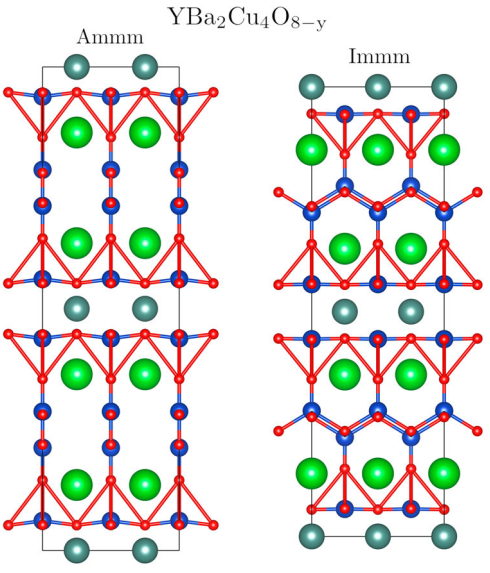


**Figure 10.** Unit cells of the ambient pressure $YBa_2Cu_4O_{8-y}$ (Y-124) structure (*Ammm*) and high pressure structure (*Immm*) projected onto the ac plane. The chains begin to cant under pressure and eventually collapse to form a three dimensional $CuO_2$ network near 11 GPa, greatly suppressing superconductivity. Oxygen tetrahedra drawn to emphasize formation of a 3D Cu-O network. Unit cell dimensions and atomic positions from Nakayama et al. [177].

different *P-T* paths resulting in different, and occasionally contradictory, results. Experiments show structural phase transitions occurring anywhere from 1.1 GPa [175,176] to 3.7 GPa [174]. It is debated if these transitions are orthorhombic to tetragonal transitions as proposed by Akhtar et al. [175], isostructural transitions to a collapsed orthorhombic phase observed by Fietz et al. [15], or to a disordered state as observed by Calamitou et al. [174]. The data suggest that the temperature at which the pressure is changed (and vice versa) significantly alter the properties observed in Y-123 under compression.

Unlike Y-123, Y-124 is much less prone to hysteresis effects. The phases observed in Y-124 are mostly independent of the *P-T* path taken by the sample. Calamiotu et al. [174] observed Y-124 to undergo a structural phase transition near 11 GPa, from the orthorhombic *Ammm* structure to a higher pressure orthorhombic *Immm* phase. In high pressure samples a small amount of the low pressure phase was observed to remain [177–179], Nakayama et al. [177] estimated that 8.7% of the sample remained in the *Ammm* phase. Nakayama et al. [177] also determined that the *Immm* high pressure phase still contains the $CuO_2$ planes common to all HTS cuprates. In the high pressure phase the chains severely tilt and collapse to form a three-dimensional Cu-O network (Figure 10). Nakayama et al. [177] found $T_c$ to decrease in the high pressure phase, coinciding with the collapse of the chains. Transport data by Van Eenige et al. [31] and Scholtz et al. [33] exhibit a kink in the $T_c$ versus pressure relation at the same conditions ($P \sim 11$ GPa), albeit with a much less drastic change than reported by Nakayama et al. [177]. This structural transition was shown to be reversible upon release of pressure by Souliou et al. [11], indicating that the chains are not irreversibly destroyed and tend to reform upon decompression.

### 4.2. $T_c$ under pressure in YBCO

At pressures below the observed structural transitions in Y-123 [44,136,180] and Y-124 [181], the critical temperature versus pressure curves appear to track the effect of doping on $T_c$. Pressure induced doping is believed to be the most significant contribution to the pressure dependence of the critical temperature up to ~20 GPa [135–137]. The parabolic trajectory of $T_c$ continues up to a maximum critical temperature of 108 K in Y-124 at 12 GPa [31,130]. With further increase in pressure, $T_c$ then decreases forming an inverted dome (Figure 11). These observations led Chen et al. [181] to cast the pressure dependence of $T_c$ in terms of two variables, the charge carrier density in the $CuO_2$ planes ($n_H$) and the effective pairing potential ($V_{eff}$),

$$T_c(P) = T_c[n_H(P), V_{eff}(P)]. \tag{4}$$

The authors then used the measured $T_c(P)$ and $dT_c/dP$ values [136] as inputs to an experimentally motivated *d*-wave gap (Equation 2) additional constraints were provided by a hole concentration constraint

$$n_H = \frac{1}{2} - \frac{1}{2N}\sum_k \tanh\left(\frac{\epsilon_k - \mu}{2T_c}\right), \tag{5}$$

and an experimentally measured dispersion relation

$$\epsilon_k = 0.16625\cos(k_x)\cos(k_y) + 0.046\big(\cos(2k_x) + \cos(2k_y)\big), \tag{6}$$

with a *d*-wave gap determined for cuprates in general via ARPES [150,182,183]. (for discussions of the YBCO gap see Lu et al. [184] and Damascelli et al. [185] for additional discussion of the gap in general). Chen et al. [181] argued that irrespective of the pairing

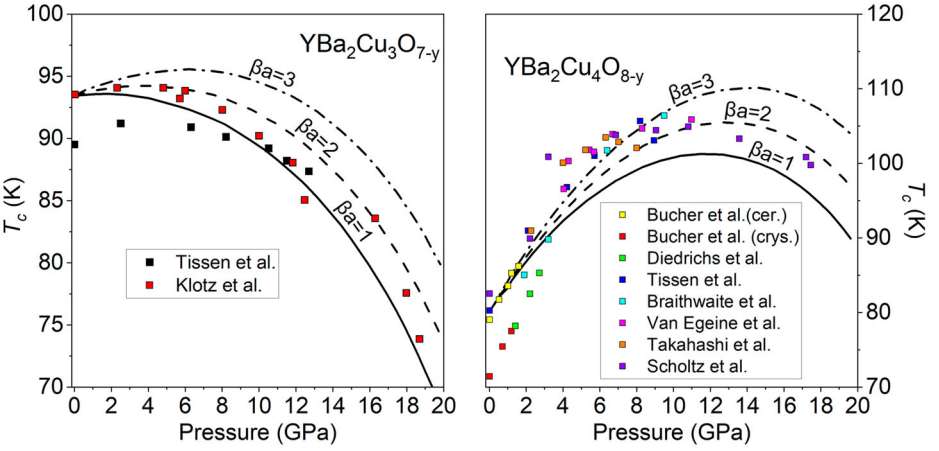


**Figure 11.** Left: Evolution of $T_c$ with pressure for optimally doped Y-123. Data for Y-123 from Tissen et al. [25] and Klotz et al. [26] Right: Evolution of $T_c$ with pressure for UD Y-124 including three calculated curves utilizing different coupling strengths ($\beta a$ = 1,2,3) calculated by Chen et al. [181] using the methods described in the text. Data from Bucher et al. [27] Diedrichs et al. [28] Tissen et al. [29] Braithwaite et al. [30] Van Eenige et al. [31] Takahashi et al. and [32] Scholtz et al. [33] Figures adapted from Chen et al. [181].

mechanism, the effective attractive potential varies with the $a$ lattice parameter as $V_{eff} \sim {}^{1}/_{a}\, e^{-\beta a}$, with $\beta > 0$ being a material dependent quantity. Solutions to the gap equation with these constraints were then calculated. The pressure dependence of the critical temperature for various values of $\beta a$ along with experimentally determined $T_c$ versus pressure data are presented in Figure 11. The calculated curves show a roughly parabolic behavior and are in agreement with experimentally measured values of $T_c$. The above observations led to the proposal that pressure alters the oxygen ordering within the $CuO_2$ planes and chains of YBCO, and therefore $T_c$, in a manner analogous to oxygen doping [172,186]. According to this picture charge carriers originate in the chains and are then transferred to the $CuO_2$ planes as they deform under pressure [110,187]. Pressure induced charge transfer increases and then suppresses $T_c$. In Y-124 this continues up to a structural phase transition at 11 GPa, where the chains buckle and superconductivity is suppressed.

Neumeier et al. [135,188] reported that in Pr doped Y-123 [$(Y_{1-x}Pr_x)Ba_2Cu_3O_{7-\delta}$], upon increasing the Pr concentration the value of $dT_c/dP$ upon initial pressurization increases, maximizes at $x = 0.3$ , and then becomes negative. This behavior is in contrast to that of pure YBCO, which retains a positive $dT_c/dP$ upon initial compression for all doping levels. Maple et al. [189] were able to describe this behavior in a phenomenological model by assuming the pressure effect on $T_c$ to have two contributions: the hybridization of the 4f electrons with the valence band of the $CuO_2$ planes, and the scattering of superconducting electrons by the Pr magnetic moments. The model assumes a constant oxygen doping, consistent with the notion that the suppression of superconductivity in this system is primarily due to effects of the Pr dopants.

### 4.3. Raman spectroscopy of YBCO

As an optical technique, micro-Raman spectroscopy is well suited to high pressure measurements using DACs. The technique has been used for studies of HTS cuprates, in particular for measurements of vibrational spectra, including detailed analyses of vibrational line shapes, electronic scattering signal, and attempts to directly measure the superconducting gap. The results provide important constraints on physical properties and, in principle, aid in developing a theory of the superconducting mechanism [190,191]. Moreover, the initial phase characterization of YBCO [192] was greatly aided by advances in micro-Raman spectroscopy, a technique developed for the measurement of Raman spectra at high pressure. Ambient pressure Raman measurements of YBCO show changes in spectra below $T_c$, with the electronic scattering signal being suppressed below 150 $cm^{-1}$ and spectral weight shifting to a broad feature between 350 $cm^{-1}$ and 450 $cm^{-1}$ . These changes have been interpreted by Monien et al. [193] as arising from the opening of a superconducting gap. The depletion of electrons around the Fermi level would then suppress any scattering from modes with a frequency below the gap energy, $\omega < 2\Delta$. A smaller depletion is observed below $T^*$ and has been interpreted as signature of the pseudogap by Nemetschek et al. [194]. Despite the depletion in spectral weight in the spectrum, scattering from the electronic excitations is not completely suppressed; these results have been interpreted as further evidence for gap anisotropy, *i.e.* a *d*-wave order parameter [195,196].

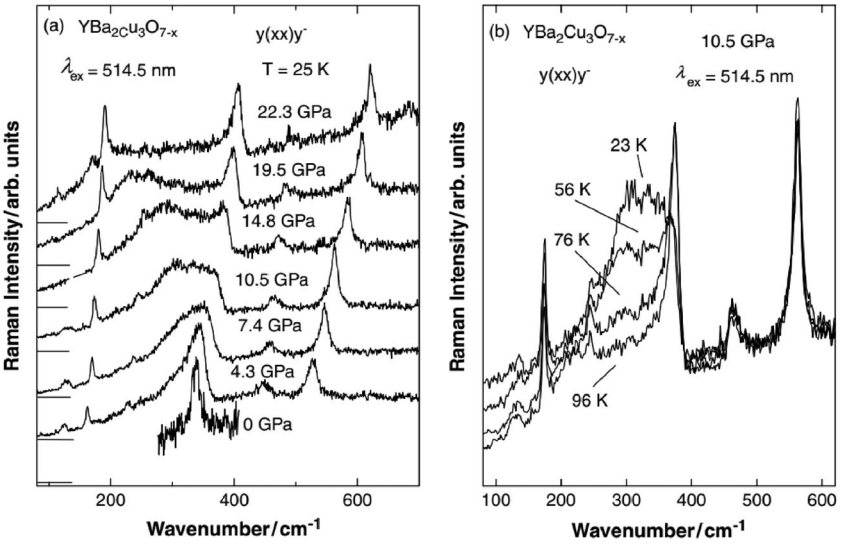


**Figure 12.** Left: Raman spectra of nearly optimally doped $YBa_2Cu_3O_{7-x}$ (Y-123) at various pressures in the superconducting phase measured at $T = 25$ K [199]. A large broadening of the electronic background is present around 300 $cm^{-1}$ which was attributed to an enhancement of electron-phonon coupling. Right: Y-123 at 10.5 GPa and various temperatures above and below $T_c$. With increasing pressure the scattering at low wave numbers decreases and spectral weight shifts to a broad feature around 300 $cm^{-1}$, consistent with the opening of the superconducting gap [197]. Spectral weight is never fully suppressed within the spectral gap region indicating the *d*-wave character of the gap, *i.e*. points exist on the Fermi surface where the gap is zero. Despite the sample being nearly optimally doped, electronic Raman features appear to match those of overdoped samples while under pressure. Figure from Goncharov and Struzhkin [197] reproduced with permission.

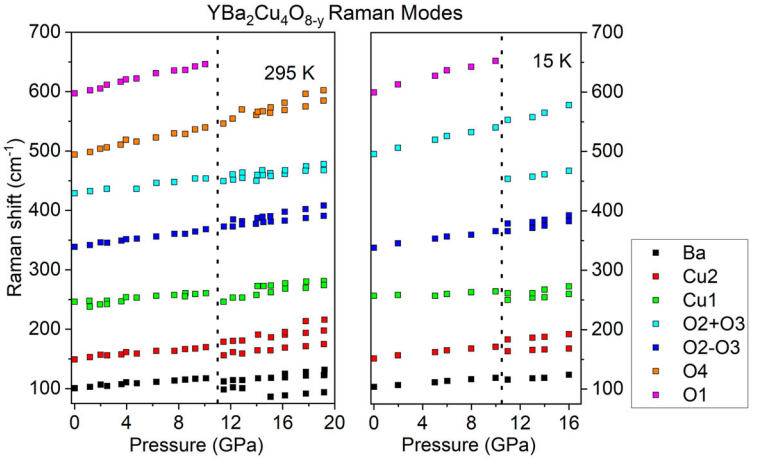


**Figure 13.** *P* dependence of Raman mode frequencies of $YBa_2Cu_4O_{8-y}$ (Y-124) in the normal (left) and superconduting state (right). The intensity of the O1 and Cu1 dominant modes are greatly reduced at pressures above the structural phase transition (vertical dashed line) that is associated with the destruction of the $CuO_2$ chains and formation of the 3D $CuO_2$ network. At low temperatures an additional peak associated with the formation of the 3D $CuO_2$ network formed from the collapsed chains appears at 450 $cm^{-1}$. Peaks split at pressures above the transition. Figure adapted from Souliou et al. [11].

Similar phenomena are apparent in high pressure Raman spectra reported for Y-123 [174,197–199] and Y-124 [11,174,200]. These Raman spectra all show a shift in the 500 $cm^{-1}$ peak that has been correlated to the oxygen doping at ambient pressure. Goncharov et al. [197] used the behavior of this peak to estimate the hole doping ($n_H$) under pressure. Above 7 GPa broad features emerge between 200 $cm^{-1}$ to 400 $cm^{-1}$, which appear similar to those observed in overdoped samples at ambient pressure Figure 12 [197]. The reported temperature dependence of the spectra is presented in Figure 12. The results indicate that nearly optimally doped Y-123 behaves like an overdoped cuprate under pressure; *i.e.* $T_c$ is slightly lower than the critical temperature at optimal doping and Raman shifts are consistent with those of overdoped Y-123 [197,201].

The Raman peaks observed in the normal and superconducting states of Y-124 above 11.2 GPa indicate a hardening and splitting of the modes associated with the chain copper and oxygen sites [11] Figure 13. The effects are interpreted as arising from collapse of the chains to form the three dimensional Cu-O network of the *Immm* structure as described in the previous section [11,200,202]. The other peaks in the Raman spectrum of the high pressure phase of Y-124 are broadly similar to those of the low pressure spectrum, which is consistent with the observation that the only major change in the Y-124 structure is the collapse of the chains to form the 3D Cu-O network.

### *4.4. Charge density waves under pressure in YBCO*

Charge density waves (CDW) have been measured in YBCO at ambient pressure using nuclear magnetic resonance (NMR) [203] and x-ray diffraction [204,205]. The CDW

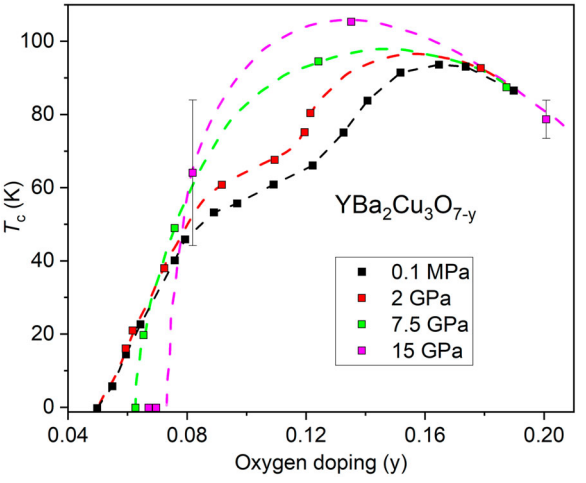


**Figure 14.** Effect of pressure on the doping-temperature phase diagram of $YBa_2Cu_3O_{7-y}$ (Y-123). The suppression in the superconducting dome around $y \sim 0.12$ has been attributed to the competition between the superconducting phase and stripe formation [206]. Measurements of the dome at 2 GPa (red), 7.5 GPa (green), and 15 GPa (pink) are presented. Lines inserted as a guide to the eye. Error bars inserted when reported. Figure adapted from Cyr-Choiniere et al. [142].

competes directly with superconductivity around an oxygen doping of $x \sim 0.13$. The phase competition is demonstrated by a noticeable dip in the $T_c$ versus doping curve (Figure 14). Inelastic *x*-ray scattering by Souliou et al. [170] and resonant soft *x*-ray scattering by Huang et al. [169] indicate a suppression of electronic order in the Y-123 compounds under pressure. LeBoeuf et al. [206] has attributed the suppression of $T_c$ with pressure in Y-123 and Y-124 to the destruction of charge density waves and the corresponding destruction of the electron like pockets in the Fermi surface. LeBoeuf et al. [206] further argued that as the CDW appears to be completely destroyed by 1 GPa, the destruction of the CDW under pressure alters the $T_c$ versus doping relation shifting the optimal doping parameter to $n_H \sim 0.13$ at 15 GPa (Figure 14). Furthermore, the destruction of the CDW through pressure causes the superconducting dome in YBCO to approach the parabolic relation described above (Equation 1) [51].

Under pressures measured to date parameters associated with charge order, such as slow quantum oscillations (particularly in Y-123) [207] and the presence of a negative Hall number [208] are hardly changed from the ambient pressure values. These results are particularly evident in the NMR experiments reported by Vinograd et al. [171], where it appears that both long and short range CDW both exist appear to be nearly unaffected by pressures up to at least 1 GPa. As the authors state, it is not clear if these discrepancies are due to experimental constraints or a more complicated interplay between the CDW and superconductivity under pressure than previously assumed [209].

### *4.5. Nuclear magnetic resonance of YBCO*

Nuclear magnetic resonance (NMR) probes the electronic environment around specific NMR active nuclei in a material. Due to the relatively large sample size needed for meaningful NMR data, NMR measurements have not yet been reported above several GPa [210,211]. Meissner et al. [212] and Zheng et al. [213] reported NMR measurements of Y-123 under pressure, and both found that on compression, the samples began to behave like a Fermi liquid. Up to ~6 GPa, all NMR peaks shift to higher frequencies, with the most dramatic shift present in peaks associated with the planar oxygen. The shift indicates an increase in the spin susceptibility of the superconducting $CuO_2$ planes with pressure.

The collapse in the Knight shift at temperatures above $T_c$ at ambient pressure has been interpreted as the opening of the pseudogap [214]. The collapse is observed to lessen in magnitude as pressure is increased and the sample effectively becomes more overdoped [171,212,215] Figure 15. Similar effects have been observed on increasing oxygen doping of Y-123 at ambient pressure by Alloul et al. [216]. These measurements are consistent with the hypothesis that pressure increases the effective hole doping within the $CuO_2$ planes, *i.e*. both changes result in the electronic properties of cuprates approaching that of a Fermi liquid.

Recently, Jurkutat et al. [217] reported the use of NMR to probe $n_H$ within the $CuO_2$ planes in Y-123 as a function of pressure, specifically by tracking the quadrupole splitting of the Cu and O frequencies and relating the magnitude of the splitting to the hole concentrations within the planes [171,209]. Unlike many other techniques for directly

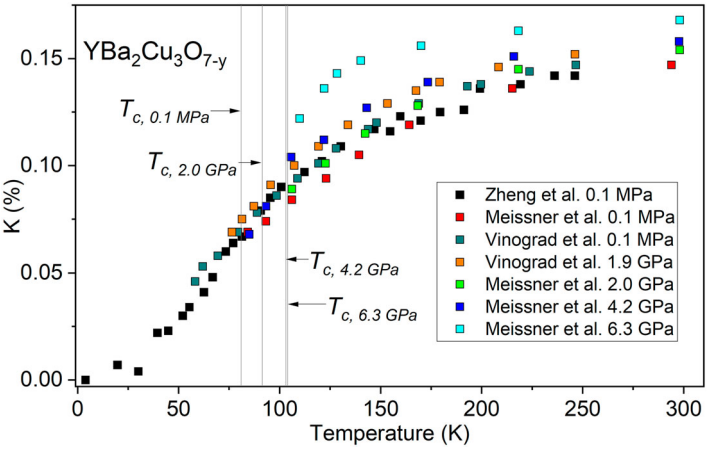


**Figure 15.** Knight shift of $^{17}O$ from the planar oxygens in UD $YBa_2Cu_3O_{7-y}$ (Y-123). At ambient pressure there is a collapse in the Knight shift at temperatures greater than $T_c$ indicating a removal of conduction electrons attributed to the pseudogap. Measured $T_c$ values indicated by vertical lines. As pressure is increased the decrease is lessened, indicating the magnitude of the pseudogap is decreasing as the behavior of the sample approaches that of a Fermi liquid. Data from Meissner et al. [212], Zheng et al. [215] and Vinograd et al. [171].

determining the hole concentration, NMR is not directly sensitive to the stoichiometric doping parameter (y) and is able to determine the relative hole contribution from the Cu $d_{x^2-y^2}$ orbitals ($n_{H,Cu}$) and the O $p_{x,y}$ orbitals ($n_{H,O}$). It was empirically determined that the relative hole contents are related through the equation

$$1 + y = n_{H,Cu} + 2n_{H,O}, \tag{7}$$

with $y$ representing the usual stoichiometric oxygen doping parameter. The ratio of $n_{H,Cu}$ to $n_{H,O}$ is then a material dependent parameter which is roughly constant at ambient pressure, irrespective of chemical doping [218].

Under pressure $n_{H,O}/n_{H,Cu}$ is reported to no longer remain constant, so equation 7 must be modified as $n_H$ is no longer directly proportional to $1-y$. Replacing $y$ with the hole-doping concentration as measured by NMR generalizes the relation to samples under pressure [217]. Pressure is observed to increase the overall value of $n_H$, but with holes being preferentially injected into (electrons being removed from) the oxygen $p$ orbitals. These observations imply that the pressure induced doping contribution to the trajectory of $T_c$ under pressure is directly related to the magnitude of $n_H$, corroborating data from of other probes. The change in the ratio of $n_{H,O}$ to $n_{H,Cu}$ would then be a material dependent quantity responsible for differences in $T_c$ between cuprates.

### *4.6. Pseudogap under pressure in YBCO*

Relatively few high pressure studies of YBCO in regions of the phase diagram that exhibit the pseudogap have been reported (For a general review see Vovk and Solovjov [219]). Similar to observations for LBCO/LSCO, the value of $T^*$ appears to be

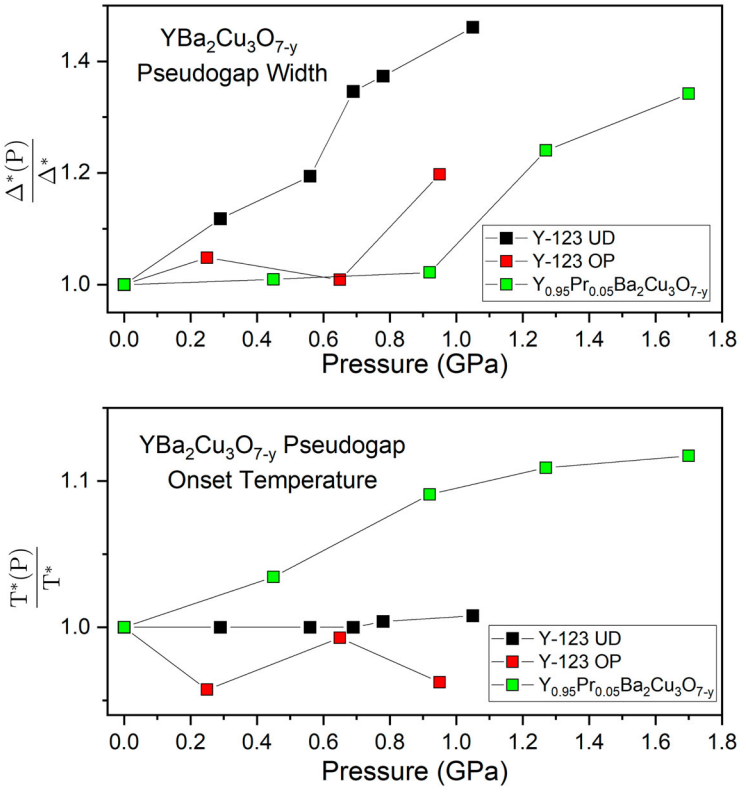


**Figure 16.** Top: Pressure dependence of normalized $\Delta^*$ (pseudogap width) versus pressure for underdoped and optimally doped $YBa_2Cu_3O_{7-y}$ and optimally doped $Y_{0.95}Pr_{0.05}Ba_2Cu_3O_{7-y}$. In all samples the maximum gap width is reported to significantly increase under pressure, with the most drastic broadening occuring in the underdoped samples (black) and in samples doped with Pr doped samples (green). $\Delta^*$ was determined using the methods described by Solovjov and Dmitrev [231]. Bottom: Pressure dependence of $T^*$ for the same samples. $T^*$ in pure YBCO $T^*$ shows little to no pressure dependence, whereas Pr doped YBCO shows an increase in $T^*$ from 110 K at ambient pressure to 122.9 K at 1.7 GPa. Data from Solovjov et al. [220,227,232].

relatively insensitive to pressure [220,221]. As the transition from the strange metal state to the pseudogap appears to be a continuous crossover, there is some ambiguity in determining the exact value of $T^*$. Values of $T^*$ range from 135 K to 141 K for all pressures below 1.75 GPa. These observations do not definitively prove that there is no pressure effect on $T^*$, but only that any effect is of a magnitude to the experimental resolution. Additionally, very few data points of $T^*$ above 1.7 GPa have been reported.

Numerous reported experiments indicate the replacement of Y in Y-123 with other rare earth elements cause little change in the resistive properties of these compounds [222], other than replacement of Y with Pr [223–226]. This observed 'praseodymium anomaly' is associated with a large increase in electrical resistivity and a decrease in $T_c$. It has been proposed that the anomaly is related to interactions between the $CuO_2$ planes and the 4f electrons found in Pr [188]. In addition to these peculiarities found in Pr-doped YBCO, $Y_{0.95}Pr_{0.05}Ba_2Cu_3O_{7-\delta}$ is reported to exhibit a positive

$dT^*/dP$ which appears to track the increase in $T_c$ reported by Solovjov et al. [227]. Neumeier et al. [188] note that the peculiarities found in Pr-doped YBCO may be related to the comparatively large magnetic moment of the Pr ($\sim 3.58\ \mu_B$) [228] which is significantly larger than other rare earth elements, possibly providing valuable data on the impact of magnetism on the pseudogap and HTS in general [229,230]. Unlike $T^*$, the pseudogap width $\Delta^*$ is observed to vary with pressure in YBCO, with the gap width increasing up to 46%. All $T^*$ and $\Delta^*$ data under pressure is presented in Figure 16. Absent a complete theory, most of these analyses are phenomenological in nature.

### 4.7. Uniaxial compression of YBCO

In addition to hydrostatic (or quasi-hydrostatic) compression, YBCO has been studied under uniaxial stress. Both $T_c$ and $dT_c/dP_i$ (i=$a$, $b$, $c$) vary considerably depending on the axis of compression and the initial doping of the sample. Kraut et al. [233] have shown it is possible to model $T_c$ as the sum of uniaxial compression effects with $dT_c/dP$ written as

$$\frac{dT_c}{dP} = \sum_i \frac{dT_c}{dP_i} = \frac{dT_c}{dP_a} + \frac{dT_c}{dP_b} + \frac{dT_c}{dP_c}, \tag{8}$$

where $P_i$ is the stress along the $a$, $b$, and $c$ crystallographic axis.

In Y-123 it appears that uniaxial stress along the $a$ or $b$ axes produces effects on $T_c$ unrelated to doping. Upon initial compression, $dT_c/dP_a$ and $dT_c/dP_b$ differ in sign and nearly cancel each other under hydrostatic pressure [233,234]. For all dopings the $a$, $b$, and $c$ derivatives appear to sum together to give the observed hydrostatic value. An initial large value of the pressure derivative around a doping level of x = 6.73 corresponds to a structural anomaly involving a decrease in orthorhombicity (similar to the 1/8 anomaly in LBCO) and a change in sign of $dT_c/dP_a$ [233] Figure 17. The considerable differences in the effects of uniaxial stress bring into question many of the contradictory results from high pressure experiments on YBCO, as many were conducted under non-hydrostatic stress conditions [235–237].

In addition to uniaxial stress effects on transport properties, there is a noticeable effect on the charge density waves in Y-123. [240,241]. A slight compression in the $a$($b$) axis enhances the correlation along the $b$($a$) charge density waves measured by resonant inelastic X-ray scattering (RIXS). Compression along the $a$ direction leads to a new set of Bragg reflections observed in RIXS which are consistent with a new long range 3D CDW order that competes directly with superconductivity [240]. The 3D CDW that emerges under uniaxial stress is distinct from the 2D CDW observed at ambient pressure in that it is coherent over a much longer range. The 3D CDW is completely destroyed when the material enters the superconducting state, unlike the 2D CDW, which can persist in vortices pinned to defects. A long range 3D CDW was also observed in YBCO when exposed to high magnetic fields (~10 T) [242–244].

Mito et al. [12,245,246] reported that uniaxial strain destroys superconductivity in single crystal Y-124. In optimally doped Y-124 the Meissner signal was reported to

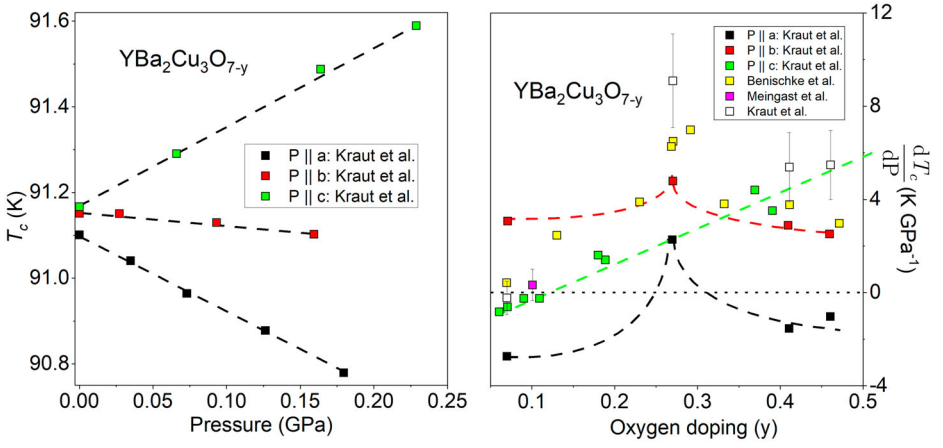


**Figure 17.** Left: Uniaxial stress dependence of $T_c$ in nearly optimally doped Y-123 for stress applied along the a, b, and c directions. up to 0.3 GPa. Data from Kraut et al. [233]. Right: Uniaxial pressure coefficient upon initial pressurization, $dT_c/dP_i$ ($i = a,b,c$), versus oxygen doping parameter up to y = 0.5. $dT_c/dP_b$ is always initially positive with the largest values for those samples near y = 0.25. Hydrostatic pressure dependence from Kraut et al. [233], Meingast et al. [238] (both calculated from thermal expansivity measurements), and Benischke et al. [239] (calculated from transport measurements) are also plotted.

disappear at 10 GPa when stress was applied along the *c* axis [246]. Mito et al. [247] also reported that doping of Ca into Y-124 allowed the Meissner signal to persist up to a uniaxial stress of 15 GPa along the *c* axis [248,249]. Zhang et al. [164,250] reported epitaxial strain induced by *CuO* intergrowths in a $La_{2/3}Ca_{1/3}MnO_3/YBa_2Cu_3O_{7-\delta}$ heterostructure to decrease $T_c$. Films grown a using pulsed laser deposition process known to induce such intergrowths [251] were reported to exhibit $T_c$ values of 60 K as opposed to films with no measured intergrowths. STEM measurements indicated that a doubling up of the CuO chains were present in the strained samples, driving the system to form a significant amount of Y-247 that suppressed superconductivity [251].

## 5. $Bi_2Sr_2Ca_{n-1}Cu_nO_{2n+4+\delta}$, $Tl_mSr_2Ca_{n-1}Cu_nO_{2n+m+\delta}$, and $HgBa_2Ca_{n-1}Cu_nO_{2n+2+\delta}$ under pressure

The majority of other commonly studied cuprate superconductors are structurally similar to each other and consist of alternating layers of flat $CuO_2$ planes and metallic charge reservoir layers as discussed above. These materials include bismuth-based $Bi_2Sr_2Ca_{n-1}Cu_nO_{2n+4+\delta}$ (BSCCO), thallium-based $Tl_mSr_2Ca_{n-1}Cu_nO_{2n+m+\delta}$ (TBCCO), and mercury-based $HgBa_2Ca_{n-1}Cu_nO_{2n+2+\delta}$ (HgBCCO). All families contain compounds with one to five adjacent layers of $CuO_2$ planes in a unit cell. These cuprates are all orthorhombic, due to a Jahn-Teller distortion along the *b* axis. The distortion is small, below the resolution of many probes. As a result these cuprates are often referred to as pseudo-tetragonal despite being orthorhombic; the higher symmetry is used to describe their structures.

As found for other cuprates, pressure can produce higher critical temperatures for near optimally doped samples. High pressure measurements by Montiverde et al. [19] and

Yamamoto et al. [41] show that at 30 GPa fluoridated $HgBa_2Ca_2Cu_3O_{8+\delta}$ exhibits the onset of superconductivity at 166 K and a zero resistivity temperature of 133 K, the highest $T_c$ values observed in a cuprate to date. Gao et al. [18] observed a similar enhancement of $T_c$ from 130 K to 164 K at 31 GPa.

Two common representations have been used to describe the structure of these cuprates that depend on the reference with respect to the $CuO_2$ planes. Most experimental papers use a primitive unit cell, with boundaries along the Cu-O bonds. This representation results in $a$ and $b$ lattice parameters of $\sim$ 3.85 Å. The crystallographic cell is rotated by 45$^o$ in order to place the unit cell boundary along the Cu-Cu boundary giving a unit cell $a$ and $b$ parameter that is larger by a factor of $\sqrt{2}$ as shown in Figure 18. The $c$ parameter is extended by the same length in both representations. It is also common to assume the unit cells are tetragonal instead of orthorhombic in many calculations, as any orthorhombicity is below the resolution of many probes. In the discussion below we use the smaller unit cell unless specified otherwise.

The bismuth-bearing cuprates, have the chemical formula $Bi_2Sr_2Ca_{n-1}Cu_nO_{4+2n+\delta}$, where $\delta$ is the doping parameter and n is the number of $CuO_2$ layers in a unit cell. Setting $n$ =1–4 generates the formula for the four stable forms of BSCCO. The compounds are abbreviated using the stoichiometry of the metallic elements (Bi, Sr, Ca, and Cu) as a suffix with Bi-2201 being the single layered member ($Bi_2Sr_2Cu_1O_{6+\delta}$), Bi-2212 having two layers ($Bi_2Sr_2CaCu_2O_{8+\delta}$), and Bi-2223 having three ($Bi_2Sr_2Ca_2Cu_3O_{10+\delta}$). A four layer Bi-2234 compound is also possible, but it does not form large single phase crystals and has not been studied as extensively under pressure [252,253]. BSCCO unit cells are presented in Figure 19. TBCCO and HgBCCO are abbreviated in the same manner.

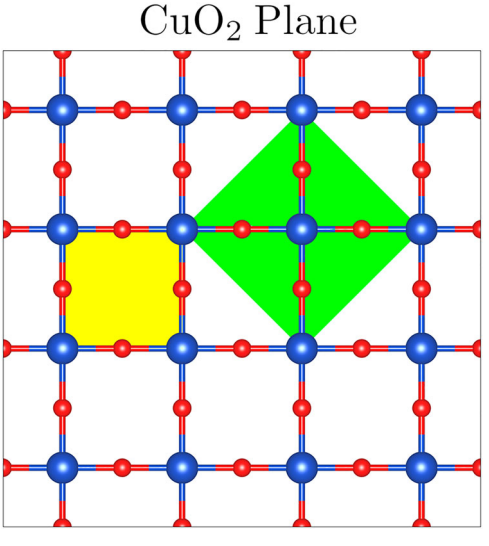


**Figure 18.** Superconducting $CuO_2$ plane common to all cuprates with the crystallographic cell (green, $a \sim$ 5.4 Å) and the smaller cell (yellow, $a \sim$ 3.8 Å) typically used for electronic structure calculations.

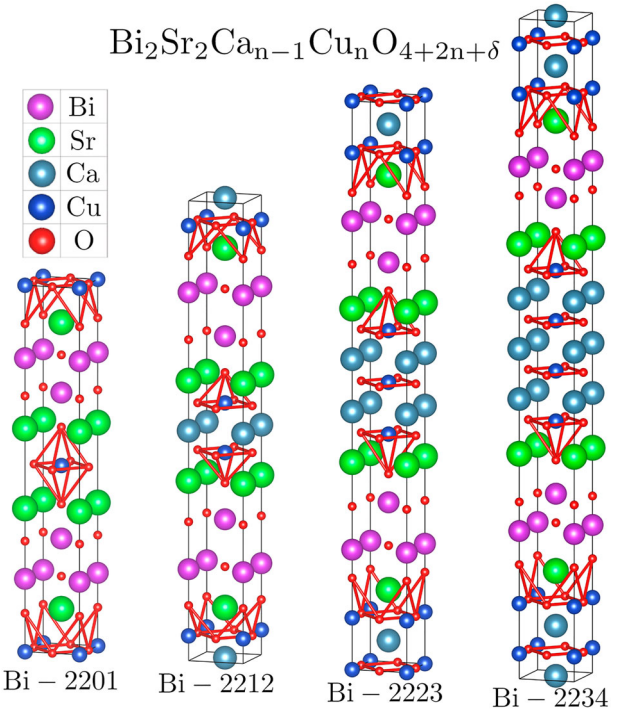


**Figure 19.** Unit cells of Bi-2201, Bi-2212, Bi-2223, and Bi-2234 presented in a tetragonal ($I4/mmm$) representation. Oxygen bonds drawn to show apical oxygen sites out of the $CuO_2$ planes. For Bi-2223 there is a single inequivalent central plane with no associated apical oxygen site. Bi-2234 contains two central planes with no associated apical oxygen. As n increases the observed orthorhombic distortion tends to decrease. Structural parameters used for Bi-2201 ($a = 3.80$Å, $c = 24.6$Å) from Matheis et al. [253], for Bi-2212 ($a = 3.80$Å, $c = 30.9$Å) and Bi-2223 ($a = 3.80$Å, $c = 38.2$Å) from Wesche et al. [254], and for Bi-2234 ($a = 3.80$Å, $c = 44.3$Å) from Hatano et al. [252].

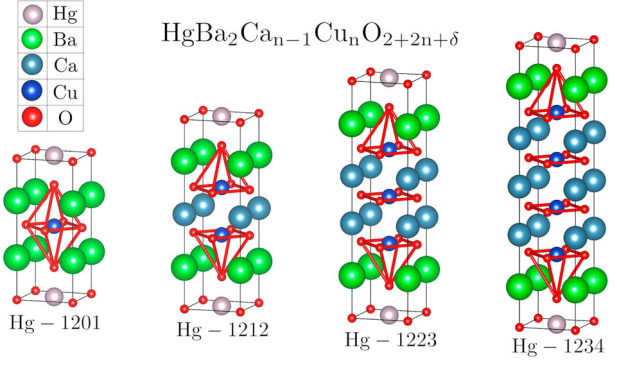


**Figure 20.** Crystal structures of $HgBa_2Ca_{n-1}Cu_nO_{2+2n+\delta}$ for $n = 1$ (Hg-1201), $n = 2$ (Hg-1212), $n = 3$ (Hg-1223), and $n = 4$ (Hg-1234) presented in a tetragonal ($P4/mmm$) representation. Data used to generate image of Hg-1201 ($a = 3.88$Å, $c = 9.50$Å) from Legros et al. [259], Hg-1212 ($a = 3.86$Å, $c = 15.8$Å) from Gatt et al. [260], Hg-1223 ($a = 3.70$Å, $c = 15.1$Å) from Hassun et al. [261], and Hg-1234 ($a = 3.85$Å, $c = 18.9$Å) from Lokshin et al. [262].

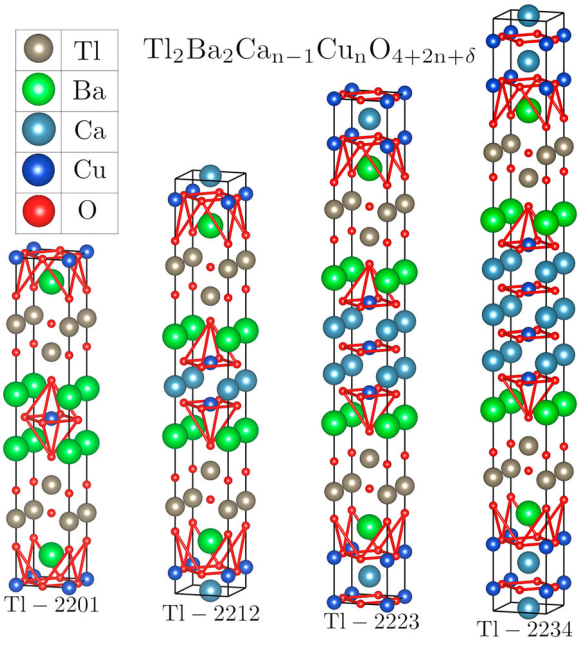


**Figure 21.** Unit cells of $Tl_2Ba_2Ca_{n-1}Cu_nO_{4+2n+\delta}$ for $n = 1$ (Tl-2201), $n = 2$ (Tl-2212), $n = 3$ (Tl-2223), and $n = 4$ (Tl-2234), presented in a tetragonal ($I4/mmm$) representation. Data used to generate image of Tl-2201 ($a = 3.88$Å, $c = 23.2$Å) from Kajitani et al. [263], Tl-2212 ($a = 3.86$Å, $c = 29.3$Å) from Subramanian et al. [264], Tl-2223 ($a = 3.84$Å, $c = 35.9$Å) from Torardi et al. [265], and Tl-2234 ($a$∼3.9Å, $c$∼42Å) from Matheis et al. [253].

Olsen et al. [255] first reported that BSCCO is structurally stable (or at least metastable on room temperature compression) up to 60 GPa. Unlike many of the other cuprates, BSCCO has no CDW phase competing with superconductivity, greatly simplifying data analysis due to the absence of competing electronic or magnetic effects. These properties, along with the wealth of information already gathered from other ambient pressure measurements of BSCCO, make it the ideal candidate to understand the effects of pressure on the superconducting properties of cuprates.

Members of the BSCCO family have an orthorhombic unit cell (*Ammm*), but due to the close *a* and *b* parameters (within 0.1 Å) all BSCCO varieties are often described using a tetragonal representation ($I4/mmm$). BSCCO also contains offset $CuO_2$ planes which result in much larger unit cells compared to many other cuprates due to the length of the *c* axis. The offset planes allow for an easy cleaving interface along the weakly bonded BiO layers resulting in clean nearly flat surfaces, making BSCCO amenable to ARPES and other surface-sensitive probes.

As discussed above, the mercury-bearing cuprates, $HgBa_2Ca_{n-1}Cu_nO_{2n+2+\delta}$, $n = 1,2,3$, possess the highest $T_c$'s at ambient conditions and under pressure [9,19,39,256]. They are typically described with a tetragonal $P4/mmm$ structure with a slight orthorhombic distortion Figure 20. HgBCCO lacks offset $CuO_2$ planes, resulting in smaller *c* parameters and fewer atoms per unit cell than BSCCO. Variable $T_c's$ have been reported for many of the mercury-cuprates in part due to a broadening of the resistivity versus temperature curve under pressure; *e.g.* in the single layer Hg-1201 the temperature at which the

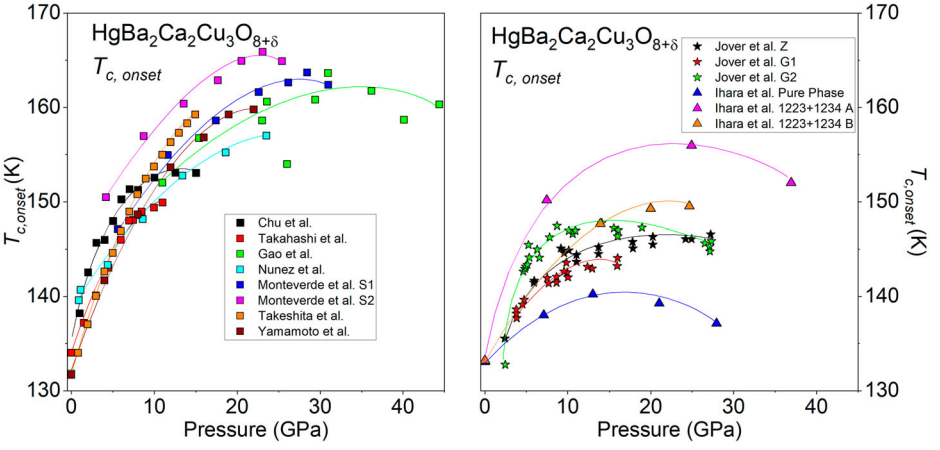


**Figure 22.** Left: Onset $T_c$ versus pressure plots for slightly underdoped $HgBa_2Ca_2Cu_3O_{8+\delta}$ (Hg-1223) versus hydrostatic pressure showing a saturation in $T_c$ at 30 GPa. Data from Chu et al. [39], Takeshita et al. [20], Gao et al. [18], Nunez et al. [40] Monteverde et al. [19], and Yamamoto et al. [41]. $T_c$ of near optimally doped single phase Hg-1223 appears to rise and then fall with pressure superficially similar to increasing $\delta$ through oxygen doping. Right: $T_c$ versus pressure for uniaxial compression of Hg-1223 (stars) from Jover et al. [42] and for different mixtures of Hg-1223 and Hg-1234 (triangles) from Ihara et al. [43]. $T_c$ in the mixed phase samples are lower than pure phase Hg-1223, presumably due to intercalation of the four layer Hg-1234. Uniaxially compressed samples also exhibit lower values of $T_c$ for all pressures. Data from the above references. Lines are guides to the eye.

resistivity begins to trend toward zero was reported to increase with pressure but the zero resistivity temperature decreases. [41,42,257]. The broadening of the critical temperature is especially prominent in Hg-1212; Yamamoto et al. [41] report a difference of $T_{c,onset} - T_{c,zero} \sim 25\ K$ at ambient pressure which increases to $T_{c,onset} - T_{c,zero} \sim 45\ K$ near 18 GPa. The HgBCCO cuprates are prone to oxygen relaxation effects similar to Y-123, further complicating their study under pressure [258].

Finally, the thallium-bearing cuprates, $Tl_mBa_2Ca_{n-1}Cu_nO_{2n+m+2}$ behave similarly to the bismuth-bearing family but with slightly higher $T_c$'s. TBCCO exist in some compounds that are isostructural to BSCCO (Figure 21) and some isostructural to HgBCCO, with Tl replacing the Bi or the Hg. Like the other cuprate superconductors, they can be described using a tetragonal structure exhibiting a small orthorhombic distortion. The Tl based family has been studied relatively little under pressure and, similar to Y-123, are prone to large oxygen relaxation effects upon changing pressure [34].

### *5.1. Transport measurements on the Bi, Tl, and Hg based Cuprates*

The Bi, Tl, and Hg based cuprates have been characterized by electrical resistivity and magneto-transport measurements at ambient [266,267] and high pressures [14,35,131,268]. Like the simpler cuprates, the shift in $T_c$ has been associated with structural and doping effects as well as a suppression of competing phases [139,142]. Below $\sim 40\ GPa$, $T_c$ appears to track the parabola-like doping versus $T_c$ curve with a small offset due to structural effects [142]. As for LBCO/LSCO and YBCO the largest contribution

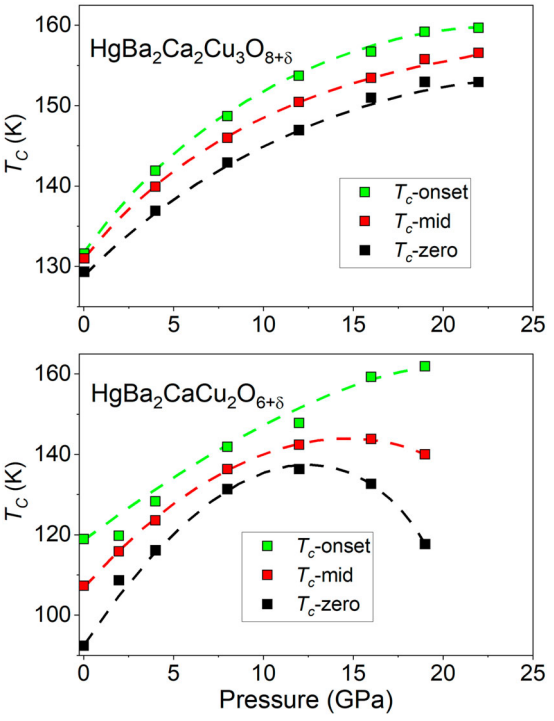


**Figure 23.** Top: Pressure dependence of $T_{c,onset}$, $T_{c,zero}$ and the midpoint of the two values for slightly underdoped $HgBa_2Ca_2Cu_3O_{8+\delta}$ (Hg-1223) as determined by susceptibility measurements. Both the onset and zero resistivity value rise upon compression up to the limit of the experiment, with both values exhibiting the same trend under pressure. Bottom: $T_{c,onset}$, $T_{c,zero}$ and the midpoint of the two values for slightly underdoped $HgBa_2CaCu_2O_{6+\delta}$ (Hg-1212). As opposed to what is observed in Hg-1223, $T_{c,onset}$ and $T_{c,zero}$ exhibit different trends under pressure in Hg-1212. $T_{c,zero}$ is observed to decrease above 11 GPa in Hg-1212 $T_{c,onset}$ appears to grow to the limit of the experiment. Lines are guides to the eye. Figures adapted from Yamamoto et al. [41].

to the trajectory of $T_c$ under pressure is attributed to pressure induced doping for a wide range of pressures.

Reported pressure dependencies of $T_c$ for the Hg bearing cuprates are presented in Figure 22. The data show the current highest $T_c$ in a cuprate HTS as reported by Monteverde et al. [19], $T_c$ onset at 166 K in fluorinated Hg-1223 at 23 GPa. There is some ambiguity in the interpretation of transport data for HgBCCO, as many papers report $T_{c,onset}$ (the temperature where the resistivity versus temperature relation deviates from linearity) as the transition temperature and others report the zero resistivity temperature. The ambiguity complicates interpretation, as many of the Hg compounds show a broadening of the transition under pressure. In Hg-1223 $T_{c,onset}$ appears to track $T_{c,zero}$ reasonably well, but in Hg-1212 the two temperature scales behave differently. Yamamoto et al. [41] reported a large difference of almost 45 K between the onset of superconductivity and the zero temperature resistivity in Hg-1212. A comparison between the behavior of $T_c$ under pressure for Hg-1223 and Hg-1212 is presented in Figure 23. In Hg-1212 $T_{c,onset}$ appears to rise monotonically with pressure, even though $T_{c,zero}$ drops.

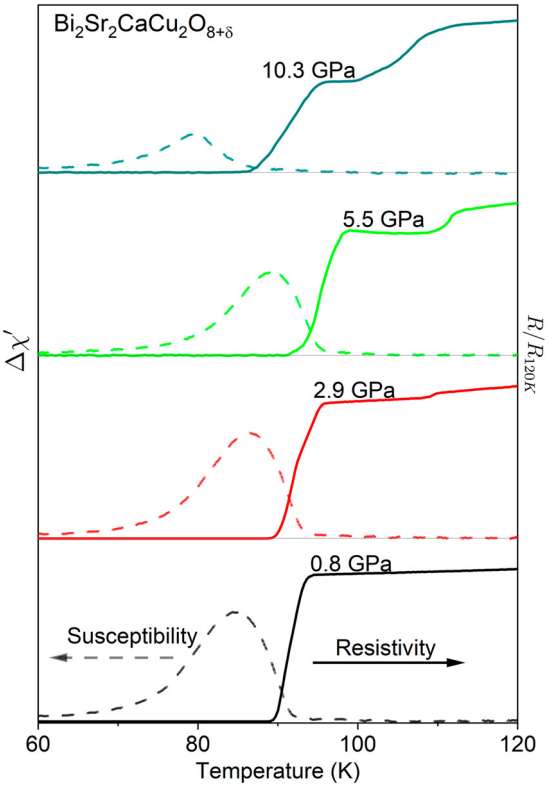


**Figure 24.** Normalized magnetic susceptibility ($\Delta\chi'$, dashed) and normalized in-plane (parallel to the $CuO_2$ planes) resistance data (solid) for optimally doped Bi-2212 at several different pressures from Guo et al. [280]. A noticeable step-like behavior emerges in the in-plane resistivity as pressure is increased. The expected Meissner effect was observed in the susceptibility for the lower superconducting $T_c$, but no signal in the susceptibility occurs at higher temperatures. Guo et al. [280] interpreted these observations as arising from as an upper two-dimensional superconducting $T_c$ that emerges at higher pressures and a shifting of the lower three-dimensional $T_c$ observed at ambient pressure.

At low pressures the non-doping related effects of pressure on $T_c$ are typically large, causing $T_c$ to initially rise irrespective of oxygen doping as observed in Bi-2212 [268], Tl-1212 [269], Hg-1212 [270], and Hg-1223 [270]. Sieburger et al. [271] found that upon initial pressurization of Bi-2212 the intrinsic term dominates and almost no pressure-induced doping effects are present for a range of oxygen dopings up to 1.5 GPa. For cuprates in the same family the initial $dT_c/dP$ appears to be identical, with Klehe et al. [270] reporting a value of $dT_c/dP = 1.75 \pm 0.03\ K/GPa$ for HgBCCO. As stated by Klehe et al. [270,272] a more relevant physical parameter for this low pressure regime, where doping effects are small, would be the relative volume derivative $d\,ln(T_c)/d\,ln(V)$ as it accounts for the different compressibilities between cuprate families. For low pressures the value of the derivative appears to be universal; $d\,ln(T_c)/d\,ln(V) \sim -1.2$ was measured in Hg-1201, Hg-1212, Hg 1223 by Klehe et al. [273], in Y-123 by Neumier et al. [135] and Jorgensen et al. [187] and in Tl-1212 and Bi-2212 by Schilling et al. [274]. The apparent universality of the relative volume derivative indicates that the intrinsic effects that

cause $T_c$ to initially rise on compression are common to cuprates in general and is most likely related to the compression of the $CuO_2$ planes common to all cuprate superconductors.

As observed in most cuprates at higher pressures ( *e.g.* $P > 1.5$ GPa in HgBCCO), the doping effectdominates and $T_c$ rises and then drops following the $T_c$ – doping relation [275]. Chu et al. [39] argue that this observation implies that the highest values of $T_c$ should be attained in slightly underdoped samples as the intrinsic and doping terms are both initially positive. So far, this hypothesis appears to hold experimentally [19].

A major complication in data interpretation is the influence of pressure induced relaxation effects on $T_c$. The properties of both the TBCCO family [269] and the HgBCCO family [257] demonstrate a level of hysteresis upon pressurization. The value of $T_c$ under pressure depends on the detailed temperature and pressure history along with doping for the materials. In general, the hysteresis adds an additional time contribution to the pressure dependence of $T_c$ that depends on how long after a change in pressure $T_c$ is measured. Sadewasser et al. [257] modeled the hysteresis effect as

$$T_c(t)|_{relax} = T_c(\infty) - \left[T_c(\infty) - T_c(0)\right] \exp\left\{-\left(\frac{t}{\tau}\right)^{\alpha}\right\}, \tag{9}$$

where $\alpha$ is a phenomenological fitting parameter [130].

The value of $\tau$ was fit to $T_c$ relaxation curves and used to estimate the time scale of the relaxation effect. The application of pressure on overdoped Hg-1201 drastically increases $\tau$ from an ambient pressure value of $3.4 \pm 0.6$ hours to $17.5 \pm 5.4$ hours at 0.15 GPa. Looney et al. [269] and Sieburger et al. [271] also observed similar increases in relaxation times in the Tl-based cuprates under pressure. Further complications arise when annealing history is taken into account. Sieburger et al. [271] reported that these lengthy relaxation times were not evident the BSCCO samples that they studied. The number of $CuO_2$ layers is also shown to have a large effect on $T_c$ and its pressure dependence [276,277]. As the inner layers of cuprates with $n>3$ are protected from doping [278], pressure can potentially drive holes into these protected layers dramatically increasing $T_c$. Finally, many of the discrepancies between experiments in the Bi, Tl, and Hg bearing cuprates could be due to non-hydrostatic effects in the sample environment. Compression in a non-hydrostatic medium tends to produce lower maximum values of $T_c$ when compared to hydrostatic or quasi-hydrostatic compression, as observed in the HgBCCO cuprates by Jover et al. [42].

Measurements of $T_c$ via other techniques are in agreement with the $T_c$ – pressure relationship obtained by tracking the magnetic susceptibility [14]. Through careful biasing and noise reduction techniques Timofeev et al. [279] introduced a very sensitive four coil technique for measuring $T_c$ in diamond anvil cells by detecting the Meissner effect. Upon compression, $T_c$ in near optimally doped Bi-2223 was observed to rise and then fall as one would expect by increasing the doping. Unexpectedly, $T_c$ was then observed to rise once more as discussed in the next section.

Guo et al. [280] reported a step-like resistivity - temperature relationship in Bi-2212 Figure 24. The authors [280] proposed a superconducting 2D→3D crossover, similar to the 2D→3D crossover observed by Takeuchi et al. [281] in overdoped ambient pressure BSCCO and the proposed strain induced crossover proposed to exist in LBCO [159].

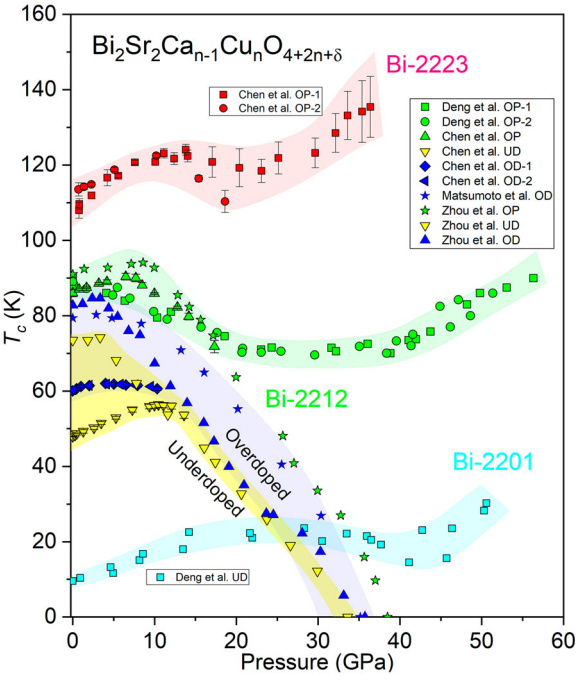


**Figure 25.** $T_c$ pressure dependence of $Bi_2Sr_2Ca_{n-1}Cu_nO_{4+2n+\delta}$ (BSCCO, $n = 1,2,3$). Data are presented for optimally doped Bi-2223 [14] (red), optimally doped Bi-2212 [35,268] (green), overdoped Bi-2212 [37,268] (blue), underdoped Bi-2212 [268] (yellow), and underdoped Bi-2201 [35] (cyan). Upon compression all samples, irrespective of doping, experience a small rise in $T_c$. $T_c$ is reported to reach a maximum and then decrease, similar to other cuprates. Superconductivity was only reported to be destroyed in overdoped Bi-2212 by Matsumoto et al. [37] when compressed in a cubic boron nitride pressure transmitting medium. At higher pressures, $T_c$ has been reported to increase once again in optimally doped Bi-2212 and Bi-2223, and in underdoped Bi-2201.

However, no step like feature was observed in the resistivity of BSCCO at ambient pressure. This upper $T_{c,2D}$ value does not appear to coincide with any susceptibility signal Figure 24. Huang et al. [282] reported a similar step-like feature in the resistivity of Fe-doped LSCO, which they attributed to pair density wave (PDW) order. This commonality might imply that pressure can alter the interplay between the CDW and SDW order and therefore create/destroy PDW order. Additional measurements are needed to determine the nature of this feature.

### *5.2. Pressure-driven effects of $T_c$ in BSCCO*

We now discuss the unusual pressure dependence of $T_c$ in BSCCO in more detail. At a critical pressure, the pressure response of $T_c$ in the bismuth-based cuprates departs from that expected from the critical temperature versus pressure dome and $T_c$ begins to rise once again. All $T_c$ versus pressure data for members of the BSCCO family under pressure is presented in Figure 25, Data from Bi-2201 and Bi-2212 by Deng et al. [35] and Bi-2223 by Chen et al. [14]. We are not aware of any transport data on the $n = 4$ compound under pressure.

The reported critical temperature as a function of pressure for Bi-2201, Bi-2212, and Bi-2223 are presented in Figure 25. In underdoped Bi-2201 $T_c$ was observed to rise and then fall upon compression, tracing out the superconducting dome. Beginning at 40 GPa, the rise in $T_c$ is observed with no saturation to at least 50 GPa, the pressure limit of the experiment [35]. Studies of optimally doped Bi-2212 by Deng et al. [35] and Chen et al. [14] report $T_c$ to slightly rise upon initial compression irrespective of doping level. The doping-maximized $T_c$ then began to fall, tracking the superconducting dome. After appearing to saturate from 20 GPa to 40 GPa, $T_c$ was then observed to rise once more [35]. Additionally, one compression experiment for underdoped Bi-2212 reported by Chen et al. [268] demonstrates $T_c$ increasing to a maximum and then falling. The result suggests that the samples became effectively overdoped with pressure. All these samples initially show a small enhancement in $T_c$ before pressure causes them to behave similarly to overdoped samples and superconductivity is suppressed. Matsumoto et al. [37] reported a compression experiment on single crystal Bi-2212 that showed a destruction of superconductivity at 35 GPa. Unlike other electrical conductivity experiments, cubic boron nitride was used as the pressure transmitting medium on single crystal samples. The use of such a stiff pressure transmitting medium likely resulted in strong shearing or destruction of the single crystal samples. In underdoped Bi-2223 Chen et al. [14] reported $T_c$ following the trend predicted by the PICT model for slightly underdoped Bi-2223 until deviating from its dome like behavior at 22 GPa and rising until the maximum pressure of the experiment [14].

Recently Zhou et al. [36] reported pressure-induced electronic phase transitions in Bi-2201, Bi-2212, and Bi-2223 where the materials become insulating and superconductivity is destroyed at a critical pressure. These observations are in contrast to the reports of Deng et al. [35] and Chen et al. [14]. All experiments where superconductivity is reported to be destroyed were carried out under non-hydrostatic conditions [37] or when using pressure transmitting media known to develop non-hydrostatic stress under pressure [36]. These results indicate that superconductivity in cuprates under pressure is strongly dependent on the degree of hydrostaticity of the sample environment.

Chen et al. [14] proposed a pressure induced inner plane doping optimization mechanism to explain the rise in $T_c$ observed in the three layer Bi-2223. According to this charge transfer model, the inner $CuO_2$ planes present in cuprates with more than two planes per unit cell have $\delta$ optimized with pressure. Since these inner planes are known to be less doped than the planes adjacent to the charge reservoirs [283,284], pressure induced doping would enhance $T_c$. Auvray et al. [285] reported different pressure dependence of the dopings in the inner and outer planes of the HgBCCO family, and it is expected that a similar degree of charge imbalance between the inner and outer planes exists in Bi-2223. This hypothesis would suggest a second maximum in the pressure dependence of $T_c$ at more extreme pressures. As no second maximum has been observed to date, it is unclear if this is a driving mechanism behind the second rise in $T_c$ in Bi-2223.

It appears as if inner plane optimization is not the only effect contributing to the rise in $T_c$ under pressure. Deng et al. [35] reported that $T_c$ of Bi-2201 and Bi-2212 to rise under pressure, both being cuprates with no inequivalent inner plane. The results suggest that there is some more fundamental mechanism common to cuprates (or at least the members of the BSCCO family) behind the rise in $T_c$. The number of layers does, however, appear to be related to the critical pressure where $T_c$ begins to increase. The

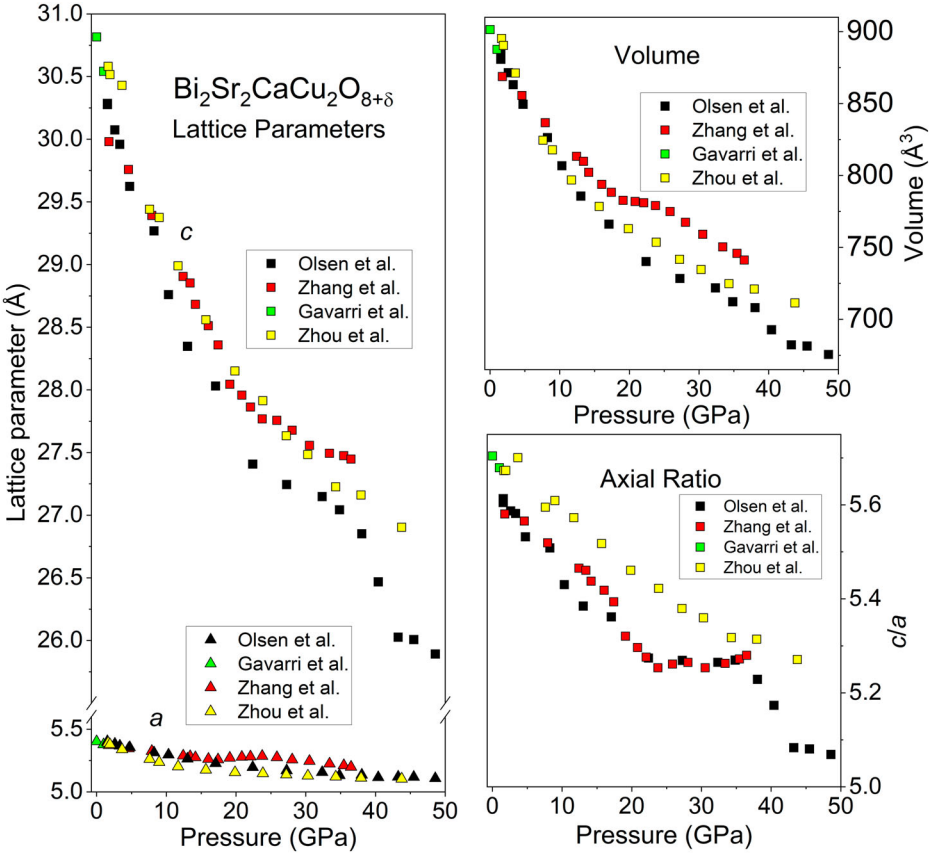


**Figure 26.** Left: *a* and *c* unit cell lattice parameters for $Bi_2Sr_2CaCu_2O_{8+\delta}$. Olsen et al. [255] fit the data to a tetragonal (*I*4/*mmm*) space group, whereas Gavari et al. [294] and Zhang et al. [293] used an orthorhombic representation (*Amaa*). Zhang et al. [293] observed increases in the *a*(*b*) parameter with pressure between 18 GPa and 25 GPa. Top: Unit cell volume of Bi-2212 as a function of pressure. Olsen et al. [255] reported an anomaly at 38 GPa interpreted as a 'possible planar collapse' where the *c* parameter suddenly shrinks. Zhang et al. [293] shows anomalies at 20 GPa related to the growth of the *a* and *b* parameter. Bottom: Pressure dependence of the axial ratio (*c*/*a*) for Bi-2212 from Olsen et al. [255], Zhang et al. [293], Gavarri et al. [294], and Zhou et al. [36]

pressure at which the increase becomes apparent is approximately 20 GPa lower in Bi-2223 than in Bi-2201 and Bi-2212 (Figure 25).

To explain the rise in $T_c$ in the $n = 1,2$ compounds, Deng et al. [35] suggested a possible Lifshitz transition similar to the change in Fermi surface topology observed through doping [286,287]. As it is unlikely that this trend continues indefinitely, bringing these cuprates to higher pressures in search of a saturation $T_c$ should help in the understanding of these phenomenon.

### *5.3. Structural studies of Bi, Tl, and Hg based cuprates*

Unlike other cuprates that undergo structural changes as a function of doping or pressure [64,200,288], the three major stoichiometries of BSCCO are reported to maintain an

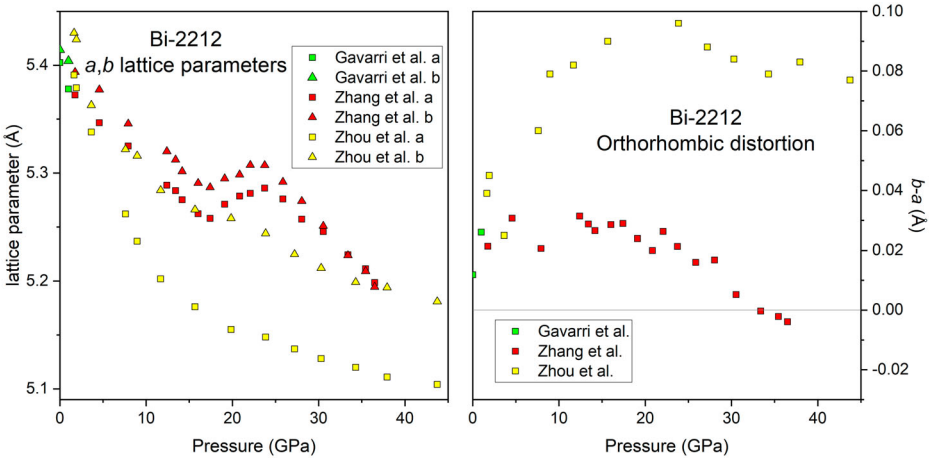


**Figure 27.** Left: *a* and *b* parameters of Bi-2212 under pressure. Zhang et al. [293] observed growth in both *a* and *b*. Zhou et al. [36] report *a* to shrink much more quickly upon the application of pressure than *b*. Right: Orthorhombic distortion of the data from the left panel. Zhang et al. [293] reported the distortion to remain constant up to 20 GPa where it then decreases and appears to vanish. Zhou et al. [36] report the distortion to increase until possibly saturating at 20 GPa. Data from Gavarri et al. [294], Zhang et al. [293], and Zhou et al. [36].

orthorhombic perovskite *Amaa* structure under pressure [289–291]. The unit cell is nearly tetragonal ($a - b \approx 0.1$ Å) such that all three variants are typically described with an *I*4/*mmm* tetragonal structure.

Compression experiments were performed on Bi-2212 to 50 GPa by Olsen et al. [255] who fit their data to a Murninghan equation of state [292]. Contradicting reports on the lattice parameters of Bi-2212 have been reported above 15 GPa. Olsen et al. [255] observed a 'possible planar collapse' at 40 GPa where the *c* parameter dramatically decreased. Deng et al. [35] pointed out that this structural anomaly coincided with the anomalous rise in $T_c$ observed in transport measurements. Zhang et al. [293] reported a stiffening in the *a* and *b* parameters of Bi-2212 at 15 GPa. Recently, Zhou et al. [36] reported compression experiments on Bi-2212 that fit the Bi-2212 cell to an orthorhombic *Ammm* space group and did not exhibit a saturation in the axial ratio or a stiffening in the *c* parameter. All compression data is presented in Figure 26. Similar to compression data for YBCO, Many of the experiments on BSCCO were performed in pressure transmitting media known to develop non-hydrostatic stresses [235–237].

Common in most compression experiments on Bi-2212 is an increase in the bulk modulus around 15 GPa. Below 22 GPa the extrapolated zero pressure bulk modulus is in agreement with ambient pressure ultrasonic measurements [295]. At 22 GPa the ratio appears to saturate with pressure as the *c* axis stiffens. At pressures above the aforementioned 'planar collapse' reported by Olsen et al. [255] at 40 GPa the *c*/*a* ratio was found to suddenly decrease and to saturate once again as pressure was further increased.

Although BSCCO compounds are nearly tetragonal, and commonly described with an *I*4/*mmm* space group, differences in the *a* and *b* parameter have been reported in the literature, with several experiments fitting the Bi-2212 cell to an orthorhombic *Amaa* space group and reporting a pressure dependent orthorhombic distortion ($b - a$) [36,293,294]. Experiments in which a significant orthorhombic distortion was observed were mostly in

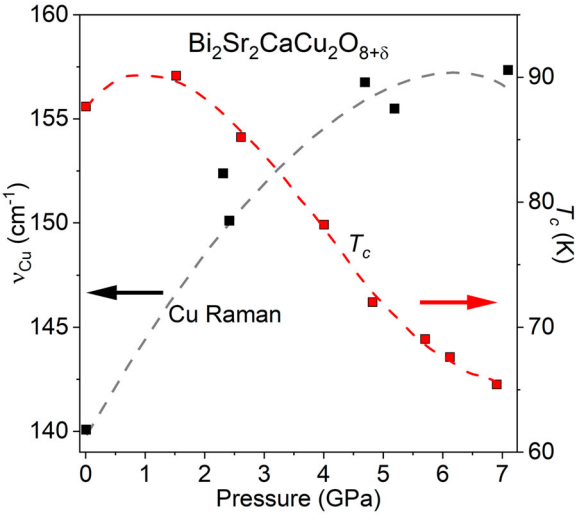


**Figure 28.** Correlation of pressure dependence of the critical temperature (red) and Raman frequency dominated by motion of planar Cu (black) for $BiSr_2CaCu_2O_{8+\delta}$. The pressure derivative of the Raman shift, $d\nu_{Cu}/dP$, deviates from linearity within the same pressure range over which $T_c$ begins to decrease (red). A similar deviation from linearity was reported in Y-123 by Kakihana et al. [202] Data from Klotz and Schilling [236].

pressure transmitting media known to be highly non-hydrostatic above several GPa [36,237,293]. The pressure dependence of $a$, $b$ and $a - b$ are presented in Figure 27

### *5.4. Raman spectroscopy of Bi, Tl, and Hg based cuprates*

As with most materials, many of the vibrational Raman peaks observed in the Bi, Tl, and Hg based cuprates systemically broaden and shift to higher frequencies under pressure [196]. A noticeable exception is the 470 cm$^{-1}$ mode associated with the $c$ axis vibration of the O(3) site in Bi-2212 – corresponding to the vibration of the out of plane apical oxygen – as observed by by Kendziora et al. [296] Osada et al. [133] reported that in overdoped Bi-2212 this peak shifts to higher frequencies under pressure, while in underdoped samples The O(3) peak does not appear to shift at all up to at least 18 GPa.

Feiner et al. [297] and Zhou et al. [298] have proposed that the weakly bonded apical oxygen present in many cuprates might have a significant influence on the charge carrier density of the $CuO_2$ planes. The weak pressure dependence of the vibrational mode associated with the apical oxygen [O(3)] might be indicative of slow pressure induced oxygen ordering above $T_c$, similar to what was observed by Sadewasser et al. in Y-123 [172] and in Hg-1201 [257] where the temperature at which the pressure was changed – and vice versa – drastically altered the values of $T_c$ the sample exhibited. In addition to the unusual behavior of the O(3) mode, Osada et al. [133] observed a correlation between the pressure dependence of $T_c$ and the frequency of the Raman mode associated with the planar Cu in overdoped Bi-2212. This correlation was proposed to be related to pressure-induced charge redistribution *i.e.* pressure-induced doping. The pressure dependence of the frequency of the Cu mode (observed at 140 cm$^{-1}$ at

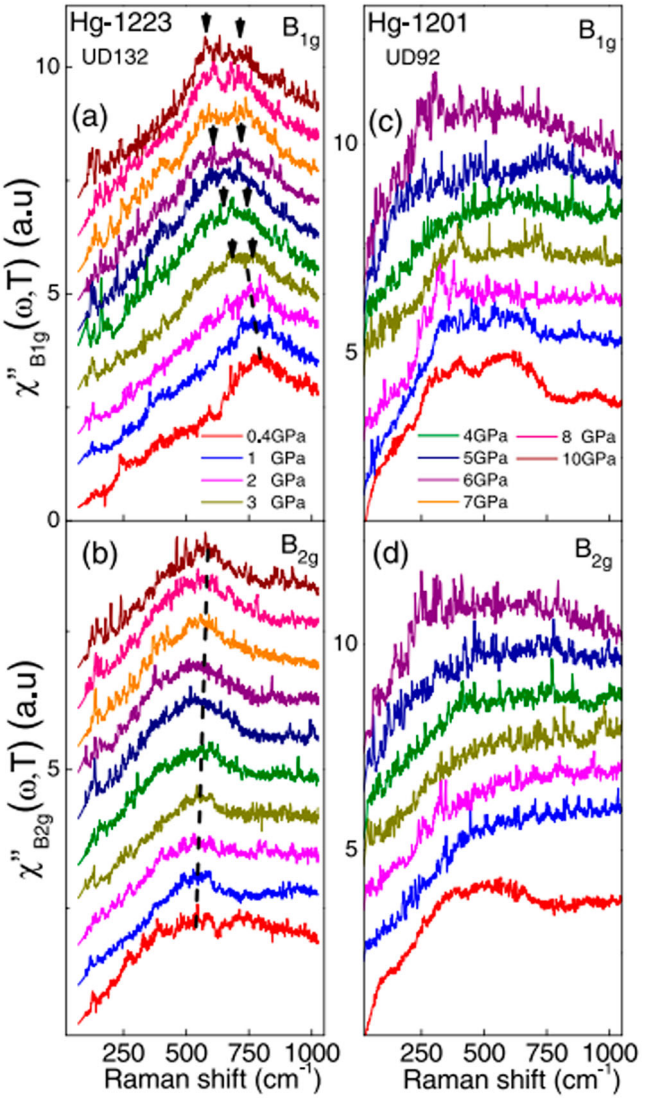


**Figure 29.** Polarized Raman spectra plotted in terms of relative scattering cross section at selected pressures for $HgBa_2Ca_2Cu_3O_{8+\delta}$ (Hg-1223, Left) and $HgBa_2Cu_1O_{4+\delta}$ (Hg-1201, Right). Under pressure the $B_{2g}$ spectra lack pronounced features as expected from the nodal region of the Fermi surface [299]. The $B_{1g}$ spectra shows a shift in the broad feature associated with electronic excitations to lower pressures, with the feature appearing to split at higher pressures in Hg-1223 (arrows in panel a). This split has been interpreted as pressure induced doping preferentially altering the outer $CuO_2$ planes, resulting in a less doped inner plane and the coexistence of two superconducting gaps. Figure reproduced from Auvray et al. [285] with permission.

ambient pressure) was reported to deviate from linearity around 2 GPa, which is close to the pressure at which $T_c$ begins to drop Figure 28.

Electronic Raman scattering – the light scattering off of electronic excitations – has been extensively used to characterize the properties of cuprate superconductors (see

Klein et al. [299] for a general review of electronic Raman scattering applied to superconductors). Features diagnostic of the superconducting gap and the pseudogap have been reported in electronic Raman measurements; specifically through reports of a depletion in signal from the lower energy background and a shift of spectral weight to higher wavenumbers [296,300–302]. The reduction in the electronic background is most clearly observed in the cross polarized spectrum, where a new peak emerges around 400 $cm^{-1}$, indicating some degree of electron-phonon coupling.

Early Raman measurements of the electronic measurements of cuprates, such as those by Lyons et al. [303] and Hackl et al. [304] suggested a degree of gap anisotropy not present in the *s*-wave superconductors. Devereaux et al. [305,306] elaborated on this observation, demonstrating how electronic Raman scattering can be a powerful tool for constraining the electronic structure of cuprates. With this technique, different regions of the Brillouin zone are probed by different polarizations of light, *e.g.* with $B_{1g}$ and $B_{2g}$ polarizations probing the antinodal and nodal regions of the Fermi surface respectively. This opening of the gap is most prominent in the $B_{1g}$ symmetry and hardly visible in the $B_{2g}$, as expected for a *d*-wave gap which is maximal at the antinodal region and minimal at the Fermi surface nodal region [67].

High pressure Raman scattering has been used to measure a pressure induced doping of the $CuO_2$ planes. Under pressure, a shift in spectral weight analogous to the change observed upon an increase in doping was observed in Hg-1201 and Hg-1223 by Auvray et al. [285], and a novel $Bi_{1.98}Sr_{2.06}Y_{0.68}Cu_2O_{8+\delta}$ cuprate by Cuk et al. [307] The evolution of this gap-like feature under pressure has been correlated with the degree of charge transfer into the $CuO_2$ planes, which in turn is heavily influenced by the compressibility

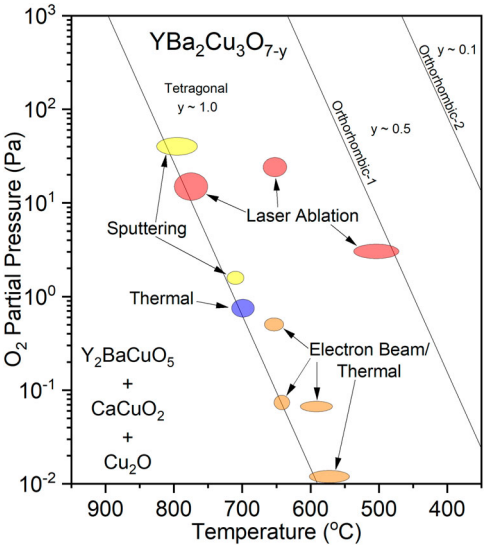


**Figure 30.** Oxygen partial pressure versus temperature for different structures of YBCO reported by Hammond and Bormann [310]. y indicates the oxygen content ($YBa_2Cu_3O_{7-y}$). Diagonal lines are phase boundaries. From left to right the presented phases are, precursor materials, non-superconducting tetragonal phase, oxygenated orthorhombic superconducting phase (Y-123, $T_c \sim 50\,K$), and a second orthorhombic superconducting phase (Y-124, $T_c \sim 94\,K$). Colored ovals indicate stable phase formation for the specified technique. Figure adapted from Hammond and Bormann [310].

of the material [308]. Auvray et al. [285] also reported differences in the electronic Raman response of the one- and three-layer mercury cuprates on compression. While the features associated with the electronic background associated with pair-breaking energy shifts to lower energies in Hg-1201, the feature broadens significantly and appears to split in Hg-1223 as presented in Figure 29. The breadth of this feature has been interpreted as arising from a lower doping of the inner plane under pressure in Hg-1223, causing two superconducting gaps to coexist; *i.e.* the inner and outer planes exhibit gaps corresponding to different hole doping levels.

## 6. Synthesis of cuprates under pressure

In addition to the use of pressure to explore and understand the physical properties of the cuprates, pressure has been used to synthesize the common cuprate families discussed above [309]. Moreover, high pressure synthesis has been used to create altogether new superconducting cuprates as discussed in the next section. Soon after the discovery of YBCO, Hammond and Bormann [310,311] showed that adjusting the oxygen partial pressure during synthesis can be used to control which structure forms as well as tune the doping level in the oxygen-doped materials. Stability fields for different phases can thus be mapped as a function of temperature and oxygen partial pressure. Phase boundaries for Y-123 as a function of synthesis conditions are

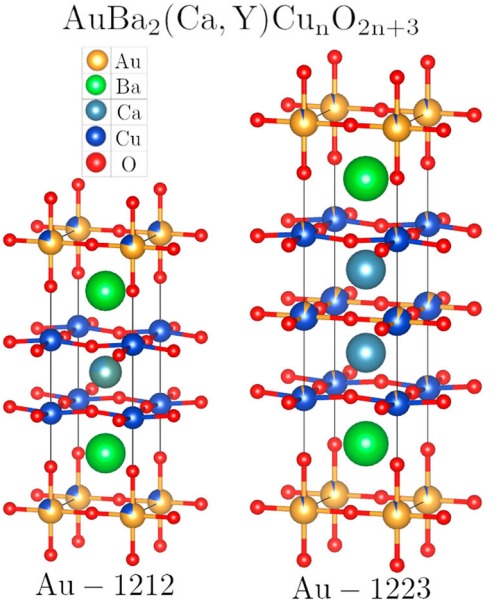


**Figure 31.** Unit cell of $AuBa_2(Ca, Y)Cu_nO_{2n+3}$ for $n = 1$ (Au-1212) and $n = 2$ (Au-1223). All members of the Au-bearing cuprates are described with an orthorhombic (*Pmmm*) space group and have structures similar to YBCO, but with up to 40 % of the Cu replaced by Au. The ratio of gold to blue spheres in above images represents the relative occupancy of Au/Cu at each site, with Au preferentially replacing chain copper sites (up to 80% of chain sites can be occupied by Au in the Au-1223 structure). Au-1212 data ($a = 3.850$ Å, $b = 3.826$ Å, $c = 12.07$ Å) used to draw structure from Bordet et al. [318] Au-1223 data ($a = 3.812$ Å, $b = 3.856$ Å, $c = 15.44$ Å) from Kopnin et al. [321].

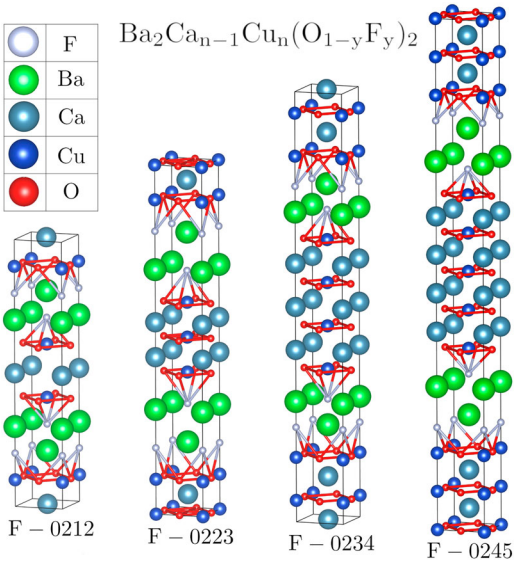


**Figure 32.** Crystal structure of $Ba_2Ca_{n-1}Cu_n(O_{1-y}F_y)_2$ for $n$ =1–5. All structures are described by a tetragonal ($I4/mmm$) space group. Fluorine dopants preferentially replace the apical oxygen sites in order to increase hole doping. Similar to BSCCO, unit cells are offset in the c direction, allowing an easy cleavage plane along the Ba layer for surface sensitive probes. Structural data from Iyo et al. [322] for F-0212 ($a$ = 3.89 Å, $c$ = 20.9 Å), F-0223 ($a$ = 3.86 Å, $c$ = 27.5 Å), F-0234 ($a$ = 3.86 Å, $c$ = 33.8 Å), and F-0245 ($a$ = 3.86 Å, $c$ = 40.2 Å).

shown in Figure 30. Elevated oxygen pressures are required for Y-124 [312] and Y-247 [166] to form.

High oxygen partial pressures are needed to grow cuprates with more than three $CuO_2$ layers per unit cell. Pressure is required for the samples to be adequately doped and therefore superconduct [312]. Schwer et al. [313] demonstrated that high inert gas partial pressures are also needed for $n$>6 layered compounds ( *e.g.* $Hg_{0.75}Re_{0.22}Ba_2Ca_5Cu_6O_{15}$ and $Hg_{1-x}Re_xBa_2Ca_6Cu_7O_{16+4x+\delta}$), in order to stabilize the larger structures and prevent decomposition into the $n$ = 1,2,3 members.

Capponi et al. [314,315] demonstrated that the mercury-bearing cuprates can be doped by the use of high oxygen partial pressure during growth. As observed in the synthesis of the $n$ = 5 and $n$ = 6 HgBCCO compounds (Hg-1245 and Hg-1256) elevated oxygen partial pressure is required to stabilize the structures and ensure the doped superconducting phase forms. These studies indicated that without an oxygen partial pressure of 500 – 1300 bar, the high n compounds are underdoped and contain appreciable defects that inhibit superconductivity.

## 7. Novel structures

We now discuss novel superconducting cuprate systems that have been reported to be synthesized only under pressure. These families include the gold-doped cuprates, the fluorine bearing $Ba_2Ca_{n-1}Cu_nO_{2n}(O, F)_2$, the $Ca_{1-x}R_xCuO_2$ infinite layer materials, and the Ba-Ca-Cu-O systems.

### 7.1. Gold-doped cuprates

Analogous to the La – Y chemical pressure conjecture for LBCO, Bordet et al. [316] proposed that replacing Hg with Au might raise $T_c$ of HgBCCO. The authors [316] reported that these gold-bearing phases are isostructural with HgBCCO, and have up to 40% of the Hg sites replaced by Au. Bordet et al. [316] synthesized these Au/Hg cuprates using a belt-type apparatus at pressures up to 1.8 GPa and temperatures of 600–900 °C . These materials had slightly smaller lattice parameters than HgBCCO, $a(b)$ and $c$ shrink by approximately 0.004 Å and 0.044 Å respectively. The critical temperature was observed to be slightly lower than optimally doped HgBCCO, suggesting these samples were effectively overdoped by the 'chemical pressure' from the Au substitution.

Bordet et al. [317] used high pressure synthesis to create an entirely new family of gold-bearing cuprates with the nominal formula $AuBa_2(Ca, Y)_{n-1}Cu_nO_{2n+3}$ abbreviated as Au-12 $(n-1)n$ with $n = 1,2,3,4$ reported to be synthesized. These gold bearing compounds have a structure similar to YBCO, but with gold partially substituting up to 80% of the chain copper sites. The unit cells of Au-1212 and Au-1223 are presented in Figure 31. All compounds of the gold-doped family require synthesis pressures greater than 6 GPa and temperatures above 1000 °C to form. Structurally, these phases are characterized by long range zig-zag units formed within the Cu-O/Au-O chains [318]. This pattern is a result of the Au-O bonds being slightly longer than the Cu-O bonds. The consequence of these structural features on the electronic properties of the gold bearing cuprates has not been explained. The onset of superconductivity for optimally doped gold-bearing cuprates was observed to be 19 K in Au-1201, 82 K in Au-1212, 30 K in Au 1223, and 99 K in Au-1234 [317–320]. Kopnin et al. [321] suggested that the decrease in $T_c$ for Au-1223 is likely due to an increased gold concentration within the $CuO_2$ planes as opposed to the chains.

### 7.2. Fluorine-bearing cuprates

Iyo et al. [322] reported a series of HTS cuprates with the formula $Ba_2Ca_{n-1}Cu_n(O_{1-y}F_y)_2$ ( $n$ =2–5, Figure 32), that can be grown under high $P$-$T$ conditions. These materials are doped via the replacement of the apical oxygen sites with fluorine and have optimally doped $T_c$ values ranging from 90 – 120 K [322–324]. The fluorine doped materials are unique in the fact that they contain no rare earth elements to stabilize the structure and that, once synthesized, are relatively defect free, even for the $n \geq 3$ compositions [322].

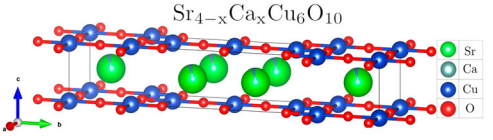


**Figure 33.** Crystal structure of the superconducting phase of $Sr_{3.83}Ca_{0.17}Cu_6O_{10}$ in an $I4/mmm$ representation. Unlike other superconducting cuprates, these infinite layer compounds consist of layers of $CuO_2$ with only a single layer of atoms between them. $CuO_2$ planes are not composed of checkerboard patterns like other cuprates, but instead form ribbon like structures with $CuO_2$ blocks running along the $a$ axis. Doping is controlled by Ca substitution into the Sr sites. Unit cell parameters ($a = 3.930$ Å, $b = 19.39$ Å, $c = 3.4358$ Å) from Schwer et al. [332].

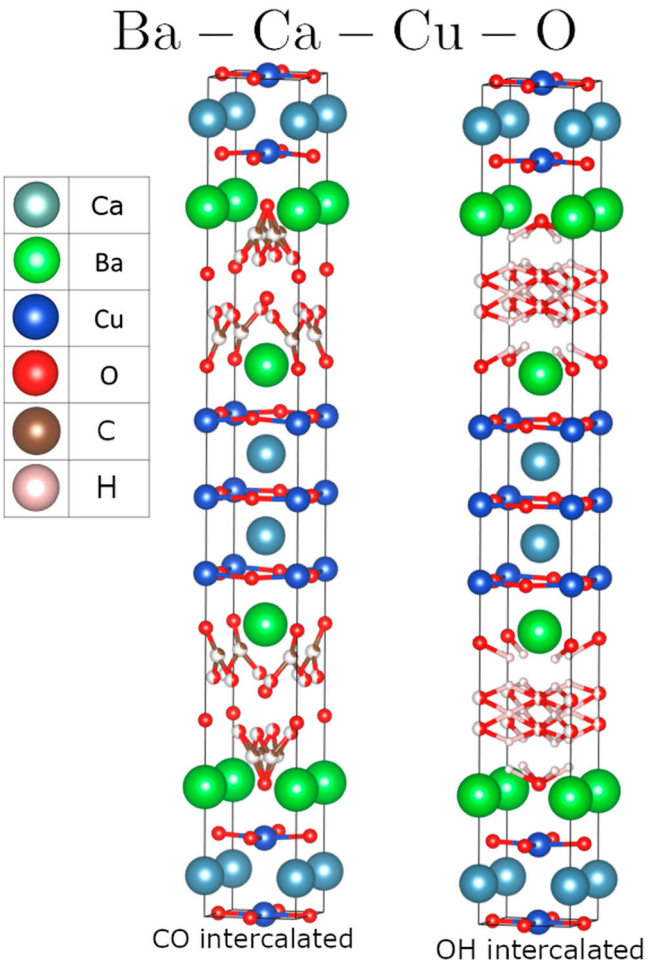


**Figure 34.** Left: Proposed crystal structure of (Ca, Cu, H, $CO_2)_2Ba_2Ca_2Cu_3O_{8+\delta}$ showing C and O intercalated between the BaO charge reservoir planes. The fraction of each sphere that is filled corresponds to the approximate occupancy of that site in the proposed structure. Right: Proposed structure of (Ca, Cu, H, $Co_2)_2Ba_2Ca_2Cu_3O_{8+\delta}$ showing H and O intercalated between the charge reservoir layers. Structural parameters ($a = 3.848$ Å, $c = 33.98$ Å) from Hosomi et al. [339].

All compounds of this family require high synthesis pressures typically applied using a cubic anvil press. Shirage et al. [325,326] reported requiring 5 GPa to synthesize the $n = 2$ compound and Iyo et al. [323,324] required a pressure of 4.5 GPa to form the $n$ =3–5 compounds. The pressure dependence on $T_c$ after synthesis has not been reported. The stability and purity of the $n$>3 compounds after synthesis allows for probes into the undoped central $CuO_2$ planes. NMR studies by Shimizu et al. [284,327–329] indicated that the central planes in the $n = 3 - 5$ members are protected from the doping effects induced by the charge reservoir layers. This protection allows for superconductivity to occur in the more doped outer planes while the AFM Mott insulating properties of the parent compound dominate the undoped central planes. An ARPES study by Kunisada et al. [278] supported the proposed phase coexistence. Electron-like pockets present in the Fermi surface were attributed to the strongly correlated AFM phase in the central

plane of the structure. Mukuda et al. [283] elaborated further on this co-existence and how it may provide insight to the cuprate pairing mechanism.

### 7.3. Infinite layer structures

Several infinite layer structures consisting of parallel copper oxide planes can be synthesized under pressure [320], many of which are superconducting, with the general formula $Sr_{n-1-x}M_xCu_{n+1}O_{2n}$ ( $n = 1,3,5$ ); M = Nd [330], La [331], Ca [320,332,333] ( Figure 33). These structures are unlike other cuprates in that the charge reservoir layer is a single layer of atoms instead of the usual rock-salt like structure as exhibited in the cuprates described above. All members of the infinite layer group seem to have an optimally doped $T_c$ of about 40 K [330]. Instead of n corresponding to the number of layers per unit cell, it describes the number of ribbon like structures in the $CuO_2$ plane. Unlike many of the other cuprates discussed in this review, the infinite layer compounds are electron-doped as opposed to hole-doped [334]. Smith et al. [335] reported the synthesis of the $n = 1$ Nd doped infinite layer cuprate at 2.5 GPa using a belt-type apparatus. Kazakov et al. [330] describe the synthesis of the $n = 3,5$ compounds requiring significantly higher pressures to form (5-8 GPa). Er et al. [331] reported the $n = 1$ La doped system requiring 4 GPa to form .

### 7.4. Ba-Ca-Cu-O systems

High pressures have been used in the synthesis of various Ba-Ca-Cu-O superconducting cuprates. Chu et al. [336] reported the formation of Ca and Cu doped $Ba_2Ca_{n-1}Cu_nO_x$ [abbreviated 02 $(n-1)n$-Ba] with a $T_c$ of 126 K, the highest reported $T_c$ in a cuprate without a volatile toxic element. The $n = 3,4$ compounds were formed at 5–6 GPa in a multianvil device [337], and were found to have a tetragonal $I4$ symmetry [338]. The structures of the 02 $(n-1)n$-Ba compounds are unusual among the hole doped cuprates in that the charge reservoir blocks are comparatively simple, consisting of only tetragonal BaO substructures. The intercalation of Ca and Cu in between the charge reservoir layers allows for the doping of the $CuO_2$ planes. These 02 $(n-1)n$-Ba are unstable in air, with the relatively open charge reservoir layer readily accepting $OH^-$ and $CO^{2-}$ ions into the structure. This reaction reduces $T_c$ from 126 K to 90 K as the more stable lower $T_c$ phase forms [336,339]. Structures of the lower $T_c$ phase for the $n = 3$ compound $[(Ca, Cu, H, Co_2)_2Ba_2Ca_2Cu_3O_{8+\delta}]$ with the positions of the possible $OH^-$ and $CO^{2-}$ contaminants in the charge reservoir layers, are presented in Figure 34.

Wu et al. [340] reported the synthesis of a related superconducting cuprate with formula $CaBa_2Ca_2Cu_3O_{9-\delta}$ [abbreviated Ca-12 $(n-1)n$-Ba] with a $T_c$ of 107 K. The Ca-12 $(n-1)n$-Ba compounds are structurally similar to the Tl-doped cuprates and were synthesized at 6 GPa in a similar multianvil setup to that used in the synthesis of 02 $(n-1)n$-Ba . The Ca-12 $(n-1)n$-Ba are reported to be stable in ambient conditions and do not readily absorb $OH^-$ and $CO^{2-}$ from air.

## 8. Electron-doped cuprates

Electron-doped cuprates exhibit pressure-induced effects on superconductivity similar to those found for the hole-doped cuprates. Electron doped cuprates typically have smaller

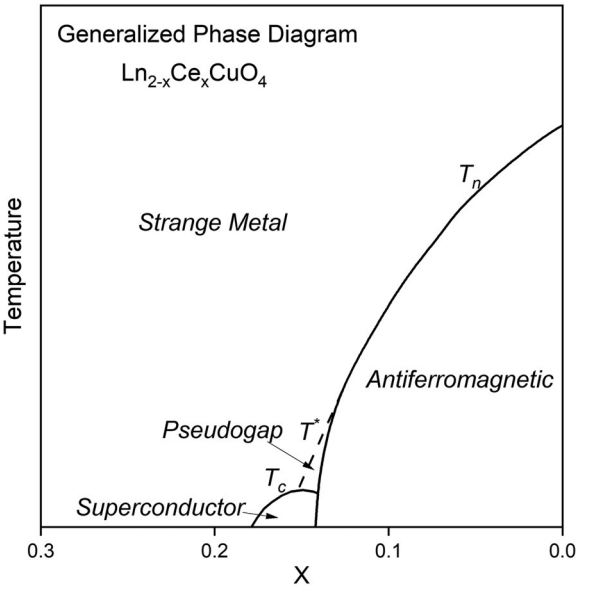


**Figure 35.** Generalized phase diagram for the electron doped cuprates at ambient pressure, showing a significantly larger region of stability for the Antiferromagnetic phase, along with a much smaller superconducting phase. Phase boundaries adapted from [106,345,346].

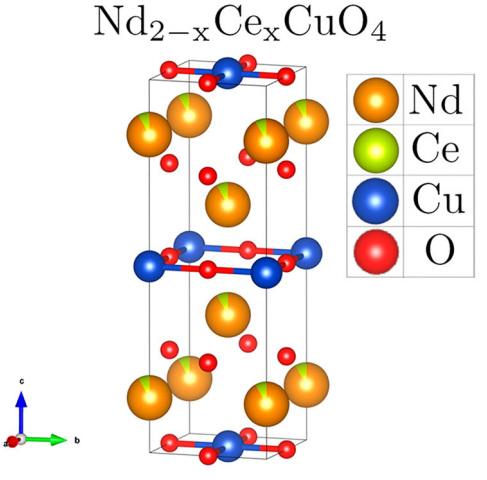


**Figure 36.** Crystal structure of electron doped $Nd_{2-x}Ce_xCuO_4$ in the superconducting T′ phase, presented in an *I*4/*mmm* representation. Charge carrier doping is controlled by Ce substitution into the Nd sites. Unit cell parameters ($a$ = 3.942 Å, $c$ = 12.06 Å) from Paulus et al. [347].

$T_c$'s and significantly stronger antiferromagnetic effects than hole-doped cuprates [341,342]. A generalized phase diagram for the electron-doped cuprates is presented in Figure 35 showing a significantly larger region of stability for the antiferromagnetic phase and a smaller superconducting dome which is truncated by the AFM phase

boundary. A pseudogap has also been observed in electron-doped cuprates, but it occupies a much smaller region of phase space compared to the pseudogap present in hole-doped cuprates [343,344]. Electron doped cuprates have been studied less than their hole doped counterparts, although many reports of pressure effects on $Ln_{2-x}Ce_xCuO_4$ (Ln = Nd, Sm, Eu, Pr) have been reported and are discussed below. Structure of the Nd doped material is presented in Figure 36

As for the hole doped cuprates, the concept of 'chemical pressure' has been used to categorize these materials. Several groups [348–350] have used the concept of chemical pressure in studies of $Ln_{2-x}Ce_xCuO_4$, generated by replacing the Ln with the smaller Sm and Eu to suppress $T_c$. Tsukada et al. [351] argued that the $T_c$-doping diagram in the electron-doped cuprates is highly susceptible $Ln^{+3}$ species, and have related this to a chemical pressure similar to what has been discussed above; *i.e.* similar to the replacement of Ba → Sr in the LBCO/LSCO hole doped cuprates [114]. In general, chemical pressure can be viewed as shrinking the area of phase space occupied by the superconducting dome and extending the antiferromagnetic phase to higher dopings [346,351–353].

The superconducting phase of many of the electron-doped cuprates exist in an $A_2^{II}B^{IV}O_4$ type solid solution. Chen and Eichhorn [354] examined the pressure response of the $A_2^{II}B^{IV}O_4$ solid solutions and found the compounds to undergo structural phase transitions under pressure. $A_2^{II}B^{IV}O_4$ type materials adopt a tetragonal $K_2NiF_4$ type lattice (T-phase), an orthorhombic distorted $K_2NiF_4$ type lattice (O-phase), and an $Nd_2CuO_4$ type lattice (T′-phase) [355]. In the electron-doped cuprates, the T′ phase has been reported to exhibit HTS [351]. Wilhelm et al. [355,356] reported a structural study of the un-doped parent $Nd_2CuO_4$ compound under pressure, where the T′ phase was destroyed at 21.5 GPa and the sample formed the T phase. Upon release of pressure the sample gradually distorted into the O phase. At 10 GPa the sample adopted the T′ phase once again. Wilhelm et al. [356] reported similar transitions from T′ to a T/O phase (a T phase with an orthorhombic distortion) in the doped superconducting cuprates, with $La_{2-x}Nd_xCuO_4$ undergoing a reversible pressure-induced T′ → T transition between 4.4 GPa for $x = 0.6$ up to ∼14 GPa for $x = 0.855$ . Similar reversible transitions that appears to restore superconductivity in the T′ phase upon the release of pressure have been found in $Nd_{2-x}Ce_xCuO_4$ [357,358], and $Pr_{2-x}Ce_xCuO_4$ [359].

The effect of pressure on $T_c$ has been reported for the electron doped cuprates. Markert et al. [349] measured $T_c$ in $L_{2-x}M_xCuO_{4-y}$ (L = Pr, Nd, Sm, Eu; M = Ce,Th) and measured the initial value of $dT_c/dP$ to be negative up to ∼0.2 GPa, in contrast to the positive value observed in the hole doped cuprates. Beille et al. [360] later observed this trend to continue up to at least 1 GPa, with nearly all $T_c$ – pressure relations being of a similar magnitude to the hole doped cuprates, but opposite in sign. Beille et al. [360] also pointed out that the volume dependence on $T_c$ ($dT_c/dV$) is at least an order of magnitude larger than that observed when changing the volume through a chemical pressure induced by isotope replacement [349]. This result suggests that chemical pressure and the application of pressure are not entirely equivalent in electron-doped as well as other cuprates. Murayama et al. [361] noted that many of the the electron-doped cuprates do not have an apical oxygen interacting with the $CuO_2$ planes, creating a significantly different electronic environment around the planes and inhibiting charge transfer upon atom replacement.

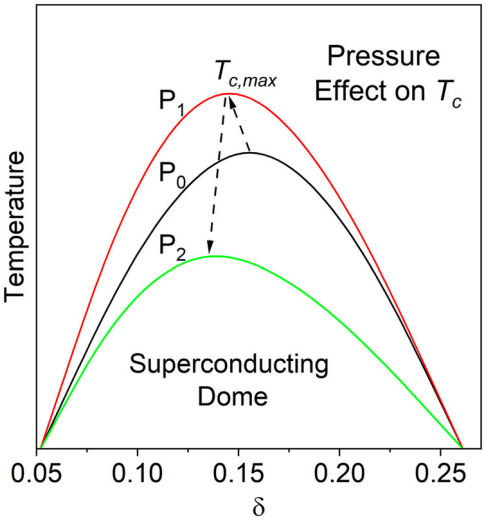


**Figure 37.** Pressure effect on the generalized superconducting dome for superconducting cuprates under pressure. As pressure is increased from ambient ($P_0$, black) to $P_1$ (red) and then $P_2$ (green), the optimal doping level of $\delta_{op} \sim 0.16$ found for most cuprates at ambient pressure tends to move to lower values, and $T_{c,max}$ first increases (red) and then decreases (green) on compression. Based on data from Doiron et al. [149], Rullier et al. [64], and Vovk and Solovjov [219,353].

Rotundu et al. [359] extend measurements of $T_c$ to higher pressures, reporting the pressure dependence of $T_c$ in single-crystal $Pr_{2-x}Ce_xCuO_4$. Optimally doped ( $x = 0.15$, $T_c = 21$ K) and over doped ( $x = 0.17$ , $T_c = 15$ K) electron-doped cuprates were measured up to 32 GPa. The optimally doped samples exhibited the T′→T structural phase transition at 2.7 GPa where the majority of the sample formed the insulating T phase and $T_c$ was suppressed from 22 K to 18.5 K. Superconductivity was reported to be completely destroyed in the optimally doped cuprates at 34 GPa. The overdoped sample, however, did not exhibit any noticeable pressure-induced effects on superconductivity, $T_c$ was relatively constant up to 32 GPa. Murayama et al. [361] also reported $T_c$ to be constant up to 2.5 GPa in electron-doped $Nd_{1.85}Ce_{0.15}CuO_{4-\delta}$.

## 9. Concluding remarks

We close with some general observations on the effect of pressure on HTS in cuprates. Pressure will likely continue to be, useful in elucidating the complex and intriguing physics found in the cuprates. Compression data obtained to date indicate that the effects of pressure on $T_c$ has close parallels to those of oxygen doping. Measurements show $T_c$ rising and then falling with increasing pressure, similar to the superconducting dome observed at ambient pressure with variable doping. Common trends in the pressure dependence of $T_c$ along with supporting data from transport [18,130], magnetization [14,131], Raman [132,133], NMR [134], and other measurements suggest pressure and doping alter the same physical parameter: the charge carrier concentration in the $CuO_2$ planes. Consequently, high pressure measurements provide a unique method to tune $n_H$ *in situ*. In the absence of structural or electronic transitions,

pressure induces doping, resulting in a deformed version of the ambient pressure doping-temperature phase diagram Figure 37. The optimal doping level $\delta_{op}$ continuously decreases with pressure, while $T_{c,max}$ rises and then falls [10,14,18–20,23,25–33,35,38–44] An apparent universality in the pressure response of $T_c$ despite existence of multiple competing phases provides evidence that superconductivity in nearly all cuprate superconductors has a common origin, presumably in the $CuO_2$ planes. The Bi-based cuprates exhibit unexplained superconducting phenomena above a critical pressure, with $T_c$ rising with no saturation observed to date [14,35]. It is unclear if the second enhancement of $T_c$ under pressure is doping related or due to a Lifshitz transition that would alter its electronic structure [35]. To address this issue, additional measurements are needed above the current maximum reported pressures of 55 GPa [35].

Unlike $T_c$, the pressure dependence of the pseudogap onset temperature ($T^*$) does not appear to be influenced by pressure-induced doping and, in the absence of magnetic dopants such as Pr [220,227,232], $T^*$ is mostly unchanged upon compression. The major pressure-induced effect is on the critical doping level at which the pseudogap disappears. Under pressure the critical doping shifts to lower doping levels as it approaches the superconducting dome [149,171,212,220,227,232]. The critical doping level coincides with a change in Fermi surface topology where a transition from hole-like → electron-like behavior is observed [156,157]. The structure of the Fermi surface in relation to the pseudogap as elucidated through high pressure experiments [149,157] may provide insight into the origin of the unexplained phenomena [362].

With recent experimental advances, critical temperatures, crystal structures, and phase transitions have been determined in quasi-hydrostatic experiments above 200 GPa in other materials exhibiting HTS; *e.g.* in the hydride superconductors [363–367]. There is an opportunity to extend techniques to cuprates at comparable pressures. The use of pressure transmitting media that remain quasi-hydrostatic to much higher pressures will allow for more accurate probes of superconductivity at these pressures [235–237] Such advances have allowed for more precise x-ray based probes into the *d*-wave nature of the superconducting gap [368], local fluctuations associated with charge order [369], and time resolved x-ray techniques that probe the charge-ordered dynamics of the $CuO_2$ planes [101,370,371]. With the development of more brilliant and coherent x-ray sources at new and upgraded synchrotron sources [372] more precise probes into local charge dynamics and structural parameters will be possible. In addition to x-ray based techniques, IR synchrotron spectroscopy provides the opportunity to probe the phenomenology and dynamics of the superconducting gap and pseudogap under pressure [373,374]. The use of pressure as a tuning parameter to adjust the hole concentration *in-situ* promises to provide data that will allow not only improved understanding of the mechanism of cuprate HTS leading to, broader practical applications of superconducting cuprates with the possibility of retaining the high-$T_c$ phases at ambient pressures.

## Acknowledgments

We are grateful to C.W. Chu, M.B. Maple, L. Deng, L. Sun, S.A. Gramsch, M. Ahart, and F. Restrepo for helpful discussions and comments on the manuscript.

## Disclosure statement

No potential conflict of interest was reported by the authors.

## Funding

This work was supported by the U.S. National Science Foundation [grant DMR-2104881] and DOE-NNSA [cooperative agreement DE-NA0003975] (Chicago/DOE Alliance Center).

## ORCID

*Alexander C. Mark* http://orcid.org/0000-0002-7579-9625
*Russell J. Hemley* http://orcid.org/0000-0001-7398-8521

## References

[1] Bednorz JG, Müller KA. Possible high $T_c$ superconductivity in the Ba-La-Cu-O system. Z Phys B. 1986 Jun;64(2):189–193.
[2] Bednorz JG, Müller KA. Perovskite-type oxides – the new approach to high-$T_c$ superconductivity. Rev Mod Phys. 1988 Jul;60(3):585–600.
[3] Schneider T, Stoll E. Metallic hydrogen II high-temperature superconductivity. Physica. 1971 Oct;55:702–710.
[4] Ashcroft NW. Metallic hydrogen: a high-temperature superconductor?. Phys Rev Lett. 1968 Dec;21(26):1748–1749.
[5] Chu CW, Hor PH, Meng RL, et al. Superconductivity at 52.5 K in the Lanthanum-Barium-Copper-Oxide system. Science. 1987 Jan;235(4788):567–569.
[6] Wu MK, Ashburn JR, Torng CJ, et al. Superconductivity at 93 K in a new mixed-phase Y-Ba-Cu-O compound system at ambient pressure. Phys Rev Lett. 1987 Mar;58(9):908–910.
[7] Michel C, Hervieu M, Borel MM, et al. Superconductivity in the Bi - Sr - Cu - O system. Z Phys B. 1987;68:421–423.
[8] Khasanova NR, Antipov EV. Bi-2201 phases synthesis, structures and superconducting properties. Physica C. 1995 May;246(3):241–252.
[9] Schilling A, Cantoni M, Guo JD, et al. Superconductivity above 130 K in the Hg-Ba-Ca-Cu-O system. Nature. 1993 May;363(6424):56–58.
[10] Chu CW, Hor PH, Meng RL, et al. Evidence for superconductivity above 40 K in the La-Ba-Cu-O compound system. Phys Rev Lett. 1987 Jan;58(4):405–407.
[11] Souliou SM, Subedi A, Song YT, et al. Pressure-induced phase transition and superconductivity in $YBa_2Cu_4O_8$. Phys Rev B. 2014 Oct;90(14):140501.
[12] Mito M, Goto H, Matsui H, et al. Uniaxial strain effects on superconducting transition in $Y_{0.98}Ca_{0.02}Ba_2Cu_4O_8$. J Phys Soc Japan. 2016 Jan;85(2):024711.
[13] Muramatsu T, Pham D, Chu CW. A possible pressure-induced superconducting-semiconducting transition in nearly optimally doped single crystalline $YBa_2Cu_3O_{7-\delta}$. Appl Phys Lett. 2011 Aug;99(5):052508.
[14] Chen XJ, Struzhkin VV, Yu Y, et al. Enhancement of superconductivity by pressure-driven competition in electronic order. Nature. 2010;466:950–953.
[15] Fietz WH, Quenzel R, Ludwig HA, et al. Giant pressure effect in oxygen deficient $YBa_2Cu_3O_x$. Physica C. 1996 Oct;270(3):258–266.
[16] Adachi S, Matsumoto R, Hara H, et al. Pressure effect in Bi-2212 and Bi-2223 cuprate superconductor. Appl Phys Express. 2019 Mar;12(4):043002.
[17] Forgan EM, Cubitt R, Wylie MT, et al. Observation of the flux-Line lattice by neutron diffraction and Muon-Spin rotation. In: Yamafuji K, Morishita T, editors. Advances in superconductivity. VII. Tokyo: Springer; 1995. DOI:0.1007/978-4-431-68535-7_91

[18] Gao L, Xue YY, Chen F, et al. Superconductivity up to 164 K in $HgBa_2Ca_{m-1}Cu_mO_{2m+2+\delta}$ ($m = 1$, 2, and 3) under quasihydrostatic pressures. Phys Rev B. 1994 Aug;50(6):4260–4263.
[19] Monteverde M, Acha C, Núñez-Regueiro M, et al. High-pressure effects in fluorinated $HgBa_2Ca_2Cu_3O_{8+\delta}$. Europhys Lett. 2005 Sep;72(3):458–464.
[20] Takeshita N, Yamamoto A, Iyo A, et al. Zero resistivity above 150 K in $HgBa_2Ca_2Cu_3O_{8+\delta}$ at high pressure. J Phys Soc Japan. 2013 Jan;82(2):023711.
[21] Wijngaarden RJ, Scholtz JJ, Eenige ENv, et al. Pressure dependence of high-$T_c$ superconductors. High Press Res. 1992 May;10(1-2):479–485.
[22] Wijngaarden RJ, Van Eenige EN, Scholtz JJ. et al Ultra high pressure experiments on high-$T_c$ superconductors. In: Winter R, Jonas J, editors. High pressure chemistry, biochemistry and materials science. Dordrecht: Springer Netherlands; 1993. p. 121–146 (NATO ASI Series).
[23] Katano S, Funahashi S, Môri N, et al. Pressure effects on the structural phase transitions and superconductivity of $La_{2-x}Ba_xCuO_4$ ($x = 0.125$). Phys Rev B. 1993 Sep;48(9):6569–6574.
[24] Hucker M, Debessai M, et al. Spontaneous symmetry breaking by charge stripes in the high pressure phase of superconducting $La_{1.875}Ba_{0.125}CuO_4$. Phys Rev Lett. 2010 Feb;104(5):057004.
[25] Tissen VG, Nefedova MV. $T_c$ depenence upon pressure to 20 GPa for $YBa_2Cu_3O_{7-\delta}$ monocrystals. Sverkhoprovodimost: Fiz Khim Tekh. 1990;3(6):999–1002.
[26] Klotz S, Reith W, Schilling JS. The dependence of the superconducting transition temperature of single-crystalline $YBa_2Cu_3O_{7-\delta}$ on hydrostatic pressure to 13 GPa. Physica C. 1991 Jan;172(5):423–426.
[27] Karpinski J, Rusiecki B, Bucher B, et al. The nonstoichiometry of the high-$T_c$ superconductor $Y_2Ba_4Cu_7O_{15_{\pm x}}$ (14 K<$T_c$<68 K). Physica C. 1989 Dec;161(5–6):618–625.
[28] Diederichs J, Reith W, Sundqvist B, et al. Critical currents in Tl-2122 and Y-124 sinters under high hydrostatic pressure. Supercond Sci Technol. 1991 Jan;4(1S):S97–S99.
[29] Tissen VG, Nefedova MV, Emel'chenko GA, et al. Disappearance of superconductivity in $YBa_2Cu_4O_8$ under pressure about 11 GPa. Sverkhoprovodimost: Fiz Khim Tekh. 1991;4(4):677–679.
[30] Braithwaite D, Chouteau G, Martinez G, et al. The superconducting properties of $YBa_2Cu_4O_8$ single crystals under hydrostatic pressure (up to 9.5 GPa). Physica C. 1991 Jul;178(1-3):75–80.
[31] Van Eenige EN, Griessen R, Wijngaarden RJ, et al. Superconductivity at 108 K in $YBa_2Cu_4O_8$ at pressures up to 12 GPa. Physica C. 1990 Jul;168(5):482–488.
[32] Takahashi H, Shaked H, Hunter BA, et al. Structural effects of hydrostatic pressure in orthorhombic $La_{2-x}Sr_xCuO_4$. Phys Rev B. 1994 Aug;50(5):3221–3229.
[33] Scholtz JJ, van Eenige EN, Wijngaarden RJ, et al. Pressure dependence of $T_c$ and $H_c$ of $YBa_2Cu_4O_8$. Phys Rev B. 1992 Feb;45(6):3077–3082.
[34] Zhang JB, Struzhkin VV, Yang W, et al. Effects of pressure and distortion on superconductivity in $Tl_2Ba_2CaCu_2O_{8+\delta}$. J Phys: Condens Matter. 2015 Oct;27(44):445701.
[35] Deng L, Zheng Y, Wu Z, et al. Higher superconducting transition temperature by breaking the universal pressure relation. Proc Natl Acad Sci. 2019 Feb;116(6):2004–2008.
[36] Zhou Y, Guo J, Cai S, et al. Quantum phase transition from superconducting to insulating-like state in a pressurized cuprate superconductor. Nat Phys. 2022;18:406–410.
[37] Matsumoto R, Yamamoto S, Takano Y, et al. Crystal growth and high-pressure effects of bi-based superconducting whiskers. ACS Omega. 2021;6:12179–12186.
[38] Gao L, Xue YY, Chen F, et al. Universal enhancement of $T_c$ under high pressure in $HgBa_2Ca_{m-1}Cu_mO_{2m+2+\delta}$. Physica C. 1994 Dec;235–240:1493–1494.
[39] Chu CW, Gao L, Chen F, et al. Superconductivity above 150 K in $HgBa_2Ca_2Cu_3O_{8+\delta}$ at high pressures. Nature. 1993 Sep;365(6444):323–325.
[40] Nuñez-Regueiro M, Tholence JL, Antipov EV, et al. Pressure-Induced enhancement of $T_c$ above 150 K in Hg-1223. Science. 1993 Oct;262(5130):97–99.
[41] Yamamoto A, Takeshita N, Terakura C, et al. High pressure effects revisited for the cuprate superconductor family with highest critical temperature. Nat Comm. 2015 Dec;6(1):8990.

[42] Jover DT, Wijngaarden RJ, Wilhelm H, et al. Pressure dependence of the superconducting critical temperature of $HgBa_2Ca_2Cu_3O_{8+y}$ and $HgBa_2Ca_3Cu_4O_{10+y}$ up to 30 GPa. Phys Rev B. 1996 Aug;54(6):4265.
[43] Ihara H, Hirabayashi M, Tanino H, et al. The resistivity measurements of $HgBa_2Ca_2Cu_3O_{8+x}$ and $HgBa_2Ca_3Cu_4O_{10+x}$ superconductors under high pressure. Jpn J Appl Phys. 1993 Dec;32(12A):L1732–L1734.
[44] Gao P, Zhang R, Wang X. Pressure induced self-doping and dependence of critical temperature in stoichiometry $YBa_2Cu_3O_{6.95}$ predicted by first-principle and BVS calculations. AIP Adv. 2017 Mar;7(3):035215.
[45] Ding H, Norman MR, Yokoya T, et al. Evolution of the Fermi surface with carrier concentration in $Bi_2Sr_2CaCu_2O_{8+\delta}$. Phys Rev Lett. 1997 Mar;78(13):2628–2631.
[46] Kamihara Y, Hiramatsu H, Hirano M, et al. Iron-based layered superconductor: LaOFeP. J Am Chem Soc. 2006 Aug;128(31):10012–10013.
[47] Kamihara Y, Watanabe T, Hirano M, et al. Iron-based layered superconductor $La[O_{1-x}F_x]FeAs$ (x = 0.05-0.12) with $T_c$ = 26 K. J Am Chem Soc. 2008 Mar;130(11):3296–3297.
[48] Oh H, Moon J, Shin D. Brief review on iron-based superconductors: are there clues for unconventional superconductivity? 2011 Dec. Available from: https://arxiv.org/abs/1201.0237v1.
[49] Hsu FC, Luo JY, Yeh KW, et al. Superconductivity in the PbO-type structure $\alpha$-FeSe. PNAS. 2008 Sep;105(38):14262–14264.
[50] Ikeda H, Arita R, Kuneš J. Doping dependence of spin fluctuations and electron correlations in iron pnictides. Phys Rev B. 2010 Jul;82(2):024508.
[51] Presland MR, Tallon JL, Buckley RG, et al. General trends in oxygen stoichiometry effects on $T_c$ in Bi and Tl superconductors. Physica C. 1991 May;176(1):95–105.
[52] Hanzawa K. Isotope effects in the cuprates. J Phys Soc Jpn. 1995 Dec;64(12):4856–4866.
[53] Reynolds CA, Serin B, Wright WH, et al. Superconductivity of isotopes of mercury. Phys Rev. 1950 May;78(4):487–487.
[54] Maxwell E. Isotope effect in the superconductivity of mercury. Phys Rev. 1950 May;78(4):477–477.
[55] zur Loye HC, Leary KJ, Keller SW, et al. Oxygen isotope effect in high-temperature oxide superconductors. Science. 1987 Dec;238(4833):1558–1560.
[56] Chen XJ, Struzhkin VV, Wu Z, et al. Unified picture of the oxygen isotope effect in cuprate superconductors. Proc Natl Acad Sci. 2007 Mar;104(10):3732–3735.
[57] Johnston S, Vernay F, Moritz B, et al. Systematic study of electron-phonon coupling to oxygen modes across the cuprates. Phys Rev B. 2010 Aug;82(6):064513.
[58] Maple MB. Interplay between superconductivity and magnetism. Physica B: Condensed Matter. 1995 Oct;215(1):110–126.
[59] Izyumov YA, Proshin YN, Khusainov MG. Competition between superconductivity and magnetism in ferromagnet/superconductor heterostructures. Phys-Usp. 2002 Feb;45(2):109–148.
[60] Shen KM, Yoshida T, Lu DH, et al. Fully gapped single-particle excitations in the lightly doped cuprates. Phys Rev B. 2004 Feb;69(5):054503.
[61] Shi M, Chang J, Pailhés S, et al. Coherent d-wave superconducting gap in underdoped $La_{2-x}Sr_xCuO_4$ by angle-resolved photoemission spectroscopy. Phys Rev Lett. 2008 Jul;101(4):047002.
[62] Honma T, Hor PH. Unified electronic phase diagram for hole-doped high-$T_c$ cuprates. 2008 Jan. Available from: https://arxiv.org/abs/0801.1537v2.
[63] Sokol A, Pines D. Toward a unified magnetic phase diagram of the cuprate superconductors. Phys Rev Lett. 1993 Oct;71(17):2813–2816.
[64] Rullier-Albenque F, Alloul H, Balakirev F, et al. Disorder, metal-insulator crossover and phase diagram in high-$T_c$ cuprates. Europhys Lett. 2008 Feb;81(3):37008.
[65] Chatterjee U, Ai D, Zhao J, et al. Electronic phase diagram of high-temperature copper oxide superconductors. Proc Natl Acad Sci. 2011 Jun;108(23):9346–9349.
[66] Timusk T, Statt BW. The pseudogap in high-temperature superconductors: an experimental survey. Rep Prog Phys. 1999 Jan;62(1):61–122.

[67] Norman MR, Pépin C. The electronic nature of high temperature cuprate superconductors. Rep Prog Phys. 2003 Sep;66(10):1547–1610.
[68] Hashimoto M, Vishik IM, He RH, et al. Energy gaps in high-transition-temperature cuprate superconductors. Nat Phys. 2014 Jul;10(7):483–495.
[69] Zaanen J, Gunnarsson O. Charged magnetic domain lines and the magnetism of high-$T_c$ oxides. Phys Rev B. 1989 Oct;40(10):7391–7394.
[70] Tranquada JM, Axe JD, Ichikawa N, et al. Coexistence of, and competition between, superconductivity and charge-stripe order in $La_{1.6-x}Nd_{0.4}Sr_xCuO_4$. Phys Rev Lett. 1997 Jan;78(2):338–341.
[71] Basov DN, Timusk T. Electrodynamics of high-$T_c$ superconductors. Rev Mod Phys. 2005 Aug;77(2):721–779.
[72] Schneider T, Baeriswyl D. Critical temperature of layered high $T_c$ superconductors. Zeitschrift Für Physik B Condensed Matter. 1988;73(1):5–8.
[73] Ando Y, Komiya S, Segawa K, et al. Electronic phase diagram of high-$T_c$ cuprate superconductors from a mapping of the in-plane resistivity curvature. Phys Rev Lett. 2004 Dec;93(26):267001.
[74] Honma T, Hor PH, Hsieh HH, et al. Universal intrinsic scale of the hole concentration in high-$T_c$ cuprates. Phys Rev B. 2004 Dec;70:214517.
[75] Batlogg B, Ramirez AP, Cava RJ, et al. Electronic properties of $La_{2-x}Sr_xCuO_4$ high-$T_c$ superconductors. Phys Rev B. 1987 Apr;35(10):5340–5342.
[76] Itoh T, Kitazawa K, Tanaka S. Specific heat and superconductivity in $BaPb_{1-x}Bi_xO_3$. J Phys Soc Japan. 1984;53(8):2668–2673.
[77] Chen SD, Hashimoto M, He Y, et al. Unconventional spectral signature of $T_c$ in a pure d-wave superconductor. Nature. 2022 Jan;601(7894):562–567.
[78] Kittel C. Introduction to solid state physics. 8th ed. United States of America: John Wiley & Sons; 2004.
[79] Scalapino DJ, Loh E, Hirsch JE. d-wave pairing near a spin-density-wave instability. Phys Rev B. 1986 Dec;34(11):8190–8192.
[80] Monthoux P, Balatsky AV, Pines D. Toward a theory of high-temperature superconductivity in the antiferromagnetically correlated cuprate oxides. Phys Rev Lett. 1991 Dec;67(24):3448–3451.
[81] Van Harlingen DJ. Phase-sensitive tests of the symmetry of the pairing state in the high-temperature superconductors – evidence for $d_{x^2-y^2}$ symmetry. Rev Mod Phys. 1995 Apr;67(2):515–535.
[82] Wollman DA, Van Harlingen DJ, Lee WC, et al. Experimental determination of the superconducting pairing state in YBCO from the phase coherence of YBCO-Pb dc SQUIDs. Phys Rev Lett. 1993 Sep;71(13):2134–2137.
[83] Ding H, Campuzano JC, Norman MR, et al. ARPES study of the superconducting gap and pseudogap in $Bi_2Sr_2CaCu_2O_{8+x}$. J Phys Chem Solids. 1998 Oct;59(10–12):1888–1891.
[84] Warren WW, Walstedt RE, Brennert GF, et al. Cu spin dynamics and superconducting precursor effects in planes above $T_c$ in $YBa_2Cu_3O_{6.7}$. Phys Rev Lett. 1989 Mar;62(10):1193–1196.
[85] Takigawa M, Hammel PC, Heffner RH, et al. 17O NMR study of local spin susceptibility in aligned $YBa_2Cu_3O_7$ powder. Phys Rev Lett. 1989 Oct;63(17):1865–1868.
[86] Takigawa M, Hammel PC, Heffner RH, et al. Spin susceptibility in superconducting $YBa_2Cu_3O_7$ from Cu Knight shift. Phys Rev B. 1989 Apr;39(10):7371–7374.
[87] Barrett SE, Durand DJ, Pennington CH, et al. 63Cu knight shifts in the superconducting state of $YBa_2Cu_3O_{7-\delta}$ ($T_c = 90$ K). Phys Rev B. 1990 Apr;41(10):6283–6296.
[88] Ding H, Yokoya T, Campuzano JC, et al. Spectroscopic evidence for a pseudogap in the normal state of underdoped high-$T_c$ superconductors. Nature. 1996 Jul;382(6586):51–54.
[89] Kaminski A, Rosenkranz S, Fretwell HM, et al. Change of Fermi-surface topology in $Bi_2Sr_2CaCu_2O_{8+\delta}$ with doping. Phys Rev B. 2006 May;73(17):174511.
[90] Norman MR, Ding H, Randeria M, et al. Destruction of the Fermi surface in underdoped high $T_c$ superconductors. Nature. 1998 Mar;392(6672):157–160.

[91] Vaknin D, Sinha SK, Moncton DE, et al. Antiferromagnetism in $La_2CuO_{4-y}$. Phys Rev Lett. 1987 Jun;58(26):2802–2805.
[92] Mitsuda S, Shirane G, Sinha SK, et al. Confirmation of antiferromagnetism in $La_2CuO_{4-y}$ with polarized neutrons. Phys Rev B. 1987 Jul;36(1):822–825.
[93] Johnston DC, Stokes JP, Goshorn DP, et al. Influence of oxygen defects on the physical properties of $La_2CuO_{4-y}$. Phys Rev B. 1987 Sep;36(7):4007–4010.
[94] Johnston DC, Sinha SK, Jacobson AJ, et al. Superconductivity and magnetism in the high $T_c$ copper oxides. Physica C. 1988 Jun;153–155:572–577.
[95] Tsuda T, Shimizu T, Yasuoka H, et al. Observation of nuclear resonance of cu in antiferromagnetic $La_2CuO_{4-d}$ and CuO. J Phys Soc Japan. 1988 Sep;57(9):2908–2911.
[96] Ando Y, Segawa K, Komiya S, et al. Electrical resistivity anisotropy from self-organized one dimensionality in high-temperature superconductors. Phys Rev Lett. 2002 Mar;88(13):137005.
[97] Ando Y, Segawa K. Magnetoresistance of untwinned $YBa_2Cu_3O_y$ single crystals in a wide range of doping: anomalous Hole-Doping dependence of the coherence length. Phys Rev Lett. 2002 Apr;88(16):167005.
[98] Tranquada JM, Sternlieb BJ, Axe JD, et al. Evidence for stripe correlations of spins and holes in copper oxide superconductors. Nature. 1995 Jun;375(6532):561–563.
[99] Tranquada JM. Stripes and superconductivity in cuprates. Physica B. 2012 Jun;407(11):1771–1774.
[100] Huang EW, Mendl CB, Liu S, et al. Numerical evidence of fluctuating stripes in the normal state of high-$T_c$ cuprate superconductors. Science. 2017 Dec;358(6367):1161–1164.
[101] Mitrano M, Lee S, Husain AA, et al. Ultrafast time-resolved x-ray scattering reveals diffusive charge order dynamics in $La_{2-x}Ba_xCuO_4$. Sci Adv. 2019;5(8):699.
[102] Hussey NE, Gordon-Moys H, Kokal J, et al. Generic strange-metal behaviour of overdoped cuprates. J Phys: Conf Ser. 2013 Jul;449:012004.
[103] Varma CM, Schmitt-Rink S, Abrahams E. Charge transfer excitations and superconductivity in ionic metals. Solid State Commun. 1987 Jun;62(10):681–685.
[104] Cooper RA, Wang Y, Vignolle B, et al. Anomalous criticality in the electrical resistivity of $La_{2-x}Sr_xCuO_4$. Science. 2009 Jan;323(5914):603–607.
[105] Proust C, Boaknin E, Hill RW, et al. Heat transport in a strongly overdoped cuprate: Fermi liquid and a pure d-Wave BCS superconductor. Phys Rev Lett. 2002 Sep;89(14):147003.
[106] Lee PA, Nagaosa N, Wen XG. Doping a Mott insulator: physics of high-temperature superconductivity. Rev Mod Phys. 2006 Jan;78(1):17–85.
[107] Hussey NE. Phenomenology of the normal state in-plane transport properties of high-$T_c$ cuprates. J Phys Condens Matter. 2008 Mar;20(12):123201.
[108] Shen KM, Davis JCS. Cuprate high-Tc superconductors. Materials Today. 2008 Sep;11(9):14–21.
[109] Scalapino DJ. A common thread: the pairing interaction for unconventional superconductors. Rev Mod Phys. 2012 Oct;84(4):1383–1417.
[110] Islam RS, Naqib SH, Islam AKMA. Modeling of the complex doping dependence of $dT_c/dP$ of $YBa_2Cu_3O_{6+x}$. J Supercond. 2000 Jun;13(3):485–490.
[111] Wesche R. A survey of superconducting cuprates. In: Wesche R, editor. High-temperature superconductors: materials, properties, and applications. Boston, MA: Springer US; 1998. p. 79–132. (Electronic Materials: Science & Technology).
[112] Radaelli PG, Hinks DG, Mitchell AW, et al. Structural and superconducting properties of $La_{2-x}Sr_xCuO_4$ as a function of Sr content. Phys Rev B. 1994 Feb;49(6):4163–4175.
[113] Momma K, Izumi F. VESTA 3 for three-dimensional visualization of crystal, volumetric and morphology data. J Appl Cryst. 2011 Dec;44(6):1272–1276.
[114] Cava RJ, van Dover RB, Batlogg B, et al. Bulk superconductivity at 36 K in $La_{1.8}Sr_{0.2}CuO_4$. Phys Rev Lett. 1987 Jan;58(4):408–410.
[115] Park C, Snyder RL. Structures of high-temperature cuprate superconductors. J Amer Ceramic Soc. 1995;78(12):3171–3194.

[116] Billinge SJL, Kwei GH, Lawson AC, et al. Superconductivity and the low-temperature orthorhombic to tetragonal phase transition in $La_{2-x}Ba_xCuO_4$. Phys Rev Lett. 1993 Sep;71(12):1903–1906.
[117] Suzuki T, Fujita T. Structural phase transition in (La1-xBax)2CuO4-$\delta$. Physica C. 1989 Jun;159(1–2):111–116.
[118] Bozin E, Zhong R, Knox K, et al. Reconciliation of local and long range tilt correlations in underdoped $La_{2-x}Ba_xCuO_4$. Phys Rev B. 2014 Dec;91:054521.
[119] Fabbris G, Hücker M, Gu G, et al. Local structure, stripe pinning, and superconductivity in $La_{1.875}Ba_{0.125}CuO_4$ at high pressure. Phys Rev B. 2013 Aug;88:060507.
[120] Axe JD, Moudden AH, Hohlwein D, et al. Structural phase transformations and superconductivity in $La_{2-x}Ba_xCuO_4$. Phys Rev Lett. 1989 Jun;62(23):2751–2754.
[121] Moodenbaugh AR, Xu Y, Suenaga M, et al. Superconducting properties of $La_{2-x}Ba_xCuO_4$. Phys Rev B. 1988 Sep;38(7):4596–4600.
[122] Chang J, Sassa Y, Guerrero S, et al. Electronic structure near the 1/8-anomaly in La-based cuprates. New J Phys. 2008 Oct;10(10):103016.
[123] Kivelson SA, Bindloss IP, Fradkin E, et al. How to detect fluctuating stripes in the high-temperature superconductors. Rev Mod Phys. 2003 Oct;75(4):1201–1241.
[124] Vojta M. Lattice symmetry breaking in cuprate superconductors: stripes, nematics, and superconductivity. Adv Phys. 2009 Nov;58(6):699–820.
[125] Xiong Q, Chu JW, Sun YY, et al. High-pressure study of the anomalous isotope effect in $La_{2-x}A_xCuO_4$ with A = Sr or Ba. Phys Rev B. 1992 Jul;46(1):581–584.
[126] Pickett WE, Cohen RE, Krakauer H. Lattice instabilities, isotope effect, and high-$T_c$ superconductivity in $La_{2-x}Ba_xCuO_4$. Phys Rev Lett. 1991 Jul;67(2):228–231.
[127] Tranquada JM, Axe JD, Ichikawa N, et al. Neutron-scattering study of stripe-phase order of holes and spins in $La_{1.48}Nd_{0.4}Sr_{0.12}CuO_4$. Phys Rev B. 1996 Sep;54(10):7489–7499.
[128] Zhou JS, Goodenough JB. Electron-lattice coupling and stripe formation in $La_{2-x}Ba_xCuO_4$. Phys Rev B. 1997 Sep;56(10):6288–6294.
[129] Guguchia Z, Maisuradze A, Ghambashidze G, et al. Tuning the static spin-stripe phase and superconductivity in $La_{2-x}Ba_xCuO_4$ (x = 1/8) by hydrostatic pressure. New J Phys. 2013 Sep;15(9):093005.
[130] Sadewasser S, Schilling JS, Paulikas AP, et al. Pressure dependence of $T_c$ to 17 GPa with and without relaxation effects in superconducting $YBa_2Cu_3O_x$. Phys Rev B. 2000 Jan;61(1):741–749.
[131] Kubiak R, Westerholt K, Pelka G, et al. Pressure dependence of the superconducting transition temperature of Bi- and Tl-based high-$T_c$ superconductors. Physica C. 1990 Apr;166(5):523–529.
[132] Osada M, Kakihana M, Asai T, et al. High-pressure Raman study of $Bi_2Sr_2CaCu_2O_{8+\delta}$:indications of strong bond-strength hierarchy and pressure-induced charge transfer. Physica C. 2000 Nov;341-348:2241–2242.
[133] Osada M, Kakihana M, Käll M, et al. Pressure-induced effects in high-$T_c$ superconductors: Raman scattering as a probe of charge-lattice dynamics under high pressure. Physica C. 2001 Sep;357-360:142–145.
[134] Rosenstein B, Shapiro BY. Apical oxygen vibrations dominant role in d-wave cuprate superconductivity and its interplay with spin fluctuations. J Phys Commun. 2021 May;5(5):055013.
[135] Neumeier JJ, Zimmermann HA. Pressure dependence of the superconducting transition temperature of $YBa_2Cu_3O_7$ as a function of carrier concentration: a test for a simple charge-transfer model. Phys Rev B. 1993 Apr;47(13):8385–8388.
[136] Almasan CC, Han SH, Lee BW, et al. Pressure dependence of $T_c$ and charge transfer in $YBa_2Cu_3O_x$(6.35<x<7) single crystals. Phys Rev Lett. 1992 Jul;69(4):680–683.
[137] Gupta RP, Gupta M. Relationship between pressure-induced charge transfer and the superconducting transition temperature in $YBa_2Cu_3O_{7-\delta}$ superconductors. Phys Rev B. 1995 May;51(17):11760–11766.
[138] Zhang JB, Struzhkin VV, Yang W. Pressure tuning of superconductivity independent of disorder in Tl, $_2Ba_2CaCu_2O_{8+\delta}$. 2015 Feb. Available from: arXiv:150202227.

[139] Ambrosch-Draxl C, Sherman EY, Auer H, et al. Pressure-induced hole doping of the Hg-based cuprate superconductors. Phys Rev Lett. 2004 May;92(18):187004.
[140] Sakakibara H, Suzuki K, Usui H, et al. First-principles band structure and FLEX approach to the pressure effect on $T_c$ of the cuprate superconductors. J Phys: Conf Ser. 2013 Aug;454:012021.
[141] Liarokapis E, Lampakis D, Palles D, et al. A Raman view of local lattice distortions and charge transfer in cuprates. J Phys Chem Solids. 2006 Sep;67(9):2065–2071.
[142] Cyr-Choinière O, LeBoeuf D, Badoux S, et al. Sensitivity of $T_c$ to pressure and magnetic field in the cuprate superconductor $YBa_2Cu_3O_y$: evidence of charge-order suppression by pressure. Phys Rev B. 2018 Aug;98(6):064513.
[143] Guguchia Z, Khasanov R, Shengelaya A, et al. Cooperative coupling of static magnetism and bulk superconductivity in the stripe phase of $La_{2-x}Ba_xCuO_4$: pressure- and doping-dependent studies. Phys Rev B. 2016 Dec;94(21):214511.
[144] Locquet JP, Perret J, Fompeyrine J, et al. Doubling the critical temperature of $La_{1.9}Sr_{0.1}CuO_4$ using epitaxial strain. Nature. 1998 Jul;394(6692):453–456.
[145] Bozovic I, Logvenov G, Belca I, et al. Epitaxial strain and superconductivity in $L_{2-x}Sr_xCuO_4$ thin films. Phys Rev Lett. 2002 Aug;89(10):107001.
[146] Machida K. Magnetism in $La_2CuO_4$ based compounds. Physica C. 1989 Apr;158(1):192–196.
[147] Ido M, Yamada N, Oda M, et al. Pressure effect on superconductivity and low-temperature phase transition in Ba-doped $La_2CuO_4$. Physica C. 1991 Dec;185–189:911–912.
[148] Yamada N, Ido M. Pressure effects on superconductivity and structural phase transitions in La2-xMxCuO4 (M Ba, Sr). Physica C. 1992 Dec;203(3):240–246.
[149] Doiron-Leyraud N, Cyr-Choinière O, Badoux S, et al. Pseudogap phase of cuprate superconductors confined by Fermi surface topology. Nat Commun. 2017 Dec;8(1):1–7.
[150] Campuzano JC, Ding H, Fretwell H. BSCCO superconductors: hole-like Fermi surface and doping dependence of the gap function. Vol. 117, 1999 Aug.
[151] Wang Y, Li L, Ong NP. Nernst effect in high-$T_c$ superconductors. Phys Rev B. 2006 Jan;73(2):024510.
[152] Wang Y, Xu ZA, Kakeshita T, et al. Onset of the vortexlike Nernst signal above $T_c$ in $La_{2-x}Sr_xCuO_4$ and $B_2Sr_{2-y}La_yCuO_6$. Phys Rev B. 2001 Nov;64(22):224519.
[153] Cyr-Choinière O, Daou R, Laliberté F, et al. Enhancement of the Nernst effect by stripe order in a high-$T_c$ superconductor. Nature. 2009 Apr;458(7239):743–745.
[154] Xu ZA, Ong NP, Wang Y, et al. Vortex-like excitations and the onset of superconducting phase fluctuation in underdoped La2-xSrxCuO4. Nature. 2000 Aug;406(6795):486–488.
[155] Fujii T, Matsushima T, Maruoka T, et al. Effect of stripe order strength for the Nernst effect in $La_2$-xSrxCuO$_4$ single crystals. Physica C: Superconductivity and Its Applications. 2010 Dec;470:S21–S22.
[156] Collignon C, Badoux S, Afshar SAA, et al. Fermi-surface transformation across the pseudogap critical point of the cuprate superconductor $La_{1.6-x}Nd_{0.4}Sr_xCuO_4$. Phys Rev B. 2017 Jun;95(22):224517.
[157] Cyr-Choinière O, Daou R, Laliberté F, et al. Pseudogap temperature $T^*$ of cuprate superconductors from the Nernst effect. Phys Rev B. 2018 Feb;97(6):064502.
[158] Daou R, Doiron-Leyraud N, LeBoeuf D, et al. Linear temperature dependence of resistivity and change in the Fermi surface at the pseudogap critical point of a high-$T_c$ superconductor. Nat Phys. 2009 Jan;5(1):31–34.
[159] Guguchia Z, Das D, Wang C, et al. Using uniaxial stress to probe the relationship between competing superconducting states in a cuprate with spin-stripe order. Phys Rev Lett. 2020 Aug;125(9):097005.
[160] Tranquada JM, Gu GD, Hücker M, et al. Evidence for unusual superconducting correlations coexisting with stripe order in $La_{1.875}Ba_{0.125}CuO_4$. Phys Rev B. 2008 Nov;78(17):174529.
[161] Takeshita N, Sasagawa T, Sugioka T, et al. Gigantic anisotropic uniaxial pressure effect on superconductivity within the $CuO_2$ plane of $La_{1.64}Eu_{0.2}Sr_{0.16}CuO_4$: strain control of stripe criticality. J Phys Soc Jpn. 2004 May;73(5):1123–1126.

[162] Kamminga ME, Krighaar KML, Rømer AT. et al Evolution of magnetic stripes under uniaxial stress in $La_{1.885}Ba_{0.115}CuO_4$ studied by neutron scattering. 2022 Mar. Available from: arXiv:220300558.
[163] Zandbergen HW, Gronsky R, Wang K, et al. Structure of $CuO_2$ double layers in superconducting $YBa_2Cu_3O_7$. Nature. 1988 Feb;331(6157):596–599.
[164] Zhang H, Gauquelin N, Botton GA, et al. Attenuation of superconductivity in manganite/cuprate heterostructures by epitaxially-induced CuO intergrowths. Appl Phys Lett. 2013 Jul;103(5):052606.
[165] Affronte M, Decroux M, Genoud JY, et al. Hall effect in YBCO "247" ceramics. Physica C: Superconductivity. 1991 Dec;185-189:1289–1290.
[166] Zhang C, Zhang H, Wei JYT. Phase transformation in ultrathin Y-Ba-Cu-O films by high-pressure oxygen annealing. Int J Mod Phys B. 2017 Oct;31(25):1745010.
[167] Junod A, Bezinge A, Graf T, et al. Structure, resistivity, critical field, specific-Heat jump at $T_c$, meissner effect, a.c. and d.c. susceptibility of the high-$T_c$ superconductor $YBa_2Cu_3O_7$. Europhysics Letters. 1987 Jul;4(2):247–252.
[168] Karpinski J, Kaldis E, Rusiecki S, et al. Two new bulk superconducting phases in the Y-Ba-Cu-O system: $YBa_2Cu_{3.5}O_{7+x}$ ($T_c \approx 40$ K) and $YBa_2Cu_4O_{8+x}$ ($T_c \approx 80$ K). J Less Common Met. 1989 May;150:129–137.
[169] Huang H, Jang H, Fujita M, et al. Modification of structural disorder by hydrostatic pressure in the superconducting cuprate $YBa_2Cu_3O_{6.73}$. Phys Rev B. 2018 May;97(17):174508.
[170] Souliou SM, Gretarsson H, Garbarino G, et al. Rapid suppression of the charge density wave in $YBa_2Cu_3O_{6.6}$ under hydrostatic pressure. Phys Rev B. 2018 Jan;97(2):020503.
[171] Vinograd I, Zhou R, Mayaffre H, et al. Nuclear magnetic resonance study of charge density waves under hydrostatic pressure in $YBa_2Cu_3O_y$. Phys Rev B. 2019 Sep;100(9):094502.
[172] Sadewasser S, Wang Y, Schilling JS, et al. Pressure-dependent oxygen ordering in strongly underdoped $YBa_2Cu_3O_{7-y}$. Phys Rev B. 1997 Dec;56(21):14168–14175.
[173] Veal B, Paulikas A, You H, et al. Observation of temperature-dependent site disorder in $YBa_2Cu_3O_{7-y}$ below 150 degrees C. Phys Rev B. 1990 Oct;42(10):6305–6316.
[174] Calamiotou M, Gantis A, Siranidi E, et al. Pressure-induced lattice instabilities and superconductivity in $YBa_2Cu_4O_8$ and optimally doped $YBa_2Cu_3O_{7-\delta}$. Phys Rev B. 2009 Dec;80(21):214517.
[175] Akhtar ZN, Akhtar MJ, Clark SM, et al. The effect of pressure on the crystal structures of some bismuth based superconductors. Solid State Commun. 1994 Nov;92(6):535–540.
[176] Fietz WH, Dietrich MR, Ecke J. Possible transformation of $YBa_2Cu_3O_7$ under pressure. Z Phys B. 1987 Mar;69(1):17–20.
[177] Nakayama A, Onda Y, Yamada S, et al. Collapse of CuO double chains and suppression of superconductivity in high-pressure phase of $YBa_2Cu_4O_8$. J Phys Soc Japan. 2014 Aug;83(9):093601.
[178] Ludwig H, Fietz W, Dietrich M, et al. X-ray investigations of $Y_1Ba_2Cu_4O_8$ under high pressure. Physica C. 1990 May;167(3-4):335–338.
[179] Nelmes R, Loveday J, Kaldis E, et al. The crystal structure of $YBa_2Cu_4O_8$ as a function of pressure up to 5 GPa. Physica C. 1990 Dec;172(3-4):311–324.
[180] McElfresh MW, Maple MB, Yang KN, et al. Onset of superconductivity at 107 K in $YBa_2Cu_3O_{7-\delta}$ at high pressure. Appl Phys A. 1988 Apr;45(4):365–368.
[181] Chen XJ, Lin HQ, Gong CD. Pressure dependence of $T_c$ in Y-Ba-Cu-O superconductors. Phys Rev Lett. 2000 Sep;85(10):2180–2183.
[182] Dagotto E, Nazarenko A, Moreo A. Antiferromagnetic and van hove scenarios for the cuprates: taking the best of both worlds. Phys Rev Lett. 1995 Jan;74(2):310–313.
[183] Weng ZY, Sheng DN, Ting CS. Isotropic dispersion, line shape, and remnant Fermi surface in one hole problem. 1999 Nov. Available from: arXiv:cond-mat/9908032.
[184] Lu DH, Feng DL, Armitage NP, et al. Superconducting gap and strong in-Plane anisotropy in untwinned $YBa_2Cu_3O_{7-d}$. Phys Rev Lett. 2001 May;86(19):4370–4373.

[185] Damascelli A, Lu DH, Shen ZX. From Mott insulator to overdoped superconductor: evolution of the electronic structure of cuprates studied by ARPES. J Electron Spectros Relat Phenomena. 2001 Jun;117-118:165–187.
[186] Metzger J, Weber T, Fietz WH, et al. Separation of the intrinsic pressure effect on $T_c$ of $YBa_2Cu_3O_{6.7}$ from a $T_c$ enhancement caused by pressure-induced oxygen ordering. Physica C. 1993 Sep;214(3):371–376.
[187] Jorgensen JD, Pei S, Lightfoot P, et al. Pressure-induced charge transfer and $dT_c/dP$ in $YBa_2Cu_3O_{7-x}$. Physica C. 1990 Oct;171(1):93–102.
[188] Neumeier JJ, Maple MB, Torikachvili MS. Pressure dependence of the superconducting transition temperature of $(Y_{1-x}Pr_x)Ba_2Cu_3O_{7-\delta}$ compounds; evidence for 4f electron hybridization. Physica C: Superconductivity. 1988 Nov;156(4):574–578.
[189] Maple MB, Paulius LM, Neumeir JJ. On the pressure dependence of $T_c$ of the $Y_{1-x}Pr_xBa_2Cu_3O_{7-\delta}$ system. Physica C: Superconductivity. 1992 May;195(1):64–70.
[190] Cardona M. Light scattering in solids I: introductory concepts. In: Cardona M, editors. Topics in applied physics. 2nd ed. Berlin Heidelberg: Springer-Verlag; 1983. (Light Scattering).
[191] Fluegel B, Mialitsin AV, Beaton DA, et al. Electronic Raman scattering as an ultra-sensitive probe of strain effects in semiconductors. Nat Comm. 2015 May;6(1):7136.
[192] Hemley RJ, Mao HK. Single-crystal micro-Raman spectroscopy of phases in the Y-Ba-Cu-O superconductor. Phys Rev Lett. 1987 Jun;58(22):2340–2342.
[193] Monien H, Zawadowski A. Theory of Raman scattering with final-state interaction in high-$T_c$ BCS superconductors: collective modes. Phys Rev B. 1990 May;41(13):8798–8810.
[194] Nemetschek R, Opel M, Hoffmann C, et al. Pseudogap and superconducting gap in the electronic Raman spectra of underdoped cuprates. Phys Rev Lett. 1997 Jun;78(25):4837–4840.
[195] Devereaux TP, Hackl R. Inelastic light scattering from correlated electrons. Rev Mod Phys. 2007 Jan;79(1):175–233.
[196] Kendziora C, Pelloquin D, Daignere A, et al. Polarized electronic Raman scattering in high-$T_c$ superconductors. Physica C. 2000 Nov;341-348:2189–2192.
[197] Goncharov AF, Struzhkin VV. Raman spectroscopy of metals, high-temperature superconductors and related materials under high pressure. J Raman Spectrosc. 2003;34(7-8):532–548.
[198] Monien H, Zawadowski A. Theory of interband electron Raman scattering in $YBa_2Cu_3O_7$: a probe of unconventional superconductivity. Phys Rev Lett. 1989 Aug;63(8):911–914.
[199] Syassen K, Hanfland M, Strössner K, et al. Effect of pressure on Raman modes in $MBa_2Cu_3O_7$-type materials. Physica C. 1988 Jun;153–155:264–265.
[200] Lampakis D, Palles D, Liarokapis E, et al. Hydrostatic-pressure-induced phase separation in the $YBa_2Cu_4O_8$ superconductor. Phys Rev B. 2005 Jul;72(1):014539.
[201] Goncharov A, Muinov T, Uvarova T, et al. Raman scattering of $YBa_2Cu_3O_x$ single crystals with different oxygen contents at high pressures. JTEP Lett. 1991;54:111.
[202] Kakihana M, Arashi H, Yashima M, et al. Anomalous behaviour of the 147 $cm^{-1}$ Cu(2) Raman mode in $YBa_2Cu_4O_8$ under high pressure, signature of change in the electronic state of the CuO2 plane. Physica C. 1994 Sep;230(1):199–206.
[203] Wu T, Mayaffre H, Krämer S, et al. Emergence of charge order from the vortex state of a high-temperature superconductor. Nat Commun. 2013 Jul;4(1):1–6.
[204] Blanco-Canosa S, Frano A, Schierle E, et al. Resonant x-ray scattering study of charge-density wave correlations in $YBa_2Cu_3O_{6+x}$. Phys Rev B. 2014 Aug;90(5):054513.
[205] Hucker M, Christensen NB, Holmes AT, et al. Competing charge, spin, and superconducting orders in underdoped $YBa_2Cu_3O_y$. Phys Rev B. 2014 Aug;90(5):054514.
[206] LeBoeuf D, Doiron-Leyraud N, Levallois J, et al. Electron pockets in the Fermi surface of hole-doped high-$T_c$ superconductors. Nature. 2007 Nov;450(7169):533–536.
[207] Putzke C, Malone L, Badoux S, et al. Inverse correlation between quasiparticle mass and $T_c$ in a cuprate high-$T_c$ superconductor. Sci Adv. 2016 Mar;2(3):e1501657.
[208] Putzke C, Ayres J, Buhot J, et al. Charge order and superconductivity in underdoped $YBa_2Cu_3O_{7-\delta}$ under pressure. Phys Rev Lett. 2018 Mar;120(11):117002.

[209] Jurkutat M, Rybicki D, Sushkov O, et al. Distribution of electrons and holes in cuprate superconductors as determined from $^{17}O$ and $^{63}Cu$ nuclear magnetic resonance. Phys Rev B. 2014 Oct;90:140504(R).
[210] Grant DM, Harris RK. Encyclopedia of nuclear magnetic resonance. Vol. 9, advances in NMR.
[211] Schrieffer JR. Handbook of high-temperature superconductivity: theory and experiment. New York: Springer-Verlag; 2007.
[212] Meissner T, Goh SK, Haase J, et al. High-pressure spin shifts in the pseudogap regime of superconducting $YBa_2Cu_4O_8$ as revealed by $^{17}O$ NMR. Phys Rev B. 2011 Jun;83(22):220517.
[213] Zeng GQ, Mito T, Yoshio K, et al. 63-Cu NMR and NQR studies of high-$T_c$ cuprates under pressure. Physica C. 1995 Mar;243(3-4):337–341.
[214] Cvitanić T, Pelc D, Požek M, et al. 17O-NMR Knight shift study of the interplay between superconductivity and pseudogap in $(Ca_xLa_{1-x})(Ba_{1.75-x}La_{0.25+x})Cu_3O_y$. Phys Rev B. 2014 Aug;90 (5):054508.
[215] Zheng Gq, Kitaoka Y, Asayama K, et al. 17O NMR study of local hole density and spin dynamics in $YBa_2Cu_4O_8$. Phys C: Superconduct Its Appl. 1992 Apr;193(1):154–162.
[216] Alloul H, Ohno T, Mendels P. 89-Y NMR evidence for a Fermi-liquid behavior in $YBa_2Cu_3O_{6+x}$. Phys Rev Lett. 1989 Oct;63(16):1700–1703.
[217] Jurkutat M, Kattinger C, Tsankov S. How pressure enhances the critical temperature for high temperature superconductivity in $YBa_2Cu_3O_{6+y}$. 2021 Sep. Available from: arXiv:210910157.
[218] Rybicki D, Jurkutat M, Reichardt S, et al. Perspective on the phase diagram of cuprate high-temperature superconductors. Nat Commun. 2016 May;7(1):11413.
[219] Vovk RV, Solovjov AL. Electric transport and the pseudogap in the 1-2-3 HTSC system, under all-around compression (Review article). Low Temp Phys. 2018 Feb;44(2):81–113.
[220] Solovjov AL, Omelchenko LV, Vovk RV, et al. Peculiarities in the pseudogap behavior in optimally doped $YBa_2Cu_3O_{7-\delta}$ single crystals under pressure up to 1GPa. Curr Appl Phys. 2016 Sep;16(9):931–938.
[221] Solovjov AL, Omelchenko LV, Vovk RV, et al. Hydrostatic-pressure effects on the pseudogap in slightly doped $YBa_2Cu_3O_{7-\delta}$ single crystals. Physica B. 2016 Jul;493:58–67.
[222] Ginsberg D. Physical properties of high temperature superconductors I. Vol. 30, Singapore: World Scientific Publishing Co. Pvt. Ltd.; 1990.
[223] Matsuda Y, Hirai T, Komiyama S, et al. Magnetoresistance of c-axis-oriented epitaxial $YBa_2Cu_3O_{7-x}$ films above $T_c$. Phys Rev B. 1989 Sep;40(7):5176–5179.
[224] Triscone JM, Fischer O, Brunner O, et al. $YBa_2Cu_3O_7PrBa_2Cu_3O_7$ superlattices: properties of ultrathin superconducting layers separated by insulating layers. Phys Rev Lett. 1990 Feb;64 (7):804–807.
[225] Vovk RV, Nazyrov ZF, Goulatis IL, et al. Metal-to-insulator transition in $Y_{1-x}Pr_xBa_2Cu_3O_{7-\delta}$ single crystals with various praseodymium contents. Phys C: Superconduct. 2013 Feb;485:89–91.
[226] Solovjov AL, Dmitriev VM. Fluctuation conductivity and pseudogap in $Y_{1-x}Pr_xBa_2Cu_3O_{7-y}$ films. Low Temp Phys. 2006 Jun;32(6):576–581.
[227] Solovjov AL, Omelchenko LV, Petrenko EV, et al. Peculiarities of pseudogap in $Y_{0.95}Pr_{0.05}Ba_2Cu_3O_{7-d}$ single crystals under pressure up to 1.7 GPa. Sci Rep. 2019 Dec;9 (1):20424.
[228] Nagasawa H, Sugawara T. The magnetism of praseodymium metal. J Phys Soc Japan. 1967 Oct;23(4):701–710.
[229] Solovjov AL, Omelchenko LV, Vovk RV, et al. Pseudogap and fluctuation conductivity in $Y_{1-x}Pr_xBa_2Cu_3O_{7-\delta}$ single crystals with different concentrations of praseodymium. Low Temp Phys. 2017 Jul;43(7):841–847.
[230] Solovjov AL, Omelchenko LV, Stepanov VB, et al. Specific temperature dependence of pseudogap in $YBa_2Cu_3O_{7-\delta}$ nanolayers. Phys Rev B. 2016 Dec;94(22):224505.
[231] Solovjov AL, Dmitriev VM. Resistive studies of the pseudogap in YBCO films with consideration of the transition from BCS to Bose-Einstein condensation. Low Temp Phys. 2006 Feb;32(2):99–108.

[232] Solovjov AL, Tkachenko MA, Vovk RV, et al. Peculiarities of fluctuation conductivity and pseudogap behavior in slightly doped $HoBa_2Cu_3O_{7-d}$ single crystals under pressure. Low Temp Phys. 2011 Oct;37(10):840–842.
[233] Kraut O, Meingast C, Bräuchle G, et al. Uniaxial pressure dependence of $T_c$ of untwinned $YBa_2Cu_3O_x$ single crystals for $x = 6.5-7$. Physica C. 1993 Jan;205(1):139–146.
[234] Welp U, Grimsditch M, Fleshler S, et al. Effect of uniaxial stress on the superconducting transition in $YBa_2Cu_3O_7$. Phys Rev Lett. 1992 Oct;69(14):2130–2133.
[235] Angel R, Bujak M, Zhao J, et al. Effective hydrostatic limits of pressure media for high-pressure crystallographic studies. J Appl Cryst. 2007 Feb;40:26–32.
[236] Klotz S, Schilling JS. Hydrostatic pressure dependence of the superconducting transition temperature to 7 GPa in $Bi_2Ca_1Sr_2Cu_2O_{8+y}$ as a function of oxygen content. Phys C: Superconduct. 1993 May;209(4):499–506.
[237] Klotz S, Chervin JC, Munsch P, et al. Hydrostatic limits of 11 pressure transmitting media. J Phys D Appl Phys. 2009 Apr;42(7):075413.
[238] Meingast C, Kraut O, Wolf T, et al. Large a-b anisotropy of the expansivity anomaly at $T_c$ in untwinned $YBa_2Cu_3O_{7-\delta}$. Phys Rev Lett. 1991 Sep;67(12):1634–1637.
[239] Benischke R, Weber T, Fietz W, et al. The effect of high hydrostatic pressure on $T_c$ of $YBa_2Cu_3O_x$ as a function of the oxygen content. Physica C. 1992 Dec;203(3-4):293–298.
[240] Kim HH, Souliou SM, Barber ME, et al. Uniaxial pressure control of competing orders in a high-temperature superconductor. Science. 2018 Nov;362(6418):1040–1044.
[241] Kim HH, Lefrançois E, Kummer K, et al. Charge density waves in $YBa_2Cu_3O_{6.67}$ probed by resonant x-ray scattering under uniaxial compression. Phys Rev Lett. 2021 Jan;126(3):037002.
[242] Chang J, Blackburn E, Ivashko O, et al. Magnetic field controlled charge density wave coupling in underdoped $YBa_2Cu_3O_{6+x}$. Nat Comm. 2016 May;7:1–7.
[243] Gerber S, Jang H, Nojiri H, et al. Three-dimensional charge density wave order in $YBa_2Cu_3O_{6.67}$ at high magnetic fields. Science. 2015 Nov;350(6263):949–952.
[244] Quilty J, Trodahl H, Pooke D. Electronic Raman scattering from doping dependence of the pseudogap and anomalous peak. Phys Rev B. 1998;57(18):R11097–R11100.
[245] Mito M, Imakyurei T, Deguchi H, et al. Uniaxial strain effects on cuprate superconductor $YBa_2Cu_4O_8$. J Phys Soc Japan. 2012 Nov;81:3709.
[246] Mito M, Imakyurei T, Deguchi H, et al. Effective disappearance of the meissner signal in the cuprate superconductor $YBa_2Cu_4O_8$ under uniaxial strain. J Phys Soc Japan. 2014 Jan;83(2):023705.
[247] Mito M, Ogata K, Goto H, et al. Uniaxial strain effects on the superconducting transition in re-doped Hg-1223 cuprate superconductors. Phys Rev B. 2017 Feb;95(6):064503.
[248] Miyatake T, Gotoh S, Koshizuka N, et al. Tc increased to 90 K in $YBa_2Cu_4O_8$ by Ca doping. Nature. 1989 Sep;341(6237):41–42.
[249] Takahashi H, Mori N, Miyatake T, et al. Pressure dependence of superconducting transition temperature in Ca-doped $YBa_2Cu_4O_8$. Phys C: Superconduct. 1990 May;167(3):297–300.
[250] Zhang H, Nguyen A, Gredig T. Strain-driven attenuation of superconductivity in heteroepitaxial perovskite/YBCO/perovskite thin films. 2017 Oct. Available from: ArXiv: 1710.10668.
[251] Fridman I, Gunawan L, Botton GA, et al. Scanning tunneling spectroscopy study of c-axis proximity effect in epitaxial bilayer manganite/cuprate thin films. Phys Rev B. 2011 Sep;84(10):104522.
[252] Hatano T, Kadowaki K, Nakamura K. Bi-2223/Bi-2234 superlattice – Its structural analysis and superconducting transition temperature. Conference on optics, electro-optics, and laser applications in science and engineering; 1994 Dec.
[253] Matheis DP, Snyder RL. The crystal structures and powder diffraction patterns of the bismuth and thallium ruddlesden-Popper copper oxide superconductors. Powder Diffr. 1990 Mar;5(1):8–25.
[254] Wesche R. High-temperature superconductors. In: Kasap S, Capper P, editors. Springer handbook of electronic and photonic materials. Cham: Springer International Publishing; 2017. p. 1–1 (Springer Handbooks).

[255] Olsen JS, Steenstrup S, Gerward L, et al. High pressure studies up to 50 GPa of Bi-based high-$T_c$ superconductors. Phys Scr. 1991 Aug;44(2):211–213.
[256] Wagner JL, Hunter BA, Hinks DG, et al. Structure and superconductivity of $HgBa_2Ca_2Cu_3O_{8+\delta}$. Phys Rev B. 1995 Jun;51(21):15407–15414.
[257] Sadewasser S, Schilling J, Wagner J, et al. Relaxation effects in the transition temperature of superconducting $HgBa_2CuO_{4+\delta}$. Phys Rev B. 1999;60(13):9827–9835.
[258] Watanabe H, Shirakawa T, Seki K, et al. Unified description of cuprate superconductors using four-band d-p model. Phys Rev Res. 2021 Aug;3(3):033157.
[259] Legros A, Loret B, Forget A, et al. Crystal growth and doping control of $HgBa_2CuO_{4+\delta}$, the model compound for high-T superconductors. Mater Res Bull. 2019 May;118:110479.
[260] Gatt R, Olsson E, Morawski A, et al. Hg-1212 and Hg-1223 single crystals: synthesis and characterisation. Phys C: Superconduct. 1997 Mar;276(3):270–276.
[261] Hassun H, Mahdi S, Al-Maiyaly BK. Study the universal behavior of $HgBa_2Ca_2Cu_{3-x}Te_xO_{8+\delta}$ superconducting thin films; 2018.
[262] Lokshin KA, Kuzemskaya IG, Kulikova LF, et al. High pressure synthesis of Hg-1234 and strongly-overdoped Hg-1223 phases. Phys C: Superconduct. 1997 May;279(1):11–17.
[263] Kajitani T, Hiraga K, Kikuchi M, et al. Structural changes of 2201-, 2212- and 2223-type Tl-oxide superconductors at temperatures below 630 K. Phys C: Superconduct. 1990 Apr;167(1):212–220.
[264] Subramanian MA, Calabrese JC, Torardi CC, et al. Crystal structure of the high-temperature superconductor $Tl_2Ba_2CaCu_2O_8$. Nature. 1988 Mar;332(6163):420–422.
[265] Torardi CC, Subramanian MA, Calabrese JC, et al. Crystal structure of $Tl_2Ba_2Ca_2Cu_3O_{10}$, a 125 K superconductor. Sciences. 1988 Apr;240(4852):631–634.
[266] Lang W, Sekirnjak C, Heine G, et al. Study of superconducting fluctuations in the high-temperature superconductors YBCO and BSCCO by magneto-transport measurements. International Conference on Science and Technology of Synthetic Metals; 1994 Jul. p. 692–692.
[267] Pradhan A. Magneto-transport and magnetization studies in BSCCO-2212 crystals. Indian J Pure Appl Phys. 1996 Sep;34:704–717.
[268] Chen XJ, Struzhkin VV, Hemley RJ, et al. High-pressure phase diagram of $Bi_2Sr_2CaCu_2O_{8+\delta}$ single crystals. Phys Rev B. 2004 Dec;70(21):214502.
[269] Looney C, Schilling JS, Shimakawa Y. The influence of pressure-induced relaxation effects on $T_c$ in $TlS_2CaCu_2O_{7-\delta}$. Physica C. 1998 Mar;297(3):239–246.
[270] Klehe AK, Schilling JS, Wagner JL, et al. Hydrostatic presure dependence of the superconducting transition temperature of $HgBa_2CaCu_2O_{6+\delta}$ and $HgBa_2Ca_2Cu_3O_{8+\delta}$. Physica C. 1994 Apr;223(3):313–320.
[271] Sieburger R, Müller P, Schilling JS. Pressure dependence of the superconducting transition temperature in $Bi_2Sr_2CaCu_2O_{8+y}$ as a function of oxygen content. Physica C. 1991 Oct;181(4):335–339.
[272] Klehe AK, Gangopadhyay AK, Diederichs J, et al. Dependence of the superconducting transition temperature of $HgBa_2CuO_{4+\delta}$ on hydrostatic pressure. Physica C. 1993 Aug;213(3):266–270.
[273] Klehe AK, Looney C, Schilling JS, et al. Pressure-induced oxygen ordering phenomena in high-c superconductors $T_c$. Physica C. 1996 Jan;257(1):105–116.
[274] Ginsberg DM. Physical properties of high temperature superconductors III. Singapore: World Scientific; 1992.
[275] de Mello EVL, Orlando MTD, Gonzaléz JL, et al. Pressure studies on a high-$T_c$ superconductor pseudogap and critical temperatures. Phys Rev B. 2002 Sep;66(9):092504.
[276] Statt BW, Song LM. Screening of the middle $CuO_2$ layer in $Bi_{1.6}Pb_{0.4}Sr_2Ca_2Cu_3O_{10}$ determined from Cu NMR. Phys Rev B. 1993 Aug;48(5):3536–3539.
[277] Scott B, Suard E, Tsuei C, et al. Layer dependence of the superconducting transition temperature of $HgBa_2Ca_{n-1}Cu_nO_{2n+2+\delta}$. Physica C. 1994 Sep;230(3-4):239–245.
[278] Kunisada S, Isono S, Kohama Y, et al. Observation of small Fermi pockets protected by clean $CuO_2$ sheets of a high-$T_c$ superconductor. Science. 2020 Aug;369(6505):833–838.

[279] Timofeev YA, Struzhkin VV, Hemley RJ, et al. Improved techniques for measurement of superconductivity in diamond anvil cells by magnetic susceptibility. Rev Sci Instrum. 2002 Feb;73(2):371–377.
[280] Guo J, Zhou Y, Huang C, et al. Crossover from two-dimensional to three-dimensional superconducting states in bismuth-based cuprate superconductor. Nat Phys. 2020 Mar;16(3):295–300.
[281] Takeuchi T, Kondo T, Kitao T, et al. Two- to three-Dimensional crossover in the electronic structure of (Bi, Pb)$_2$(Sr, La)$_2$CuO$_{6+\delta}$ from angle-Resolved photoemission spectroscopy. Phys Rev Lett. 2005 Nov;95(22):227004.
[282] Huang H, Lee SJ, Ikeda Y, et al. Two-dimensional superconducting fluctuations associated with charge density wave stripes in $La_{1.87}Sr_{0.13}Cu_{0.99}Fe_{0.01}O_4$. Phys Rev Lett. 2021 Apr;126(16):167001.
[283] Mukuda H, Shimizu S, Iyo A, et al. High-$T_c$ superconductivity and antiferromagnetism in multilayered copper oxides – a new paradigm of superconducting mechanism. J Phys Soc Japan. 2011 Dec;81(1):011008.
[284] Shimizu S, Tabata SI, Iwai S, et al. High-$T_c$ superconductivity and antiferromagnetism in multilayer cuprates: $^{63}$Cu- and $^{19}$F-NMR on five-layer $Ba_2Ca_4Cu_5O_{10}(F, O)_2$. Phys Rev B. 2012 Jan;85(2):024528.
[285] Auvray N, Loret B, Chibani S, et al. Exploration of Hg-based cuprate superconductors by Raman spectroscopy under hydrostatic pressure. Phys Rev B. 2021 May;103(19):195130.
[286] Chu CW, Smith TF, Gardner WE. Superconductivity of Rhenium and some Rhenium-Osmium alloys at high pressure. Phys Rev Lett. 1968 Jan;20(5):198–201.
[287] Lifshitz M. Anomalies of electron charactaristics of a metal in the high pressure region. Sov Phys. 1960;11(5):6.
[288] Takagi H, Cava RJ, Marezio M, et al. Disappearance of superconductivity in overdoped $La_{2-x}Sr_xCuO_4$ at a structural phase boundary. Phys Rev Lett. 1992 Jun;68(25):3777–3780.
[289] Hervieu M, Michel C, Domenges B, et al. Electron microscopy study of the superconductor $Bi_2Sr_2CaCu_2O_{8+\delta}$. Mod Phys Lett B. 1988 Mar;02(01):491–500.
[290] Shamrai VF. Crystal structures and superconductivity of bismuth high temperature superconductors (Review). Inorg Mater Appl Res. 2013 Jul;4(4):273–283.
[291] Antipov EV, Abakumov AM. Structural design of superconductors based in complex copper oxides. Phys Usp. 2008;51(2):180.
[292] Murnaghan FD. Finite deformations of an elastic solid. Am J Math. 1937;59(2):235–260.
[293] Zhang JB, Tang LY, Zhang J, et al. Pressure-induced isostructural phase transition in $Bi_2Sr_2CaCu_2O_{8+\delta}$. Chinese Phys C. 2013 Aug;37(8):088003.
[294] Gavarri JR, Monnereau O, Vacquier G, et al. Anisotropic compressibility of the orthorhombic phase $Bi_2Sr_2Ca_1Cu_2O_8$. Physica C. 1990 Dec;172(3):213–216.
[295] Yusheng H, Jiong X, Sheng J, et al. Ultrasonic investigations of the layered perovskite ceramic superconducting systems. Physica B. 1990 Aug;165–166:1283–1284.
[296] Kendziora C. Gapless superconductivity in Raman studies of cation substituted $Bi_2Sr_2CaCu_2O_{8+\delta}$. J Phys Chem Solids. 1998 Oct;59(10):1991–1993.
[297] Feiner LF, Grilli M, Di Castro C. Apical oxygen ions and the electronic structure of the high-$T_c$ cuprates. Phys Rev B. 1992 May;45(18):10647–10669.
[298] Zhou H, Yacoby Y, Butko VY, et al. Anomalous expansion of the copper-apical-oxygen distance in superconducting cuprate bilayers. Proc Natl Acad Sci. 2010 May;107(18):8103–8107.
[299] Klein MV. Electronic Raman scattering. In: Cardona M, editor. Light scattering in solids I: introductory concepts. Berlin, Heidelberg: Springer; 1983. p. 147–204. (Topics in applied physics).
[300] Yamanaka A, Kimura T, Minami F, et al. Superconducting gap excitations in Bi-Sr-Ca-Cu-O superconductor observed by Raman scattering. Jpn J Appl Phys. 1988 Oct;27(10A):L1902–L1905.
[301] Pan S, Hudson E, Ma J, et al. Imaging and identification of atomic planes of cleaved $Bi_2Sr_2CaCu_2O_{8+\delta}$ by high resolution scanning tunneling microscopy. Appl Phys Lett. 1998 Jul;73:58–60.
[302] Kendziora C, Pelloquin D, Villard G. Polarized electronic Raman scattering studies of underdoped and overdoped high-$T_c$ superconductors. J Low Temp Phys. 1999;117(5–6):1007–1011.

[303] Lyons KB, Liou SH, Hong M, et al. Raman detection of the superconducting gap in Ba-Y-Cu-O superconductors. Phys Rev B. 1987 Oct;36(10):5592–5594.
[304] Hackl R, Gläser W, Müller P, et al. Light-scattering study of the superconducting energy gap in Y Ba $_2$ Cu$_3$ O$_7$ single crystals. Phys Rev B. 1988 Oct;38(10):7133–7136.
[305] Devereaux TP, Einzel D, Stadlober B, et al. Electronic Raman scattering in high-$T_c$ superconductors: a probe of $d_{x^2-y^2}$ pairing. Phys Rev Lett. 1994 Jan;72(3):396–399.
[306] Devereaux TP, Einzel D. Electronic Raman scattering in superconductors as a probe of anisotropic electron pairing. Phys Rev B. 1995 Jun;51(22):16336–16357.
[307] Cuk T, Struzhkin VV, Devereaux TP, et al. Uncovering a pressure-tuned electronic transition in $Bi_{1.98}Sr_{2.06}Y_{0.68}Cu_2O_{8+\delta}$ using Raman scattering and x-ray diffraction. Phys Rev Lett. 2008 May;100(21):217003.
[308] Eggert JH, Hu JZ, Mao HK, et al. Compressibility of the $HgBa_2Ca_{n-1}Cu_nO_{2n+2+\delta}$ ($n$ = 1,2,3) high-temperature superconductors. Phys Rev B. 1994 Jun;49(21):15299–15304.
[309] Kopnin EM. Layered cuprates containing flat fragments: high-pressure synthesis, crystal structures and superconducting properties. Molecules. 2021 Jan;26(7):1862.
[310] Hammond R, Bormann R. Correlation between the in situ growth conditions of YBCO thin films and the thermodynamic stability criteria. Physica C. 1989 Dec;162-164:703–704.
[311] Bormann R, Nölting J. Stability limits of the perovskite structure in the Y-Ba-Cu-O system. Appl Phys Lett. 1989 May;54(21):2148–2150.
[312] Karpinski J, Schwer H, Conder K, et al. High pressure crystal growth of $Y_2Ba_4Cu_{6+n}O_{14+n}$and $HgBa_2Ca_{n-1}Cu_nO_{2n+2+\delta}$ superconductors. Solid State Ionics. 1997 Nov;101–103:985–990.
[313] Schwer H, Molinski R, Kopnin EM, et al. Structure and properties of 1256 and 1267 type $Hg_{1-x}Re_xBa_2Ca_{n-1}Cu_nO_{2n+2+4x+\delta}$ single crystals. J Solid State Chem. 1999 Mar;143(2):277–284.
[314] Capponi JJ, Tholence JL, Chaillout C, et al. High pressure synthesis and properties of the $HgBa_2Ca_{n-1}Cu_nO_{2n+2+\delta}$ ($n$ =1–6) superconductors. Physica C. 1994 Dec;235–240:146–149.
[315] Capponi JJ, Kopnin EM, Loureiro SM, et al. High-pressure synthesis and heat treatments of the $HgBa_2Ca_4Cu_5O_{12+\delta}$ and $HgBa_2Ca_5Cu_6O_{14+\delta}$ phases. Physica C. 1996 Jan;256(1):1–7.
[316] Bordet P, Le Floch S, Capponi JJ, et al. Gold substitution in mercury cuprate superconductors. Physica C. 1996 May;262(3):151–158.
[317] Bordet P, LeFloch S, Chaillout C, et al. $AuBa_2(Y_{1-x}, Ca_x)Cu_2O_7$: a new superconducting gold cuprate with $T_c$ above 80 K. Physica C. 1997 Mar;276(3):237–244.
[318] Bordet P, Kopnin EM, Sato A, et al. Structure analysis of superconducting Au-1212 cuprate. Supercond Sci Technol. 2003 Apr;16(6):685–689.
[319] Kopnin EM, Loureiro SM, Asaka T, et al. New family of Au-based superconductors $AuBa_2Ca_{n-1}Cu_nO_{2n+3}$ ($n$ = 3,4). Chem Mater. 2001 Sep;13(9):2905–2908.
[320] Kopnin EM, Schwer H, Jun J, et al. $Ca_{1-x}R_xCuO_2$ (R = Sr, La) single crystals with infinite-layer structure: high Ar gas pressure synthesis and properties. Physica C. 1997 Aug;282–287:483–484.
[321] Kopnin EM, Sato A, Asaka T, et al. Structure analysis of Au-containing cuprate of $Au_{1+x}Ba_2Ca_2Cu_{3-x}O_9$ (Au-1223). Physica C. 2003 May;387(3):406–410.
[322] Iyo A, Tanaka Y, Tokumoto M, et al. High-pressure synthesis and properties of $Ba_2Ca_{n-1}Cu_nO_{2n}(O, F)_2$ ($n$ =2–5) superconductors. Physica C. 2001 Dec;366(1):43–50.
[323] Iyo A, Hirai M, Tokiwa K, et al. Crystal growth of $Ba_2Ca_{n-1}Cu_nO_{2n}(O, F)_2$($n$ = 3 and 4) multi-layered superconductors under high pressure. Supercond Sci Technol. 2003 Nov;17(1):143–147.
[324] Iyo A, Hirai M, Tokiwa K, et al. Preparation of polycrystals with various $T_c$ and single crystal growth of $Ba_2Ca_3Cu_4O_8(O_{1-y}F_y)_2$ under high pressure. Physica C. 2003 Oct;392–396:140–144.
[325] Shirage PM, Shivagan DD, Crisan A, et al. Superconductivity at 108 K in the simplest non-toxic double-layer cuprate of $Ba_2CaCu_2O_4(O, F)_2$. J Phys: Conf Ser. 2008 Feb;97:012163.
[326] Shirage PM, Shivagan DD, Tanaka Y, et al. Simplest nontoxic double-layered cuprate $Ba_2CaCu_2O_4(O, F)_2$ superconductor with a transition temperature of 108K. Appl Phys Lett. 2008 Jun;92(22):222501.
[327] Shimizu S, Tabata Si, Mukuda H, et al. High-$T_c$ superconductivity with $T_c$ = 52 K under antiferromagnetic order in five-layered cuprate $Ba_2Ca_4Cu_5O_{10}(F, O)_2$ with TN = 175 K: $^{19}$F- and Cu-NMR studies. J Phys Soc Japan. 2011 Apr;80(4):043706.

[328] Shimizu S, Iwai S, Tabata Si, et al. Planar $CuO_2$ hole density in high-$T_c$ cuprates determined by NMR Knight shift: $^{63}Cu$ NMR on bilayered $Ba_2CaCu_2O_4(F, O)_2$ and three-layered $Ba_2Ca_2Cu_3O_6(F, O)_2$. Phys Rev B. 2011 Apr;83(14):144523.
[329] Shimizu S, Mukuda H, Kitaoka Y, et al. Antiferromagnetic phase transition in four-layered high-$T_c$ superconductors $Ba_2Ca_3Cu_4O_8(F_yO_{1-y})_2$ with $T_c = 55$-102 K: $^{63}Cu$- and $^{19}F$-NMR studies. J Phys Soc Japan. 2009 Jun;78(6):064705.
[330] Kazakov SM, Pachot S, Kopnin EM, et al. Synthesis, neutron diffraction study and cation substitutions in $Sr_{n-1}Cu_{n+1}O_{2n}$ ($n = 3,5$). Physica C. 1997 Mar;276(1):139–146.
[331] Er G, Miyamoto Y, Kanamaru F, et al. Superconductivity in the infinite-layer compound $Sr_{1-x}La_xCuO_2$ prepared under high pressure. Physica C. 1991 Oct;181(1):206–208.
[332] Schwer H, Kopnin EM, Jun J, et al. X-ray single crystal structure analysis of the three-Leg-Ladder compound $(Sr, Ca)_4Cu_6O_{10}$. J Solid State Chem. 1997 Dec;134(2):427–430.
[333] Adachi S, Yamauchi H, Tanaka S, et al. New superconducting cuprates in the Sr-Ca-Cu-O system. Physica C. 1993 Jul;212(1):164–168.
[334] Chu CW, Deng LZ, Lv B. Hole-doped cuprate high temperature superconductors. Physica C. 2015 Jul;514:290–313.
[335] Smith MG, Manthiram A, Zhou J, et al. Electron-doped superconductivity at 40 K in the infinite-layer compound $Sr_{1-y}Nd_yCu0_2$. Nature. 1991 Jun;351(6327):549–551.
[336] Chu C, Xue Y, Du Z, et al. Superconductivity up to 126 Kelvin in interstitially doped $Ba_2Ca_{n-1}Cu_nO_x[02(n-1)n\text{-}Ba]$. Science. 1997 Aug;277(5329):1081–1083.
[337] Walker D, Carpenter MA, Hitch CM. Some simplifications to multianvil devices for high pressure experiments. American Mineralogist. 1990 Oct;75(9-10):1020–1028.
[338] Xue YY, Sun YY, Rusakova I, et al. Phase identification of the new 126 K Ba-Ca-Cu-O superconductor. Physica C: Superconductivity. 1998 Jan;294(3):316–326.
[339] Hosomi T, Suematsu H, Fjellvåg H, et al. Identification of superconducting phases in the Ba-Ca-Cu-O system: an unstable phase with $T_c \approx 126$ K and its derivative with $T_c \approx 90$ K. J Mater Chem. 1999;9(5):1141–1148.
[340] Wu NL, Du ZL, Xue YY, et al. Observation and identification of a 107 K superconducting family in the $CaBa_2Ca_2Cu_3O_{9-\delta}$ system. Physica C: Superconductivity. 1999 Apr;315(3):227–234.
[341] Alff L, Krockenberger Y, Welter B, et al. A hidden pseudogap under the 'dome' of superconductivity in electron-doped high-temperature superconductors. Nature. 2003;422(6933):698–701.
[342] Luke G, Le L, Sternlieb B, et al. Magnetic order and electronic phase diagrams of electron-doped copper oxide materials. Phys Rev B. 1990;42(13):7981–7988.
[343] Horio M, Sakai S, Koshiishi K.Common origin of the pseudogap in electron-doped and hole-doped cuprates governed by Mott physics. 2019 Mar. Available from: ArXiv: 1801.04247.
[344] Kyung B, Hankevych V, Daré AM, et al. Pseudogap and spin fluctuations in the normal state of the electron-doped cuprates. Phys Rev Lett. 2004 Sep;93(14):147004.
[345] Damascelli A, Hussain Z, Shen ZX. Angle-resolved photoemission studies of the cuprate superconductors. Rev Mod Phys. 2003 Apr;75(2):473–541.
[346] Krockenberger Y, Kurian J, Winkler A, et al. Superconductivity phase diagrams for the electron-doped cuprates $R_{2-x}Ce_xCuO_4$ (R = La, Pr, Nd, Sm, and Eu). Phys Rev B. 2008 Feb;77(6):060505.
[347] Paulus EF, Yehia I, Fuess H, et al. Crystal structure refinement of $Nd_2$-xCexCuOrm$_4$ (x = 0.05-0.30) by x-ray (295 K) and neutron (1.5 K) powder diffraction. Solid State Commun. 1990 Mar;73(11):791–795.
[348] Naito M, Hepp M. Superconducting T-$La_{2-x}Ce_xCuO_4$ films grown by molecular beam epitaxy. Jpn J Appl Phys. 2000 Jun;39(6A):L485–L487.
[349] Markert JT, Beille J, Neumeier JJ, et al. Pressure dependence of $T_c$ in $L_{2-x}M_xCuO_{4-y}$ (L = Pr, Nd, Sm, Eu; M = Ce, Th): antisymmetric behavior of electron- versus hole-doped copper-oxide superconductors. Phys Rev Lett. 1990 Jan;64(1):80–83.
[350] Ikeda M, Yoshida T, Fujimori A, et al. Effects of chemical pressure on the Fermi surface and band dispersion of the electron-doped high-$T_c$ superconductors. Phys Rev B. 2009 Jul;80(1):014510.

[351] Tsukada A, Krockenberger Y, Noda M, et al. New class of T′-structure cuprate superconductors. Solid State Commun. 2005 Feb;133(7):427–431.
[352] Kubo T, Uefuji T, Fujita M, et al. Magnetic phase diagrams of electron-doped high-$T_c$ cuprates $Pr_{1-x}LaCe_xCuO_{4-\delta}$ and $Nd_{2-x}Ce_xCuO_{4-\delta}$ studied by $\mu$SR measurements. Physica C: Superconductivity. 2002 Oct;378–381:354–359.
[353] Fujita M, Kubo T, Kuroshima S, et al. Magnetic and superconducting phase diagram of electron-doped $Pr_{1-x}LaCe_xCuO_4$. Phys Rev B. 2003 Jan;67(1):014514.
[354] Chen BH, Eichhorn BW. Alternate distortion modes and stability ranges in $A^{ii}2B^{iv}O_4$ solid solutions possessing the $K_2NiF_4$ structure type: a new structural modification of the T phase. J Solid State Chem. 1992 Apr;97(2):340–347.
[355] Wilhelm H, Cros C, Reny E, et al. Influence of pressure on the crystal structure of $Nd_2CuO_4$. J Mater Chem. 1998 Jan;8(12):2729–2732.
[356] Wilhelm H, Cros C, Arrouy F, et al. Pressure induced structural transition in the solid-Solution $La_{2-x}Nd_xCuO_4$ for $x = 0.6$, 0.7, 1.2, and 1.5. J Solid State Chem. 1996 Oct;126(1):88–94.
[357] Kamiyama T, Izumi F, Takahashi H, et al. Pressure-induced structural changes in $Nd_2$-xCexCuO$_4$ ($x = 0$ and 0.165). Physica C: Superconductivity. 1994 Aug;229(3):377–388.
[358] Glazkov VP, Savenko BN, Somenkov VA, et al. High-Pressure neutron diffraction study of the $Nd_{1.85}Ce_{0.15}CuO_4$ structure. Crystallogr Rep. 2003 May;48(3):374–376.
[359] Rotundu CR, Struzhkin VV, Somayazulu MS, et al. High-pressure effects on single crystals of electron-doped $Pr_2Ce_xCuO_4$. Phys Rev B. 2013 Jan;87(2):024506.
[360] Beille J, Gerber A, Grenet T, et al. Electrical transport properties and superconducting critical temperature of $Ln_{1.85}Ce_{0.15}CuO_{4-y}$ (Ln = Nd, Sm, Eu) under quasihydrostatic pressure up to 100 kbar. Solid State Commun. 1991 Jan;77(2):141–145.
[361] Murayama C, Môri N, Yomo S, et al. Anomalous absence of pressure effect on transition temperature in the electron-doped superconductor Nd1.85Ce0.15CuO4 − $\delta$. Nature. 1989 May;339 (6222):293–294.
[362] Wu W, Scheurer MS, Chatterjee S, et al. Pseudogap and Fermi surface topology in the two-dimensional Hubbard model. Phys Rev X. 2018 May;8(2):021048.
[363] Drozdov AP, Eremets MI, Troyan IA, et al. Conventional superconductivity at 203 kelvin at high pressures in the sulfur hydride system. Nature. 2015 Sep;525(7567):73–76.
[364] Drozdov AP, Kong PP, Minkov VS, et al. Superconductivity at 250 K in lanthanum hydride under high pressures. Nature. 2019 May;569(7757):528–531.
[365] Somayazulu M, Ahart M, Mishra AK, et al. Evidence for superconductivity above 260 K in lanthanum superhydride at megabar pressures. Phys Rev Lett. 2019 Jan;122(2):027001.
[366] Geballe ZM, Liu H, Mishra AK, et al. Synthesis and stability of lanthanum superhydrides. Angew Chem Int Ed Engl. 2018;57(3):688–692.
[367] Snider E, Dasenbrock-Gammon N, McBride R, et al. Room-temperature superconductivity in a carbonaceous sulfur hydride. Nature. 2020 Oct;586(7829):373–377.
[368] Suzuki H, Minola M, Lu Y, et al. Probing the energy gap of high-temperature cuprate superconductors by resonant inelastic x-ray scattering. NPJ Quant Mater. 2018 Dec;3(1):1–8.
[369] Lee W, Zhou KJ, Hepting M, et al. Spectroscopic fingerprint of charge order melting driven by quantum fluctuations in a cuprate. Nat Phys. 2021;17:53–57.
[370] Mitrano M, Wang Y. Probing light-driven quantum materials with ultrafast resonant inelastic x-ray scattering. Commun Phys. 2020 Oct;3(1):1–9.
[371] Mitrano M, Lee S, Husain AA, et al. Evidence for photoinduced sliding of the charge-order condensate in $La_{1.875}Ba_{0.125}CuO_4$. Phys Rev B. 2019 Nov;100(20):205125.
[372] Fornek T. Advanced photon source upgrade project final design report. 2019. (APSU–2.01-RPT-003, 1543138, 153666).
[373] Carr GL, Lobo RPSM, LaVeigne J, et al. Exploring the dynamics of superconductors by time-Resolved far-Infrared spectroscopy. Phys Rev Lett. 2000 Oct;85(14):3001–3004.
[374] Dubroka A, Yu L, Munzar D, et al. Pseudogap and precursor superconductivity in underdoped cuprate high temperature superconductors: a far-infrared ellipsometry study. Eur Phys J Spec Top. 2010 Oct;188(1):73–88.